

CASE FILE COPY

EVALUATION OF ZIRCONIA, THORIA AND ZIRCONIUM DIBORIDE FOR ADVANCED RESISTOJET USE

By Russell J. Page, Robert A. Short,
and Carl R. Halbach

MAY 1972

Prepared under Contract No. NAS1-10353 by

ADVANCED ROCKET TECHNOLOGY (ARTCOR)

Irvine, California 92664

for

NATIONAL AERONAUTICS AND SPACE ADMINISTRATION

Langley Research Center

TABLE OF CONTENTS

<u>SECTION</u>	<u>PAGE</u>
LIST OF FIGURES	iii
LIST OF TABLES	vi
SUMMARY	1
INTRODUCTION	2
SYMBOLS	4
MATERIAL PROPERTIES EVALUATION	5
Materials Surveyed	6
Properties of Candidates	13
Ranking of Materials	31
THRUSTOR DESIGN PHILOSOPHY	54
Objective.	54
Design Principles.	54
Fabrication Techniques	59
Joining Techniques	59
THRUSTOR ELEMENT FABRICATION AND TEST	61
Element Fabrication.	61
Material Test Apparatus	71
ANALYSIS OF DATA.	81
Information on As-Received Tubes	81
Tested Tubes	84
CONCLUSIONS	94
REFERENCES	95
APPENDIX A - CORRECTIONS TO OPTICAL PYROMETER TEMPERATURE MEASUREMENTS OF INDIRECTLY HEATED CERAMIC TUBE WHERE REFLECTION AND TRANSMISSION TERMS MAY BE SIGNIFICANT	A-1
APPENDIX B - DEFINITIONS OF PERFORMANCE PARAMETERS	B-1

LIST OF FIGURES

<u>Figure</u>	<u>Title</u>	<u>Page</u>
1.	Linear metal loss constants of the platinum group metals oxidized in air	8
2.	Thermal conductivity of candidate materials (all at 0% porosity)	15
3.	Linear thermal expansion of candidate materials compared with platinum	16
4.	Electrical resistivity of candidate materials compared with Re and Pt	17
5.	Elastic modulus versus temperature for $ZrB_2 + 20$ v/o SiC, MgO, ThO_2 and ZrO_2 , CaO stabilized	18
6.	Proposed phase diagram for ZrO_2 system	20
7.	Linear thermal expansion of three forms of stabilized zirconia	21
8.	Comparison of modulus of elasticity of ZrO_2 stabilized with Y_2O_3 and CaO to various degrees and for several densities	22
9.	Modulus of elasticity for cycled ZrO_2 with degrees of stabilization	23
10.	Electrical conductivity of ZrO_2 with 10 mole % Y_2O_3 (as measured by several authors)	25
11.	Electrical conductivity of ZrO_2 with 4.5 mole % Y_2O_3	26
12.	Surface sublimation rates of biowaste resistant materials in a vacuum compared to rhenium	39
13.	Surface recession rates due to sublimation of biowaste resistant materials in a vacuum compared to rhenium	40
14.	Summary of compressive creep data for thoria showing dependence on temperature and stress	43
15.	Summary of compressive creep data for stabilized zirconia	44
16.	Extrapolation of compressive creep data (for 3% total creep) to determine service life expectancy or working stress for various forms of stabilized zirconia	48
17.	Extrapolation of compressive creep data (for 3% total creep) to determine service life expectancy or working stress for thoria for a range of temperature	49

<u>Figure</u>	<u>Title</u>	<u>Page</u>
18.	Functional schematic of an advanced resistojet configuration	56
19.	Test sample configuration	64
20.	Vapor deposition process schematic	66
21.	Thermal expansion comparison of materials used in ceramic-to-metal seals	68
22.	Seal geometry	69
23.	Kovar to zirconia seal (5.5x)	70
24.	Kovar to zirconia seal - longitudinal section (11x)	70
25.	Material test apparatus	72
26.	Test schematic	73
27.	Coil heater - sample temperature difference vs electric power - Test #4	76
28.	Test heater - sample geometry	77
29.	Longitudinal cross-section of experimental apparatus	78
30.	Array of sample types	80
31.	Cross-sectional view of as-received Zircoa tubes	85
32.	After-test record photographs of representative ZrO ₂ samples	86
33.	Typical thermal shock fracture caused by contact with indirect graphite test heater. Basis for recommendation of direct ohmic heating of ceramics	90
34.	Sectional view of metal-to-ceramic fitting (Station 5.9 in. Test 13)	91
35.	Cross sections of Test 17, N ₂ , 1.7 atm. 122 hours	93
A1.	Test heater-sample geometry	103
A2.	Basis for the illustrative example of the reflection problem	106
A3.	Pyrometer indicated temperature as a function of true (one-dimensional model) tube sample temperature.	110
A4.	Basis for illustrative example of the transmitted power increment influence on pyrometer measurement	112

<u>Figure</u>	<u>Title</u>	<u>Page</u>
A5.	Calculated pyrometer indicated temperature as a function of true sample temperature for geometry of Figure A1	118
A6.	Indicated monochromatic temperature ($\lambda = 0.65\mu$) of sample and heater as a function of sample hohlraum temperature	120

LIST OF TABLES

<u>Table</u>	<u>Title</u>	<u>Page</u>
I.	Materials Considered and Basis of Decision	7
II.	Matrix - Fiber Stability Limits ($^{\circ}\text{K}$) at 10^{-4} Torr.	13
III.	Physical and Mechanical Properties of Potential Candidate Materials	14
IV.	Chemical Species Present in Typical Biowaste Propellants in Mole Fractions	33
V.	Chemical Reactions Between Gases and ZrO_2 , ThO_2 and ZrB_2 - Literature Survey	34
VI.	Specimen Summary of Compressive Creep Investigations	45
VII.	Calculated Thermal Stress Resistance Factors	53
VIII.	Advanced Resistojet Design Goals Thrust, 0.111 N (25mlb)	55
IX.	Test Matrix	62
X.	Summary of Tests	79
XI.	Axial Positions of Key Tests - mm (inches)	82
XII.	X-Ray Diffraction Data on ZrO_2	83
XIII.	X-Ray Diffraction Data on ThO_2	83
XIV.	X-Ray Diffraction Analysis of Selected Materials	87
XV.	X-Ray Fluorescence Analysis of Selected Samples	88
XVI.	Optical Micrography of Selected Materials	89
AI.	Dimensions of Heater-Sample Setup	102
AII.	Shape Factors Matrix	114
AIII.	Radiating Surface Area	115
AIV.	Consolidated Shape Factor Matrix	116
AV.	Absorption Matrix. Radiant Heat Transfer Between Surfaces	116
AVI.	Reflection Matrix	117

EVALUATION OF ZIRCONIA, THORIA, AND ZIRCONIUM DIBORIDE
FOR ADVANCED RESISTOJET USE

By Russell J. Page, Robert A. Short, and Carl R. Halbach

Advanced Rocket Technology (ARTCOR)
Irvine, California

SUMMARY

Resistojet thrusters, small rockets wherein the propellant gas is heated electrically rather than chemically, have been considered for use on manned orbital space stations using such biowaste gases as CO_2 , H_2O and CH_4 as propellants. Early versions of these thrusters were limited to 1500°K due to materials' limitations of the Group VIII metals. The purpose of the program reported here was to examine all of the high temperature materials and determine their potential applicability for use in advanced biowaste resistojets ($>2000^\circ\text{K}$).

An extensive literature survey was conducted to collect material properties data on all advanced high temperature materials. Using these data, most of the materials were eliminated leaving a few candidates. Three of these, Y_2O_3 stabilized ZrO_2 , ThO_2 , and ZrB_2 with additives of C and SiC were selected for further study. The first two were experimentally evaluated.

Stabilized ZrO_2 and ThO_2 were found to have many attractive properties, including higher temperature oxidation resistance than any metal, and great potential for use in resistojets with ZrO_2 having a slight advantage primarily because of a relatively lower electrical resistivity and sublimation and a higher creep endurance strength.

Not to be ignored, when considering the attractive properties of these materials, are their structural limitations - brittleness and susceptibility to thermal shock. As long as these limitations are considered, however, it is the authors' opinions that thruster designs employing these ceramics can certainly be successful. A preliminary thruster design philosophy is presented.

ZrO_2 and ThO_2 tubular heat exchangers, electrically heated indirectly, were evaluated in short tests (0 to 10^2 hrs) to $\sim 1900^\circ\text{K}$ in flowing CO_2 and ZrO_2 was subjected to N_2 , H_2 , H_2O and vacuum as well. X-ray diffraction and fluorescence analyses were made. No chemical incompatibility was detected. The metal-to-ceramic seal technology for ZrO_2 and ThO_2 was further developed using chemical vapor deposition of tantalum for metallizing and 82 Au - 18 Ni filler braze.

In addition, there appear to be a number of applications for these materials for which they were not previously considered due to lack of familiarity of designers with their properties. It is hoped that this work will help to provide some information and aid in the development of new applications.

INTRODUCTION

Application studies (refs. 1 and 2) have shown that the resistojet propulsion system is an attractive candidate for use in orbit keeping and desaturation of the control moment gyros on manned orbital space stations. This was particularly true when the use of available biowaste gases, such as CO_2 , H_2O , CH_4 , etc., from an open loop or a partially closed environmental control/life support system was considered as expellants. Since the energy for propulsion is not intrinsic to the expellant, it is separately supplied from the electric power supply. This raises the need for electrically heated, compact, high temperature heat exchangers, built of materials compatible with these gases.

Early ten millipound resistojets designed and tested in support of the Manned Orbiting Research Laboratory program (ref. 1) were chosen to be operable on either H_2 or NH_3 supplied specifically for this purpose. High efficiency units were built almost exclusively of the refractory, rhenium (ref. 3) and successfully life tested (ref. 4) separately on H_2 and on NH_3 for 8000 hours at wall temperatures of 2200°K .

Biowaste resistojets (ref. 5) differing from those described in Ref. 3 essentially in only the heater material, substituting a platinum iridium alloy for rhenium, were operable to 1500°K on pure CO_2 , and H_2O . However, corrosion of the metal heater material by oxidation caused early failure when small (order of 1%) quantities of free oxygen are contained in the biowaste propellant. Recent studies of the NASA Manned Space Station (ref. 6) project such oxygen contamination. A solution is needed. Either the oxygen must be completely removed by a conditioning system within the Space Station or materials more compatible with the oxidizing environment are needed in resistojet design.

The present study addressed itself to the question of the best materials choice for an advanced biowaste resistojet for both: (1) long life ($>10,000$ hours MTF) in an oxidizing atmosphere and (2) high performance ($>2000^\circ\text{K}$). The needs of the resistojet were critically assessed. The sets of environmental conditions were defined that must be met by the associated materials. The fabrication requirements were outlined to be compared against the abilities to form intricate shapes and join the candidate materials to themselves and other lower temperature parts (metal-to-ceramic seals). All advanced materials were surveyed with the metallic oxides showing the most promise but these require new design philosophies compared with earlier metallic designs.

Stabilized zirconia, thoria and modified zirconium diboride were selected for a detailed comparative survey and evaluation of their pertinent physical, chemical, electrical, and stability properties.

A key need for the study was information on the kinetics of heterogeneous reactions that can occur between these gases and material walls. Such knowledge is meager and there is scarcely a basis for an analytical solution. Experimental data are essential from carefully controlled tests over prolonged period of time, hopefully years. Prediction of the long duration exposure resistance of the material requires endurance type information such as creep and endurance stress, etc. A "time compressor" is needed to gather these data. Some analytical method for projecting such results based on short-term test is needed.

The experimental contribution of the current work is an evaluation of these materials in simulated resistojet heater configurations in the short-term exposure to the candidate gases to see if there is any major short-term barrier to their use and to gain some experience with their use in the geometries required.

Sets of heater elements were fabricated of yttria stabilized zirconia, thoria, and modified zirconium diboride. The sample tubes were 3.3 to 7.4 mm in outside diameter and 13 to 30 cm long. The evaluation consisted of subjecting these samples to an internal gas flow of 0.026 g/sec of CO₂ at total pressures of ~1 atm and an external vacuum of ~10 microns of Hg simulating an insulation jacket. The tubes were radiantly heated externally by a graphite heater to temperatures, determined by pyrometer, up to 2000°K for periods of 50 to 100 hours. A set of zirconia tubes were subjected further to propellants: H₂O (vapor), N₂ and H₂. The tubes were subjected to micrographical analysis to determine if chemical reactions had taken place.

SYMBOLS

$$\beta = \frac{r_m h}{k}$$

r_m = normal distance from center, midplane or axis to surface of specimen

h = coefficient of heat transfer between surroundings and surface

k = coefficient of thermal conductivity

E = Young's modulus

α = linear coefficient of thermal expansion

k = coefficient of thermal conductivity

$a = \frac{k}{c_p} =$ thermal diffusivity

ρ = density

c_p = specific heat

μ = Poisson's ratio

ϵ = creep rate

$S =$ structure factor $\sigma(\phi, \text{structure}, T)$

σ = applied stress

d = mean grain diameter

$Q =$ activation energy for creep

$D =$ diffusion coefficient

$k =$ Boltzmann constant

$\Omega =$ average volume of a monovacancy

MATERIAL PROPERTIES EVALUATION

One of the main purposes of this program has been the evaluation of materials that would possibly permit resistojet operation on oxidizing expellants (and perhaps the non-oxidizing high performance ones as well) at a wall temperature above 2000°K. The following criteria were applied in the screening of materials. The first two alone leave less than ten potential candidates, excluding composites, out of more than 100 high temperature materials originally considered.

- (1) The material should melt above 2500°K. The material should also be chemically stable to this temperature and not undergo any crystal structure changes.
- (2) The material should resist oxidation in flowing biowaste gases to a temperature of at least 2100°K.
- (3) Electrical resistivity should be of the order of 10^{-6} to 10^{-2} ohm-m in the temperature region of interest, or a concept must be possible employing an auxiliary heater.
- (4) No reaction, or at least only slight reactions to the extent of acceptable weight losses, ($\sim 10^{-8}$ kg/m²s) should take place between the material and flowing gases of H₂O, CO₂, CH₄, H₂, NH₃ and other species, such as CO, N₂ and some free radicals in very low concentrations.

Detrimental reactions or formation of eutectics with solid carbon should also not take place. Solid carbon deposits are possible largely from decomposition of CH₄ and partly from decomposition of CO₂.

- (5) The material should resist surface evaporation losses (corresponding to surface recession rates of 10^{-10} m/s) in flowing gases to 2100°K and in vacuum to 1800°K.
- (6) The material should have an acceptable high temperature endurance strength 100 kN/m² (15 psi) and have minimum creep behavior in 10⁴ hours.
- (7) The material should have a high thermal stress/thermal shock resistance which takes into account thermal cycling conditions. High thermal conductivity, low thermal expansion, and relatively low Young's modulus are important in this respect.
- (8) Joining capability to itself or other materials such as the platinum metals is important. This means a close match in linear thermal expansion.
- (9) With regard to availability, if the material is not available in desired shapes commercially, sufficient data

on its high temperature properties should be known and fabrication technology for the development of suitable shapes should be a state-of-the-art at least on related materials. If new materials, not available nor easily fabricated offer promise based upon the other criteria, a materials research and development effort is identified, whose primary objective would be to establish feasibility for resistojet application.

- (10) Because of the small quantity of material involved, costs per kilogram of up to \$10,000 are allowed if the properties warrant further consideration.

Materials Surveyed

Table I summarizes the materials surveyed with the primary basis for decision. The amplifying remarks by material classes follows.

Refractory metals (ref. 7). - The following elements and metals have melting points above 2500°K (listed in order of decreasing melting point): carbon and graphite, W, Re, Ta, Os, Mo, Ru, Ir, Nb, and B. Certain alloys among these and with other metals would also have sufficiently high melting points for consideration. Rhenium has been used in resistojet applications in a reducing environment, as discussed in the Introduction, but would oxidize readily at 625°K and cannot be considered here.

Of the refractories listed, the platinum group members (Os, Ru and Ir) are superior to the rest in oxidation resistance but are still inadequate for the long term. The surface mass flux-loss rates in air of the platinum group metals, (ref. 8) shown in fig. 1, are all at a higher loss than our selection criterion of $<10^{-8}$ kg/m²s. Iridium is well known as the only metal with sufficiently high melting point (2716°K) that can be used unprotected in air at temperatures up to 2600°K without undergoing catastrophic failure. However, its life is short and is inconsistent with resistojet design requirements. Two metals of lower melting points than the first criterion, platinum (m.p. 2047°K) and rhodium (m.p. 2239°K), would qualify, with regard to oxidation resistance, if the operating temperature criterion were relaxed to ~1500°K which is contemporary technology (ref. 5). The other elements listed, outside the platinum group, all oxidize below 875°K.

The above elimination of refractory metals is based mainly upon their instability towards air or pure oxygen at high temperatures. Oxygen is a diluent in the CO₂ furnished as one of the prime propellant compositions in the biowaste resistojet and approximately one order of magnitude less concentrated than in air, the basis of fig. 1. The oxidizing power of CO₂ and H₂O is considerably less than O₂ but is still considerable at high temperatures. In addition, both W and Mo react with CO₂ above 1475°K and all elements listed with the exception of Ir, Ru and possibly B, react with water vapor beginning below 1275°K.

Rhenium, for instance, reacts with pure steam (ref. 9) to give surface recession rates of 1.5×10^{-2} kg/m²s at 2000°K or six orders of magnitude higher than our fourth selection criterion.

TABLE I. - MATERIALS CONSIDERED AND BASIS OF DECISION

Material class	Materials with acceptable melting points ^a	Primary basis
Elements	C, graphite, B	Oxidize <<2000°K
Refractory metals	W, Re, Ta, Os, Mo, Nb, Hf, Ru Ir	Oxidize <<2000°K Oxidation rate high
Carbides	HfC, TaC, NbC, Ta ₂ C, ZrC, TiC, WC, W ₂ C, UC, Al ₄ C ₃ , MoC, ThC ₂ , ThC, Mo ₂ C, SiC, CeC ₂ , B ₄ C, UC ₂	} Oxidize <2000°K
Nitrides	TaN, ZrN, TiN, BN, UN, ThN	Oxidize <<2000°K
Inter-metallics	TaSi ₂ , MoSi ₂ , Mo ₃ Si, Mo ₅ Si ₃ NbSi, Nb ₅ Si ₃ , Ta ₅ Si ₃ , Ta ₉ Si ₂ Ti ₅ Si ₃ , V ₅ Si ₃ , W ₃ Si ₂ Zr ₂ Si, Zr ₃ Si ₂ , Zr ₄ Si ₃ , Zr ₅ Si ₃ Zr ₆ Si ₅ , Cr-Al, Mo ₃ Al WSi ₂ Re ₃ W ₂ Ba ₃ P ₂ CeS	} Oxidize <2000°K } Too brittle } Little information available Too volatile
Oxides	ThO ₂ , HfO ₂ , ZrO ₂ , CaO UO ₂ OsO ₄ , CeO ₂ MgO BeO ZrSiO ₄ (zircon) SrZrO ₃ , BaZrO ₃ Be ₃ Zr ₂ O ₇ , CaZrO ₃	<u>Acceptable</u> Easily oxidized Too volatile Reacts with CO, H ₂ O at elevated temperature Volatilizes in H ₂ O at 1475°K Max. cont. service:1775-2050°K } Little information available
Borides	HfB ₂ + SiC and/or C ZrB ₂ + SiC and/or C HfB ₂ , ZrB ₂ , WB, TiB ₂ , ThB ₄ MoB, Mo ₂ B	} <u>Acceptable</u> <u>Acceptable</u> Oxidize <2000°K

^a Materials not listed have melting points below 2500°K or their melting points are not known.

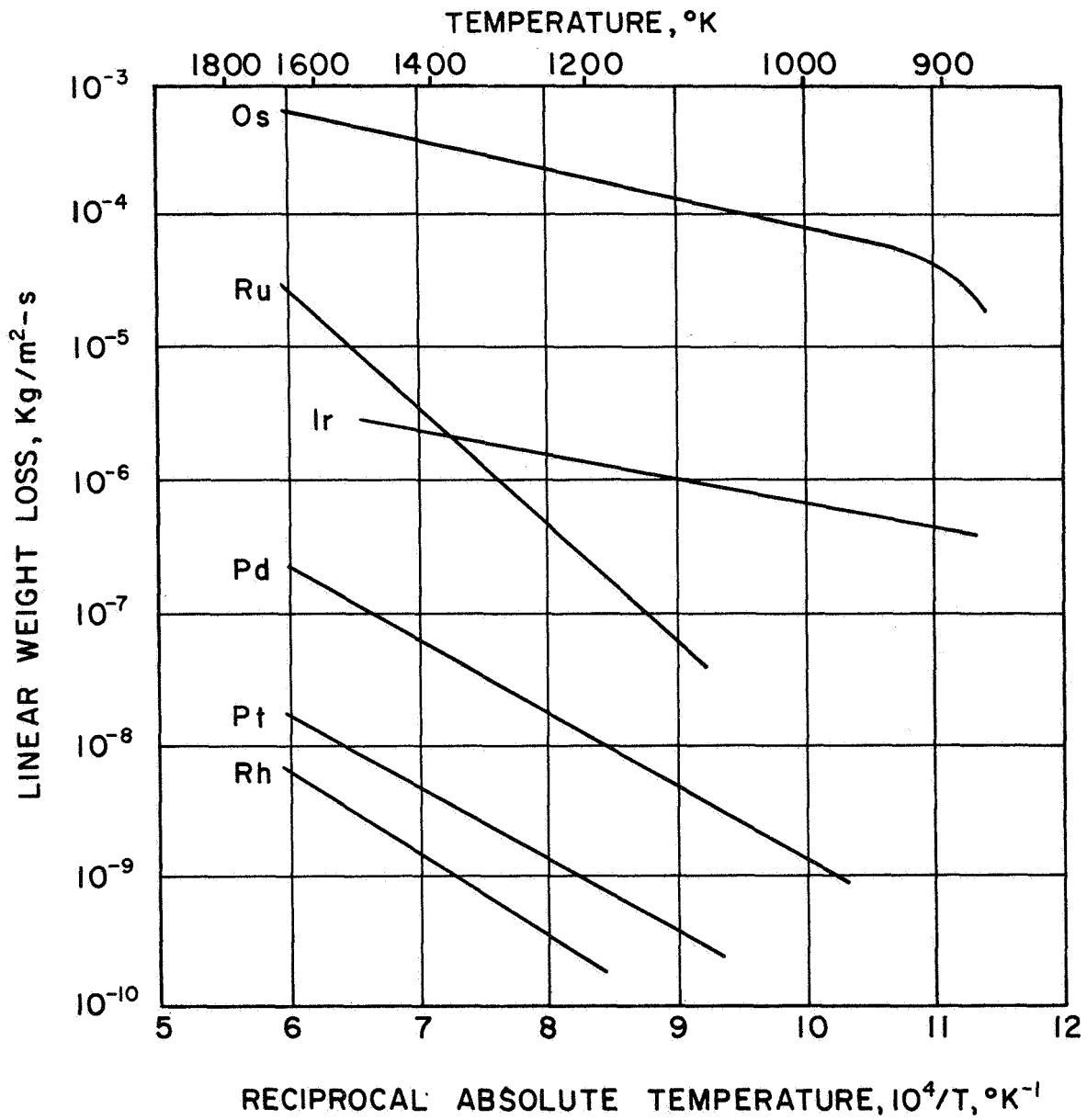


Figure 1.- Linear metal loss constants of the platinum group metals oxidized in air.

Coated refractory metals. - Since refractory metals are relatively workable and can be more readily resistance heated compared to ceramics, their use in high temperature resistojets in oxidizing gases might still be considered if oxidation resistant coatings, capable of long duration service, can be applied to the exposed surfaces. Well known oxidation resistant coatings that are available are SiC and silicides of W, Mo and Ta. An interesting combination that might lend itself to a low voltage-high current resistojet configuration is graphite coated with SiC. This coating is claimed to have excellent thermal shock and thermal fatigue resistance and to be impermeable to O₂ and H₂. No data is available on long-term resistance. Oxidation of SiC becomes severe, however, in the range 1700-2000°K.

The disilicides of W, Mo and Ta all melt above 2275°K. TaSi₂ oxidizes in air above 1775°K and MoSi₂ oxidizes severely above 1975°K. WSi₂, however, is reported to be quite stable in air to 2200°K.

Several high melting oxides and diborides of Zr and Hf with additions of SiC and C are candidates for oxidation resistant coatings on refractory metals. Oxides and diborides are also considered as candidates in bulk form. These are discussed later.

Coatings of Si₃N₄ have been considered (ref. 37) for high temperature turbines (1800°K) where the exhaust gases are very similar to the biowastes considered here. Si₃N₄ has excellent dimensional stability and oxidation resistance at temperatures up to 1700°K. Si₃N₄ is considered stable in neutral or reducing atmospheres up to 2100°K. Above 2100°K, Si₃N₄ dissociates appreciably.

The small physical size of resistojets requires thin walled tubes and parts. These are difficult to coat and inspect. Surface wear must be particularly low as a criterion. For these reasons, coatings were not considered further.

Carbides. - Carbides, as a family, have higher melting points than other refractories. The following carbides melt above 2500°K: HfC (m.p. 4165°K), TaC, NbC, Ta₂C, ZrC, TiC, WC, W₂C, VC, Al₄C₃, MoC, ThC₂, ThC, Mo₂C, CeC₂, B₄C, and UC₂. The cubic form of SiC decomposes at 2925°K. Two mixed carbides melt higher than any other material: 4TaC + HfC (m.p. 4215°K) and 4TaC + ZrC (m.p. 4205°K), and a mixed carbide/nitride, TaC + TaN also has a high melting point (3480°K).

Unfortunately, all the carbides have relatively poor oxidation resistance at high temperatures. The high melting ones corrode severely in air in the temperature range 1400-1700°K, except SiC which corrodes at 1700-2000°K, and the lower melting ones at 800-1100°K. These materials can, therefore, not be considered for resistojet applications.

Nitrides. - Nitrides that melt above 2500°K are TaN, ZrN, TiN, BN, UN, ThN, and AlN. All of these corrode severely in air at 1400-1700°K or below, often with large weight losses.

Intermetallics. - Of the numerous intermetallic compounds the silicides are generally the highest melting ones. TaSi₂, MoSi₂ and WSi₂ have already been considered (under coatings).

MoSi₂ is used as a high temperature furnace heater at 2075°K in oxidizing atmosphere with a life of approximately 1400 hours expected. In intermittent service where maximum temperature is maintained for only a few hours, only 40 - 50 cycles are obtained. Operation at lower temperatures can result in service life of one year. MoSi₂ is particularly compatible against corrosion where methane or sulfur bearing compounds are injected. Other silicides melting above 2500°K are Ta₅Si₃, Nb₅Si₃, W₃Si₂, Zr₆Si₅ and a few others. For these oxidation in air becomes severe in the range 1700-2000°K or below.

A couple of aluminides, CrAl and Mo₃Al have melting points at the border line of interest (≈2425°K). Their oxidation resistance at high temperatures is not well known, but is likely poor. Little is known about the high melting inter-metallic, Re₃W₂ (m.p. 3265°K).

While not strictly an intermetallic compound, the phosphide, Ba₃P₂ (m.p. 3475°K) is believed to be stable in air (ref. 10) but temperatures are not given. The sulfide CeS (m.p. 2615°K) is also referred to as being stable with respect to air, but its volatility is too high for consideration (ref. 10).

Intermetallic compounds are generally very brittle.

Oxides. - The oxides are natural candidates for application as structural components in oxidizing environments if their brittleness and poor thermal shock resistance can be improved or accommodated to meet the requirements of the design. Besides zirconia, the following oxides melt above 2500°K: ThO₂, UO₂, MgO, HfO₂, OsO₄, CeO₂, CaO, and BeO. The following double oxides also fall in this class: SrZrO₃, BaZrO₃, ZrSiO₄ (zircon), Be₃Zr₂O₇, and CaZrO₃. Little is known about the high temperature properties of the double oxides. Zircon is good to 2150°K in air, to 2000°K in vacuum and referred to as "fair" in a reducing atmosphere (ref. 10). Maximum continuous service temperature is 1775-2050°K without cycling, which eliminated it from consideration. Since no high temperature properties are available for the two highest melting double oxides, SrZrO₃ and BaZrO₃, they are not considered practical candidates at the present time.

Of the single oxides, BeO has a high thermal conductivity with a resultant good thermal shock resistance to 2025°K. It is useful to 2675°K in air, to 2275° in vacuum but is appreciably volatile in vacuum at 2375°K. It has excellent resistance to hydrogen. Further, it does not react with CO₂. It reacts significantly with CO at high temperatures, however. Since CO is a dissociated species of CO₂ at high temperature BeO would be unsuitable for use on CO₂ for long duration service. Most important, BeO is volatile at 1475°K in H₂O vapor and dissociates at 1875°K. It can, therefore, not be used for the intended resistojet application.

CeO₂ is easily reduced and forms hydrates in H₂O vapor. Little is known about the high temperature properties of OsO₄, but it is volatile in vacuum. More is known about UO₂, but due to the many possible valence states of U, the oxidation resistance is low and it forms hydrates in water vapor. CeO₂, OsO₄ and UO₂ are therefore excluded as candidates.

A reservation is made on considering MgO. While considered a model material and investigated thoroughly for high temperature applications, its resistance to CO is stated as poor at high temperatures and highly crystalline forms react with water vapor.

The remaining oxides, ThO₂, ZrO₂, HfO₂ and CaO are candidate materials. A reservation is made regarding HfO₂ since it undergoes a monoclinic to tetragonal transformation at about 2000°K. It preferably should be stabilized like zirconia. These oxides are all brittle, but have excellent oxidation resistance to 2675°K.

Borides. - The following borides melt above or at 2500°K: HfB₂ (m.p. 3340°K), ZrB₂ (m.p. 3275°K), WB, TiB₂, ThB₄, MoB, and Mo₂B. Corrosion becomes severe in air at 1100-1700°K for all these borides, except Mo₂B (the lowest melting of those listed), ThB₄ and HfB₂, where no information is available. The pure borides are, therefore, not good candidates.

HfB₂ and ZrB₂ with additions of SiC and/or C, however, have significantly improved high temperature properties. HfB₂ + SiC and/or C has favorable dynamic oxidation resistance to 2500°K and ZrB₂ + ZrB + SiC and/or C to 2300°K as demonstrated by short-term tests. The high temperature properties of these materials have been studied in some detail (refs. 11-15) where the preparation, microstructural, electrical, mechanical, and thermal properties, thermochemical stability and thermal stress resistance of these materials are summarized. Short-term oxidation tests of up to four hours of ZrB₂ + SiC are reported in reference 16 for 250 Torr. O₂ up to 1775°K.

Fiber reinforced ceramics. - The main purpose of using fiber reinforced ceramics is the promise of employing brittle materials such as oxides as components where loads are induced by mechanical or thermal means. The improvement in this respect of the candidate materials above, ThO₂, HfO₂, ZrO₂ and CaO and even ZrB₂ and HfB₂, would improve their chances of surviving thermal loads, thermal shock and thermal cycling for periods of time as is characteristic of resistojet operation.

An excellent summary and assessment of the potential of fiber reinforced ceramics is presented by J. Krochmal. (ref 17). The "technologically interesting" matrix-fiber combinations in Krochmal's review are: Matrices: ZrB₂, HfB₂, SiC, ZrC, HfC, TaC, WC, Al₂O₃, BeO, MgO, ThO₂, ZrO₂, MgAl₂O₄, MoSi₂, and WSi₂; fibers (or filaments or whiskers): W, Mo, Ta, B, C, SiC, B₄C, and Al₂O₃. The conclusion of the review was that no combination among these matrices and fibers offered a real solution to the brittleness problem at high temperatures in oxidizing environment, due to (1) thermochemical interaction, (2) cracking, and (3) reinforcement oxidation.

Thermochemical interactions were reactions between fiber and matrix, either at high processing or use temperatures. Low temperature hot pressing or pressure sintering would be techniques that might overcome the interactions during processing.

Microcracking, caused by differential thermal contraction following densification at high temperatures when the coefficient of thermal expansion of the matrix exceeded that of the fiber, was sometimes tolerable. It might also be avoided by lower temperature processing.

Reinforcement oxidation was a severe problem for all fibers, except Al_2O_3 , in all matrices, except Al_2O_3 and BeO . These oxides are practically impermeable to oxygen (which is not the case for the potential candidate oxides ThO_2 , HfO_2 , ZrO_2 , and CaO). Such oxidation of the fiber would either result in the mechanical disruption of the composite or reaction between oxidation product and matrix.

Since the above review was conducted, fibers of ZrO_2 have become available. If the matrix and fiber were of the same material, chemical reaction would not occur. Further, cracking due to mismatch in thermal expansion coefficient would not occur. Finally, if the fibers were the acceptable oxides and modified diborides, reinforcement oxidation would not occur.

Ceramic fiber reinforced oxides. - Hot pressing appears to be the most frequently used method to achieve densification of fiber reinforced ceramics. The fibers, filaments or whiskers (single crystal fibers) are mixed with the matrix powder and hot pressed directly. Pre-alignment of the fibers in the matrix has been practiced in order to take advantage of the extremely high tensile strength of fibers. In the systems of interest, hot pressing temperatures approaching or even above 2275°K are required to achieve the necessary density. This causes damage to the fibers. Recently developed techniques, referred to as low temperature hot pressing and pressure sintering, apparently eliminate or reduce damage to the fibers. The "Zyttrite" process (ref. 18) for low temperature hot pressing or zirconia (or cold pressing followed by sintering) and chemically activated pressure sintering of magnesia (refs. 19, 20, and 21) are examples of low temperature processing.

Due to the unavailability of other fibers, there is presently only one practical composite candidate: Yttria-stabilized zirconia matrix/yttria-stabilized zirconia fibers. The former system has been very recently studied using the "Zyttrite" zirconia at the Air Force Materials Laboratory (refs. 22 and 23).

Metal fiber reinforced oxides. - The oxide candidates, ThO_2 , HfO_2 , ZrO_2 , and CaO , as discussed later, can be solid-state electrolytes passing oxygen ions by ionic conduction. This provides a mechanism whereby reinforcement fibers of W, Mo, or Ta may be oxidized. If it were not for this above mechanism, these metals would be compatible with these ceramic oxides for resistojet use.

For applications, not having such oxidizing conditions, Table II summarizes the stability limits for the matrices and fibers shown which are collected from ref. 24 except as noted.

TABLE II. - MATRIX - FIBER STABILITY LIMITS ($^{\circ}$ K) AT 10^{-4} TORR.

Matrices	Metal Fibers		
	W	Mo	Ta
ThO ₂	2475	2175	2075 ^a
ZrO ₂	1875	2175	1875
MgO	2275 ^b	2075	2075

^aReducing conditions (ref. 25)

^bReference 26.

The system Y₂O₃-stabilized zirconia-molybdenum, however, was found to have excellent stability to 2645 $^{\circ}$ K (ref. 27).

Although composite materials have some potential for resistojet applications, they would require a considerable development effort. The fabrication of test samples was not within the scope of the present program.

Properties of Candidates

The screening criteria in the previous section passed six (6) materials that seemed to possess acceptable properties for resistojet use. These were ThO₂, HfO₂, ZrO₂, CaO, and HfB₂, and ZrB₂ with additives. Several composites were also listed as candidates, but were excluded because of lack of development. Table III lists the important properties of these materials where they are available. Figures 2 through 5 are graphical comparisons of various properties of the candidate materials with temperature.

Of the potential candidates, the reasons for selection of three (3) ZrO₂, ThO₂ and modified ZrB₂ for experimental study were as follows: From a glance at Table III it is seen that these are the ones which are more thoroughly characterized by property data. Hafnia, being more scarce than zirconia, has not been sufficiently studied with regard to stabilization of the expansion characteristics. There are no significant differences between their capabilities. The same reasons apply to the selection of zirconium diboride over hafnium diboride. For the reasons of avoiding the potential development problems and lack of availability of material, the study was narrowed to the three (3) candidates which are discussed in turn in the following section and ranked

TABLE III.- PHYSICAL AND MECHANICAL PROPERTIES OF POTENTIAL CANDIDATE MATERIALS

Property	Figure No.	Thoria ThO ₂	Hafnia HfO ₂	Calcium CaO	Zirconia ZrO ₂	Zirconium-diboride, ZrB ₂	Hafnium-diboride, HfB ₂	Platinum (for reference)
Additives	-	None	None	None	10 mole % Y ₂ O ₃	20 v/o SiC	20 v/o SiC	None
Melting point, °K	-	3540	3085	2353	2998	ca 3275	3338	2047
Specific gravity	-	9.86	9.68	3.35	5.60	5.52	9.34	21.45
Specific heat, J/kg °K	-							
@ 288°K		235	393	753	460	418	(242) ^a	133
1200°K		304	628	967	670	720	(389) ^a	158
2000°K		331			858	806	(444) ^a	180
Thermal conductivity W/m °K	2							
373°K		11.3	1.67	15.5	1.76	100	62.8	70.3
1200°K		3.0	1.67	8.0	1.88	78.3	58.6	90.4
1600°K		2.5	-	-	2.00	75.3	62.8	108.8
2000°K		2.4	-	-	-	70.7	67.0	-
Thermal diffusivity, m ² /s	-							
1200°K		9.8 x 10 ⁻⁷	4.32 x 10 ⁻⁷	2.4 x 10 ⁻⁶	4.9 x 10 ⁻⁷	1.9 x 10 ⁻⁵	1.8 x 10 ⁻⁵	2.6 x 10 ⁻⁵
2000°K		7.0 x 10 ⁻⁷	-	-	-	1.6 x 10 ⁻⁵	1.5 x 10 ⁻⁵	-
Thermal linear expansion, % (298-1800°K)	3	1.54	0.95	2.29	1.42	1.06	-	1.68
Electrical resistivity, ρ, Ω-m	4							
298°K		-	-	-	-	1.02 x 10 ⁻⁷	9.6 x 10 ⁻⁸	1.05 x 10 ⁻⁷
1200°K		4 x 10	3 x 10 ³	2 x 10 ²	2.5 x 10 ⁻¹	5.11 x 10 ⁻⁷	5.38 x 10 ⁻⁷	3.95 x 10 ⁻⁷
1600°K		1	10	-	3 x 10 ⁻²	-	-	4.95 x 10 ⁻⁷
2000°K		4 x 10 ⁻²	10 ⁻¹	-	9 x 10 ⁻³	-	-	-
Total normal emissivity, ε _n	-							
1200°K		0.29	0.81	-	0.4	(0.60) ^a	(0.51) ^a	0.12
1600°K		0.27	0.82	-	0.4	(0.78) ^a	(0.78) ^a	0.17
2000°K		0.30 - 0.55	0.82	-	0.5	0.60 (0.74) ^a	(0.82) ^a	-
Modulus of elasticity, KN/m ² x 10 ⁻⁷	5							
298°K		14.6	5.6	37.2	(15.5) ^c	54	54	17.1
1200°K		12.4	-	35.2	(13.2) ^c	52	53	-
Estimated working stress (creep) 10,000 hrs @ 1800°K, KN/m ²	-							
Sublimation recession at 1800°K, kg/sm ²	12	300	-	-	~1000	-	-	Nil
		1.7 x 10 ⁻⁸	-	-	10 ⁻⁸	e > 10 ⁻⁹	-	5 x 10 ⁻⁷

a Pure, no additives

b Zero porosity

c 8.8 mole %
- Data not available

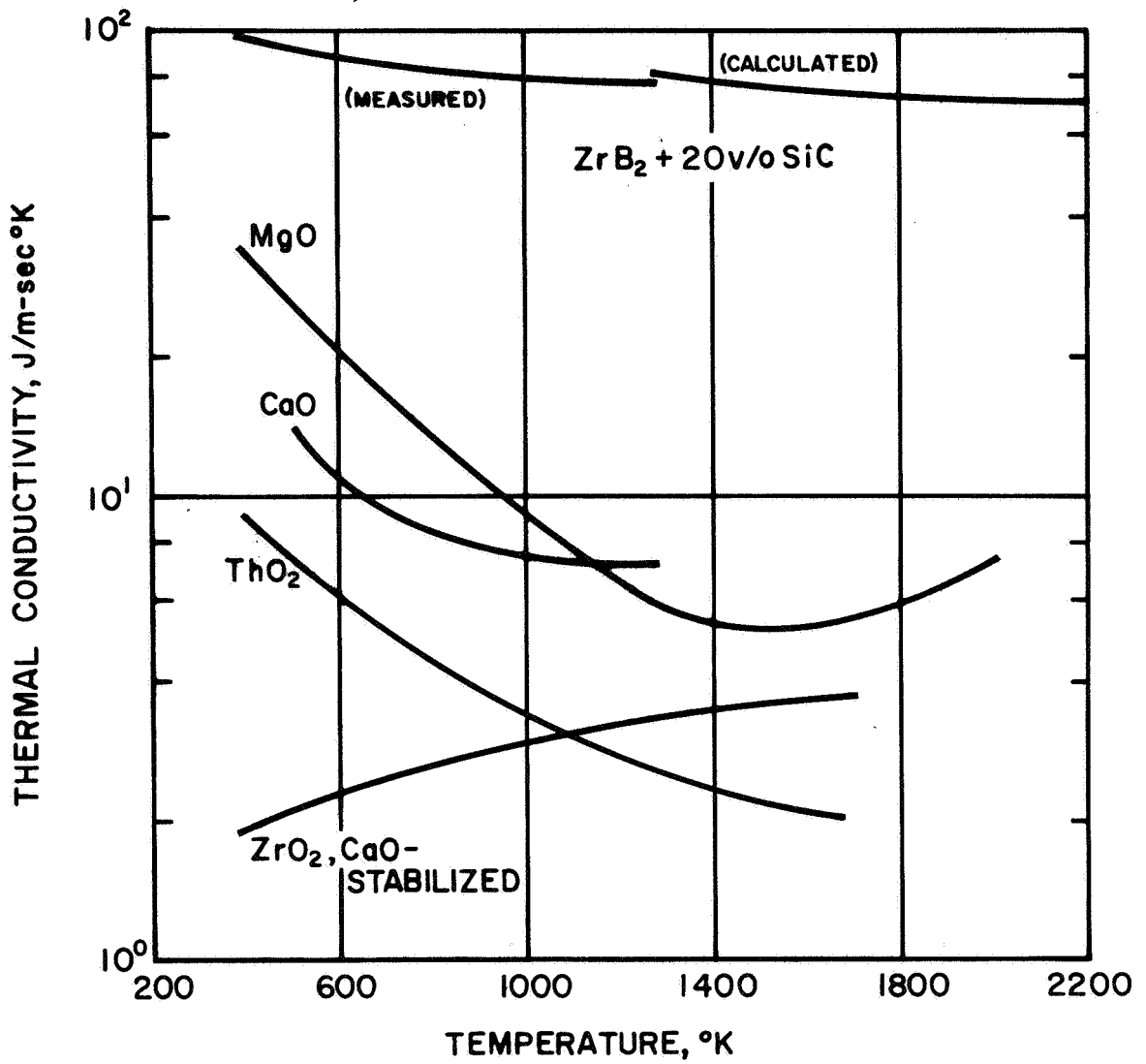


Figure 2.- Thermal conductivity of candidate materials (all at 0% porosity).

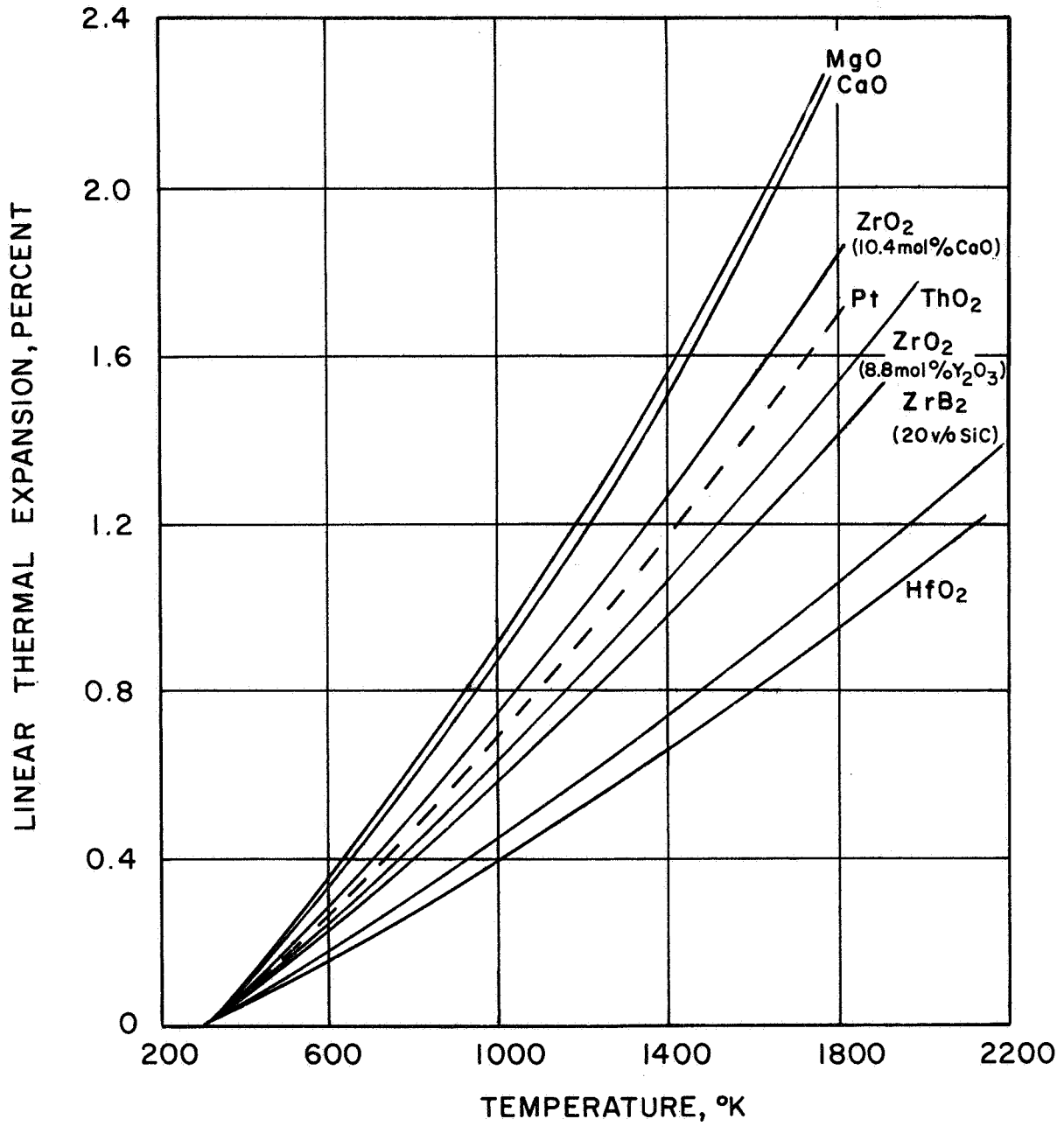


Figure 3.- Linear thermal expansion of candidate materials compared with platinum.

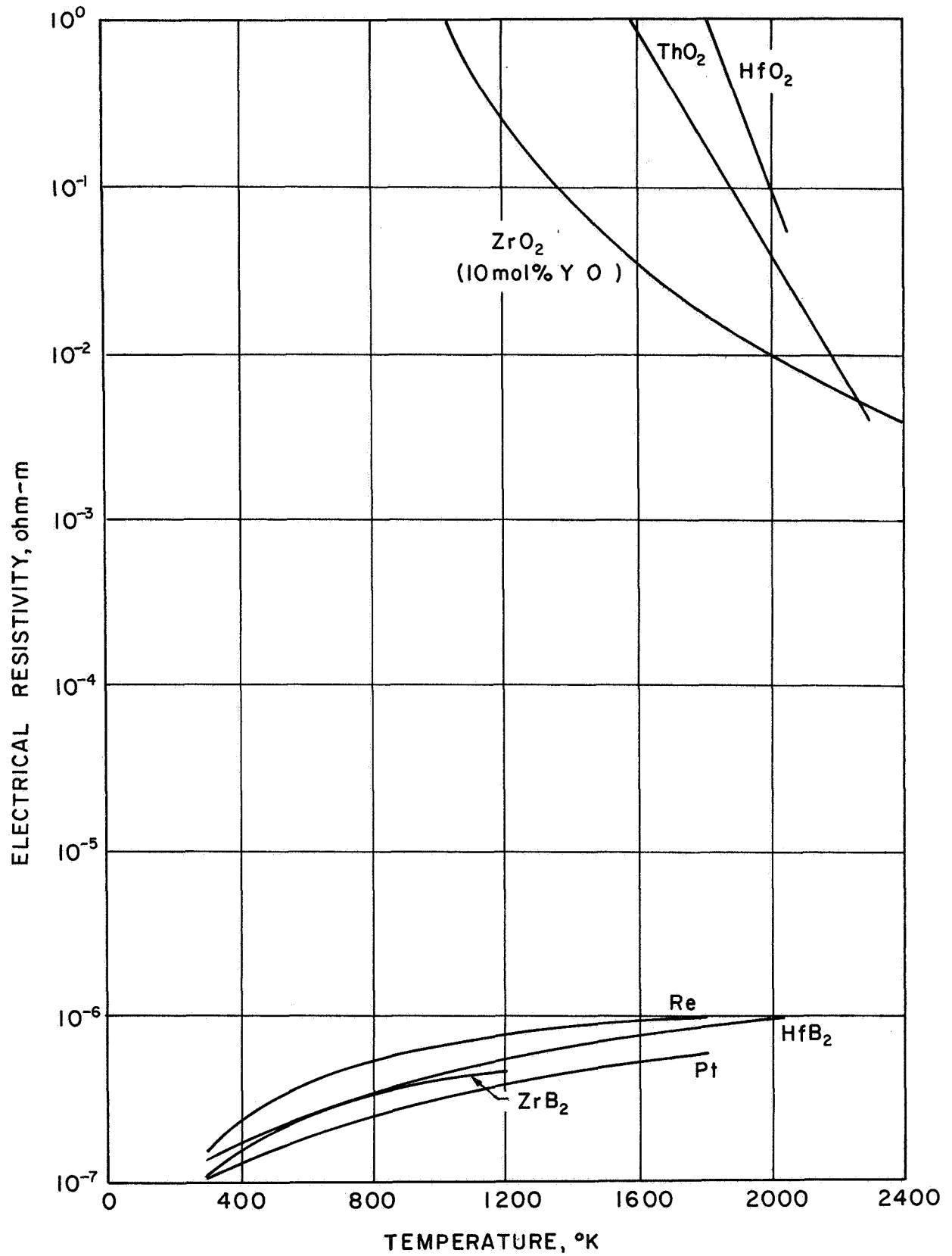


Figure 4.- Electrical resistivity of candidate materials compared with Re and Pt.

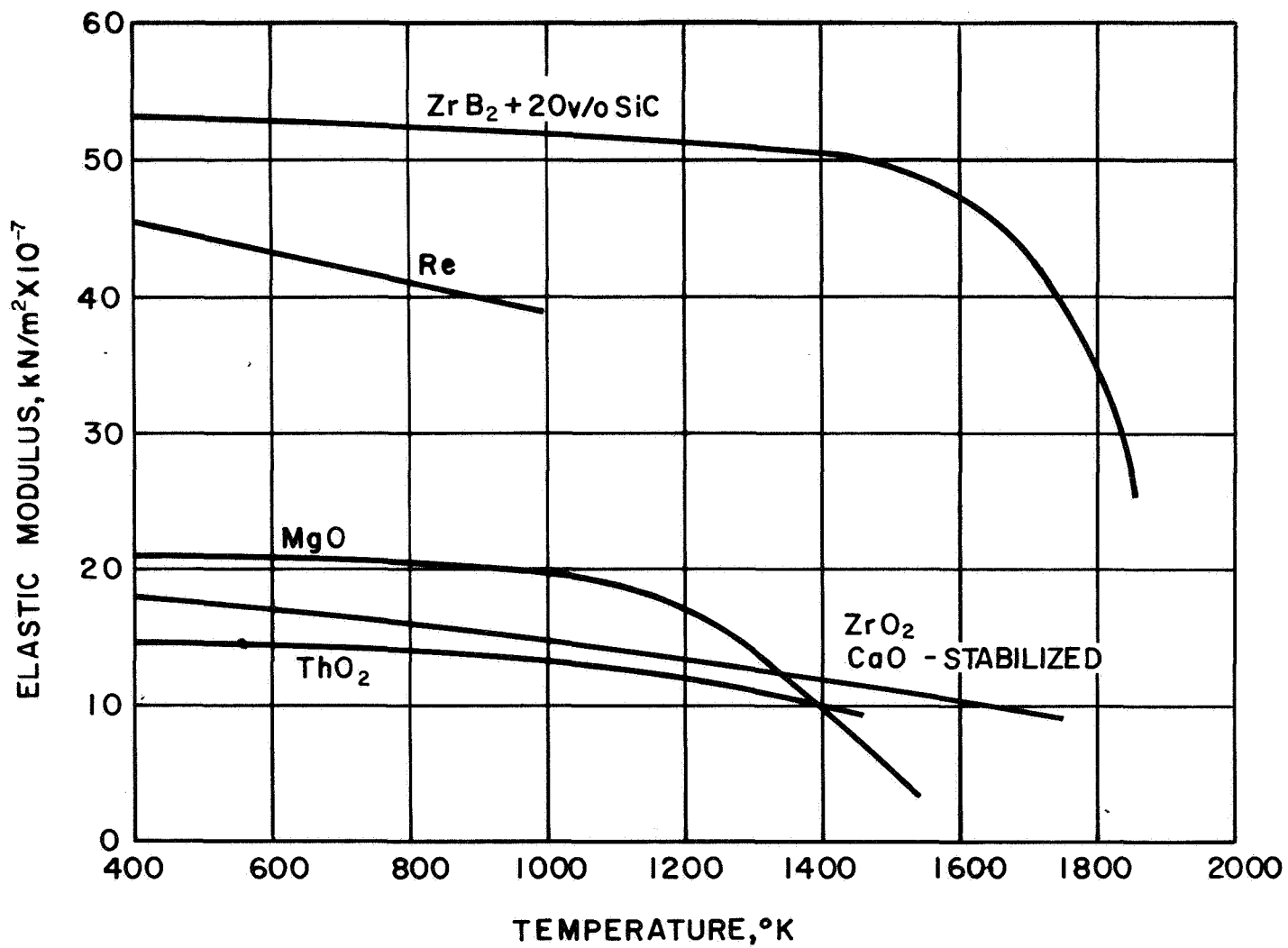


Figure 5.- Elastic modulus versus temperature for ZrB₂ + 20 v/o SiC, MgO, ThO₂ and ZrO₂, CaO stabilized.

comparatively in terms of needed characteristics for resistojets in the subsequent sections.

Zirconia. - The forms of zirconia and their relationship to desired properties are discussed in terms of a recently (1970) proposed phase diagram for the ZrO_2 system (ref. 28) shown in fig. 6. Solid lines indicate phase boundaries of stable phases and dashed lines metastable extensions of phase fields. The symbols \rightleftharpoons denote enantiotropic inversions and \rightarrow monotropic inversions. The reversible monoclinic to tetragonal transformation at atmospheric pressure occurs at about 1425°K. The monoclinic to tetragonal inversion is accompanied by a 3.2% length reduction on heating and an associated length increase (at about 1275°K) on cooling (ref. 29). Rapid cooling expansion occurs within a 10°K temperature interval to completely fragment the formed article. No usable shape can, therefore, be made of pure zirconia.

To be fabricated, zirconia must be stabilized in either the monoclinic or cubic form by adding oxides with cations of similar radius to Zr^{4+} . No one has been known to be successful in stabilizing zirconia in the monoclinic phase. A number of oxides of cubic symmetry have been added to successfully stabilize it in that phase. By such admixtures, ZrO_2 converts irreversibly to the cubic form when heated beyond 1825°K. Many oxides have been used for stabilization, but the most commonly used are CaO, Y_2O_3 , and MgO. MgO-stabilized zirconia partially reverts to the monoclinic form when cycled through the 1175-1625°K temperature zone (ref. 29). The following discussion is, therefore, limited to the CaO and Y_2O_3 stabilized forms. Zirconia is fully stabilized by the addition of 5 weight percent (10.4 mole percent) CaO or 15 weight percent (8.8 mole percent) Y_2O_3 . Smaller amounts of Y_2O_3 (~6.5 mole percent) are used for fine particle size zirconia powders (ref. 18).

Purity has an important effect on some of the thermophysical properties of zirconia. There are a large number of impurities that can be found accompanying zirconia in its natural state or unintentionally added in processing in addition to those deliberately added for stabilizing crystalline structure, enhancing electrical conductivity, etc. For instance, comparing two important stabilizers Y_2O_3 and CaO, say on the basis of cases of full stabilization, zirconia stabilized with the former is more refractory than the latter, having a melting point approximately 100°K higher. On impurities, Al_2O_3 has a strong influence on electrical conductivity acting as a poison in percentages around 2%, an undesirable additive as far as resistojets are concerned. The effects of impurities and additives on properties are discussed when known, where applicable in the sections that follow as are the influences of grain size and porosity.

Physical properties of the various forms of stabilized zirconia are presented as a function of temperature for comparison purposes. Figure 7 shows the linear thermal expansion of fully and partially calcia-stabilized zirconia (ref. 29) and of fully yttria-stabilized "Zyttrite" zirconia. The heating cycle only is shown. There is some hysteresis on cooling. The loop for the partially stabilized zirconia indicates the nonlinearity of expansion through the transition range.

The elastic modulus of ZrO_2 with various degrees of high stabilization with Y_2O_3 and CaO as a function of temperature to 1200°K is shown in fig. 8 (ref. 30). The curves indicate that a decrease in the amount of stabilizer and/or a decrease in density. Figure 9 shows for dense zirconia, stabilized with CaO and Y_2O_3

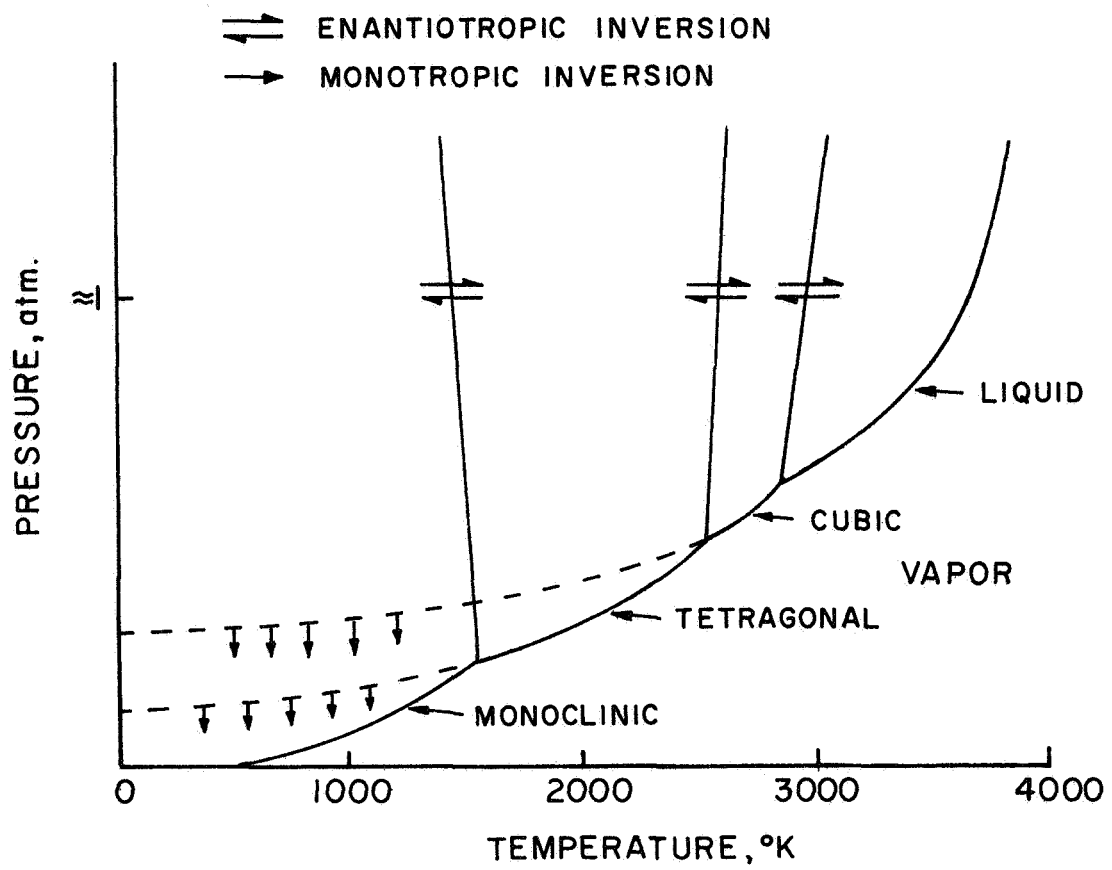


Figure 6.- Proposed phase diagram for ZrO_2 system.

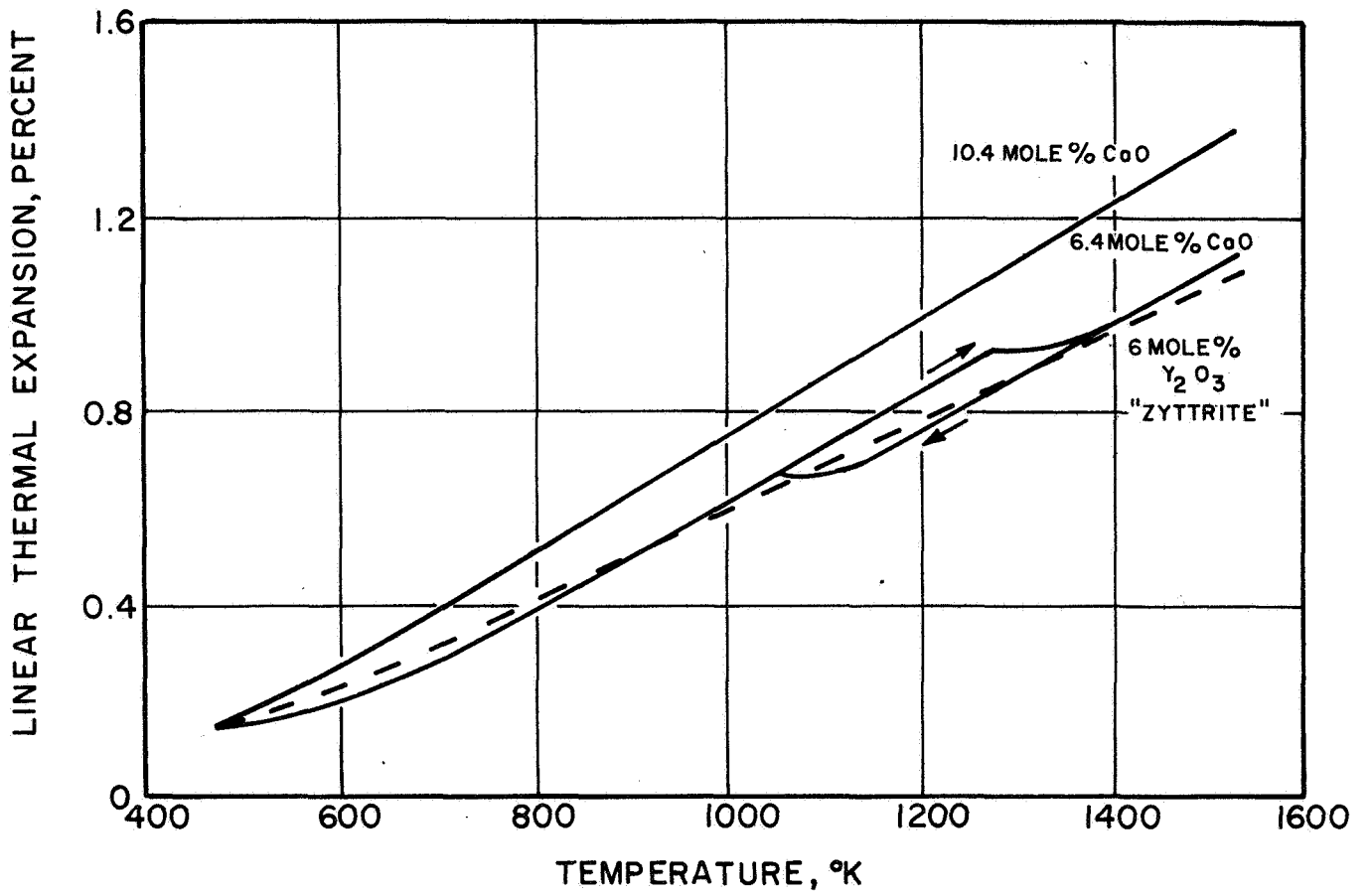


Figure 7.- Linear thermal expansion of three forms of stabilized zirconia.

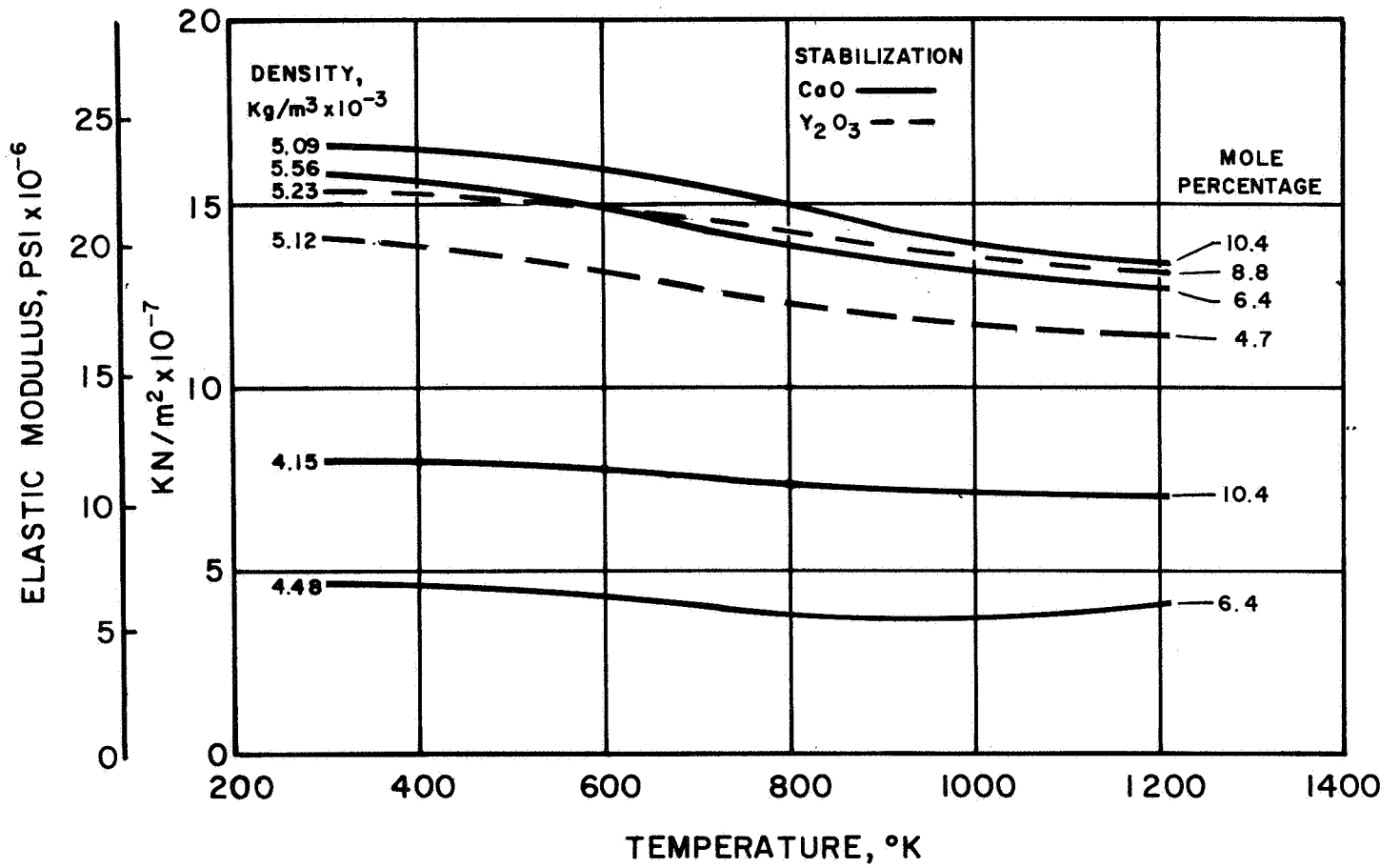
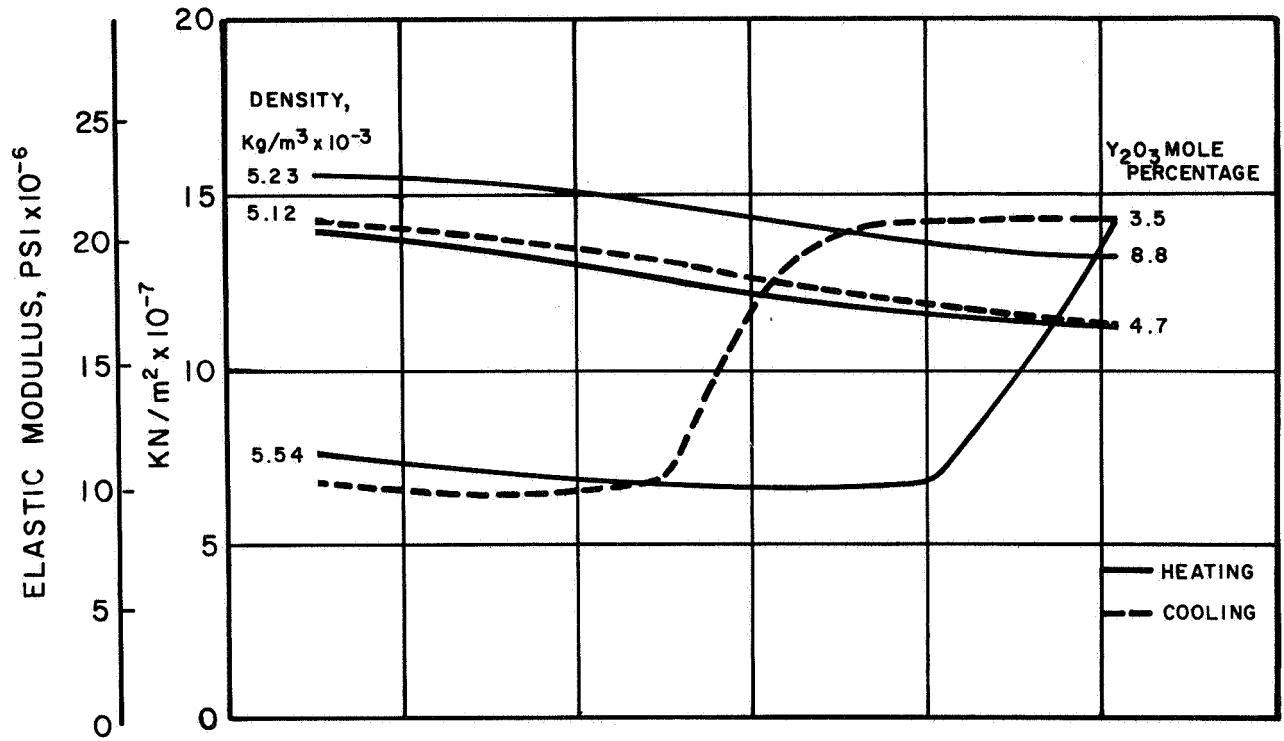
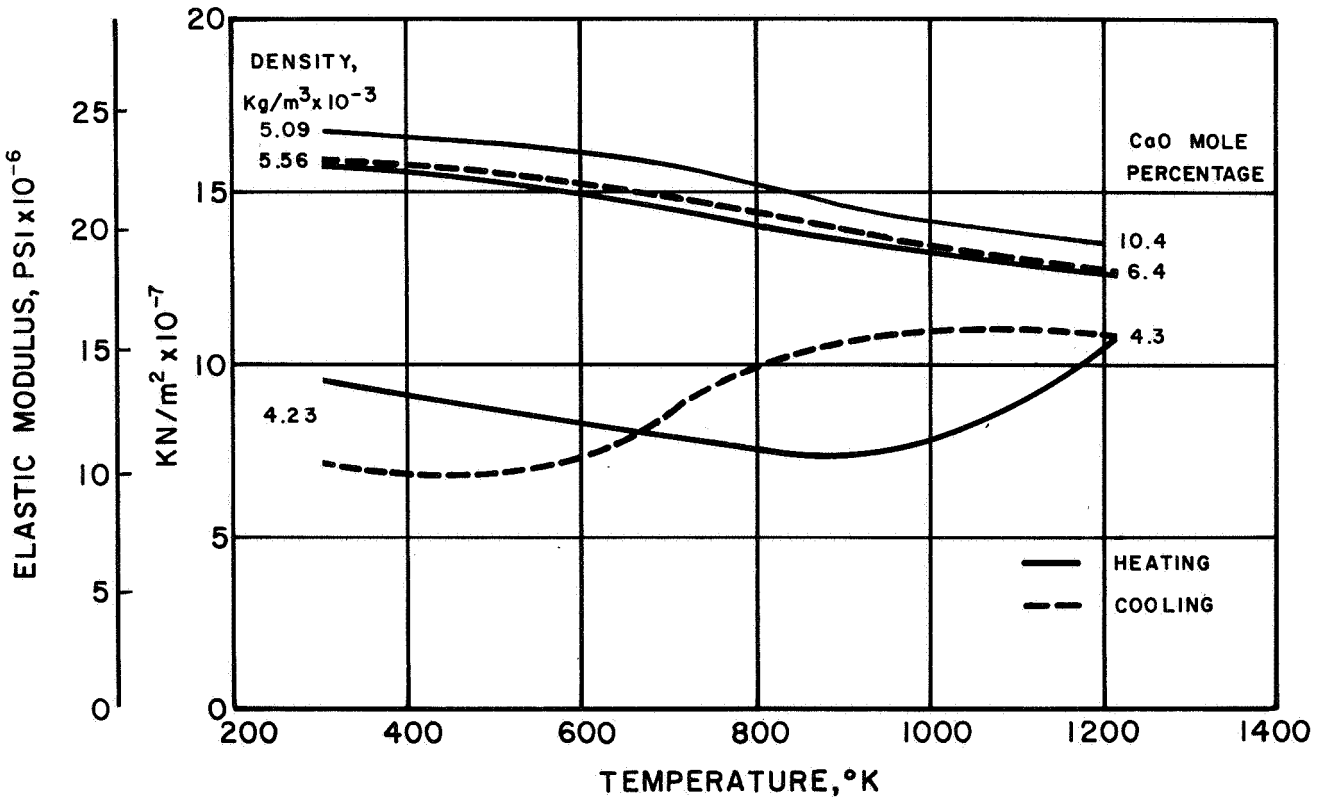


Figure 8.- Comparison of modulus of elasticity of ZrO₂ stabilized with Y₂O₃ and CaO to various degrees and for several densities.



(a) Y_2O_3 stabilized



(b) CaO stabilized

Figure 9.- Modulus of elasticity for cycled ZrO_2 with degrees of stabilization.

respectively, the influence of degree of stabilization as a function of temperature. The lowest degree of stabilization forms a hysteresis-type curve corresponding to the polymorphic transformation that occurs around 900°K. The elastic modulus for fully yttria-stabilized ZrO₂ is less than that for fully calcia-stabilized.

The tensile strength of fully calcia-stabilized zirconia at room temperature is 14,000 kN/m² (20,000 psi) and at 1575°K, 70,000 kN/m² (10,000 psi). The compressive strength at room temperature is 2,090,000 kN/m² (303,000 psi) and 690,000 kN/m² (100,000 psi) (ref. 31). These short-term values are relevant to thermal stressing conditions discussed later under Thermal Shock Resistance. These values are presented merely as representative and vary with additives.

In the life-testing of metal resistojet tubes it is found that endurance stress and creep are perhaps the most important mechanical properties. Organized information on creep has only been found for yttria and scandia-stabilized forms of zirconia. This is comparatively discussed in the section entitled "Creep."

The electrical conductivity of zirconia stabilized with 10 mole % Y₂O₃ versus temperature as measured by several authors in the range 900-2400°K is shown in fig. 10 (refs. 32, 33, and 34). Figure 11 shows a lower temperature range, 400-1100°K, for a material with 4.5 mole % Y₂O₃. (ref. 35). Although yttria-stabilized zirconia has a high temperature electrical conductivity significantly greater than that of most ceramic materials, it is still too low at room temperature to permit its use as a resistance heater without auxiliary starting. It can self-sustain joule heating above ~1100°K practically speaking.

High thermal shock resistance is another important requirement. This is comparatively discussed under the section entitled "Thermal Stress Resistance."

Thermal shock resistance of CaO-zirconia is improved by adding only 2.9 weight percent CaO as compared to fully stabilized at 5 percent. A similar situation exists for the Y₂O₃-stabilized form. These partially stabilized forms are physical mixtures of monoclinic and cubic zirconia. In the case of CaO addition, heating of the compacted blend should homogenize the CaO since a monoclinic-cubic sandwich shows CaO migration from the cubic to the monoclinic sections. Specimens of partially stabilized CaO-zirconia heated for extended periods at 2275°K still show monoclinic content (ref. 29).

A remarkable jump in thermal rupture resistance over a homogeneous partially stabilized zirconia can be obtained by a coarse matrix of zirconia filled with a zirconia grain of a different phase (ref. 29). The effect is a low elastic modulus material filling the voids of a high elastic modulus matrix. While the homogeneous partially stabilized form survived a 33°K/s temperature gradient, the heterogeneous mixture survived one of 200°K/s. It should be remarked, however, that strength decreases with cycling so that such a composition is limited to few cycles through the 1175-1625°K. The later fact disqualifies such schemes for resistojet service.

Heat exchanger tube assemblies of yttria-stabilized zirconia, in the form of hexagonally-shaped, cored bricks, have been tested for hypersonic wind tunnels at Aeronautical Research Laboratories, Wright-Patterson Air Force Base, Ohio. The zirconia material used resulted in a regenerative ceramic storage heater that

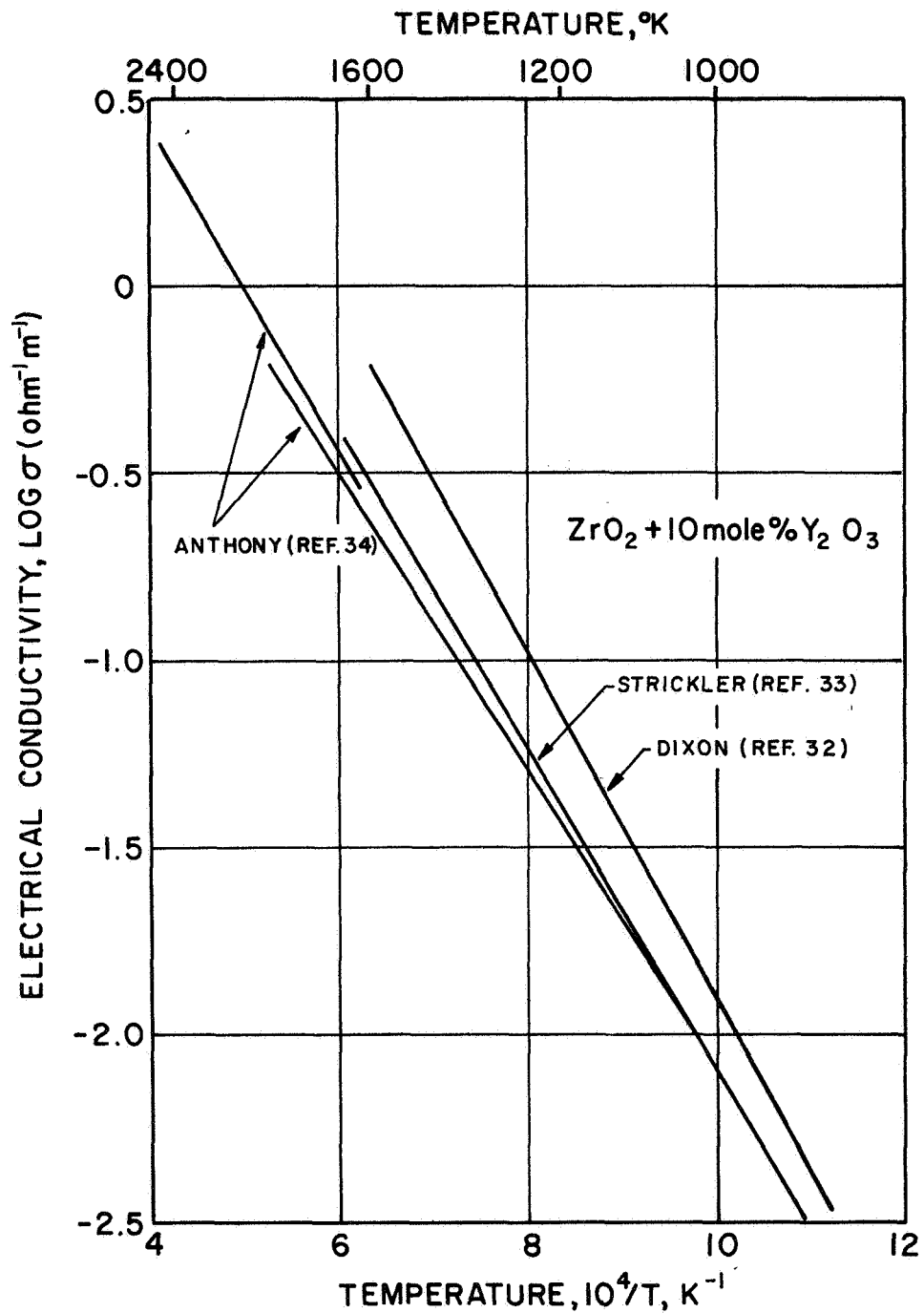


Figure 10.- Electrical conductivity of ZrO₂ with 10 mole % Y₂O₃ (as measured by several authors).

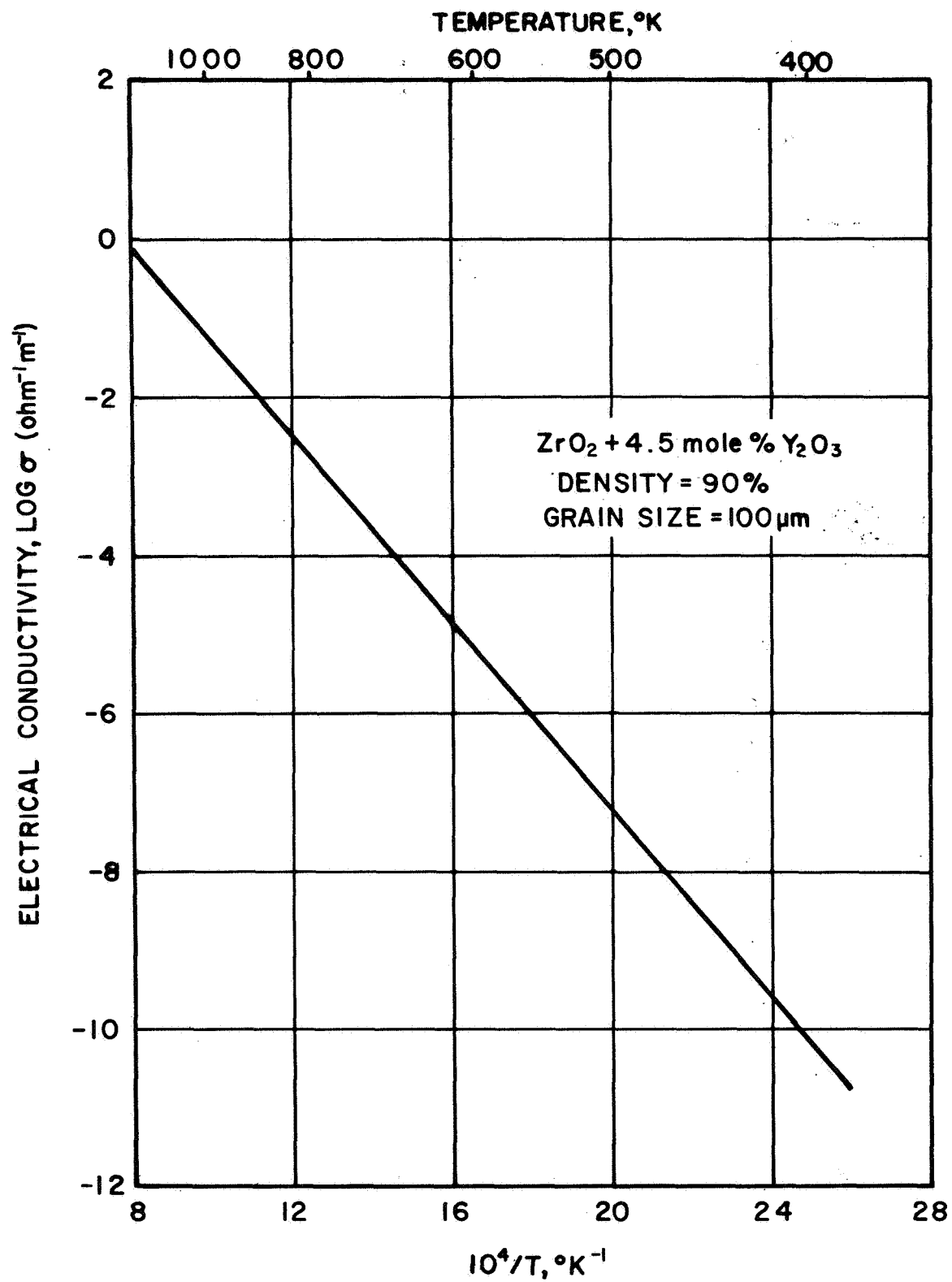


Figure 11.- Electrical conductivity of ZrO₂ with 4.5 mole % Y₂O₃.

survived air temperatures of 2600°K at very high air mass flow rates after 240 hours (ref. 36). This material was prepared by isostatic pressing.

Another form of yttria-stabilized zirconia of interest has been developed at the Air Force Materials Laboratory (ref. 18). Extremely fine particle size zirconia powders, average size 50Å, are produced by simultaneous thermal and hydrolytic decomposition of zirconium and yttrium alcoholates such as those of isopropyl alcohol. The vapor decomposition of the alkoxides to oxides produces purity in excess of 99.95%; hitherto not available from commercial sources. This high purity apparently has a definite bearing on the properties of the material. For example, while coarse grain grades of commercial zirconia have higher thermal shock resistance than fine grain grades, the finer grade has improved "Yttrite" thermal properties (ref. 38).

Cold pressing followed by sintering at 1725°K of this powder produced translucent, fully dense cylindrical and bar-shaped bodies with grain size 35-50 μ (ref. 18) and it is possible that yttria acts as a grain growth inhibitor in this case. It was possible to achieve full stabilization at a sintering temperature as low as 1075°K and with an yttria content of only 5 weight percent. Hot pressing might reduce forming temperature further.

A bar of this form of zirconia showed no change in an air atmosphere up to 2475°K for 262 hours with numerous cyclings. The material could be useful to 2775°K; the major limitation being loss of the stabilizer Y₂O₃ at the higher temperatures.

An example of the high purity is the hafnium content which is 0.5-2% in commercial grade and less than 0.05% in alkoxide-produced zirconia. Hafnia undergoes a monoclinic to tetragonal inversion at about 2000°K. This form of yttria-stabilized zirconia should be tested and compared with the commercial grades described above with respect to resistojet service. It was beyond the limited scope of the current program.

Coarse grain tubes are generally not impervious to gases and gas leakage cannot be tolerated in the operation of a resistojet. Impervious tubes of yttria-stabilized zirconia, which have a fine grain size, are available commercially and were used in the experimental phase. A tradeoff ultimately will have to be made on the advantages and disadvantages of coarse grain versus fine grain tubes and optimum grain size will have to be determined.

In brief regarding thermochemical and thermophysical properties of zirconia, its usefulness in air is stated to be up to 2675°K, in vacuum to 2475°K, and in a reducing atmosphere to 2410-2475°K. It becomes volatile in He above 2575°K, is stable in H₂ to 2475°K and reacts with N₂ at high temperature (ref. 7). The chemistry problem is treated in more detail on comparison basis with other candidates in the section "Compatibility with propellant species."

Thoria. - Thoria, ThO₂, has the highest melting point of any oxide and is for that reason alone of considerable interest for high temperature applications. Its melting point is listed in the range 3200-3600°K by various sources, the most probable figure is 3540°K according to ref. 39. It is very inert in its chemical properties.

Thoria is stable under most conditions. It requires no stabilizers.

The thermal expansion coefficient is close to that of Pt, making good compatibility with needed hermetic and electrode joints in resistojet design.

The modulus of elasticity of thoria is $14.6 \times 10^7 \text{ kN/m}^2$ (21.3×10^6 psi) at room temperature. Its compressive strength at room temperature is $1,520,000 \text{ kN/m}^2$ (220,000 psi) and it drops to $352,000 \text{ kN/m}^2$ (51,000 psi) at 1275°K and $10,340 \text{ kN/m}^2$ (1500 psi) at 1775°K . The room temperature tensile strength is $96,500 \text{ kN/m}^2$ (14,000 psi). The important creep characteristics are summarized in later sections.

Thoria is an electrical conductor and can be directly joule heated. This principle was used by the National Bureau of Standards as a high temperature furnace (ref. 40) operable in air to 2325°K . The electrical resistivity of pure ThO_2 as function of temperature is compared with the other candidates in fig. 4. The electrical resistivity of thoria is about 1 ohm-m at 1600°K (ref. 39) but 10^5 ohm-m at 775°K . Therefore, like zirconia, it must be started by auxiliary heating. Doping with CeO_2 , Y_2O_3 or La_2O_3 for various purposes was reported with starting temperatures of 1475°K for the first and latter two from 1175 to 1275°K .

The fabrication of thoria employs the same general techniques as zirconia.

On the behavior of thoria towards gases, it is useful to 2975°K in an oxidizing atmosphere and is rated as good in high temperature reducing atmospheres. It is reduced by carbon at high temperature, no temperature given (ref. 41). It is stable to high temperature in a vacuum. The compatibility with biowaste gases is discussed in detail later.

Thoria has a relatively high permeability to oxygen above 1300°K (ref. 42). The coefficient of diffusion, D , at 1375°K was measured to be of the order of $10^{-9} \text{ m}^2/\text{s}$ as compared to about $10^{-11} \text{ m}^2/\text{s}$ for alumina at 1975°K ; alumina being the least permeable to oxygen of any oxide so far found.

The radioactivity of thoria is of little concern for the quantities and exposures involved in a resistojet program. The toxicology of thorium has been summarized in an Atomic Energy Commission sponsored study (ref. 43). Thorium is unusual in that the radiological health hazards encountered in industry are not caused by Th^{232} , which is the long-lived parent isotope of the naturally occurring radioactive decay series and constitutes virtually the entire mass of natural thorium. Rather, the hazards arise from isotopes of a variety of elements that are present in the decay chain of Th^{232} , some of which are Ra^{228} , Ac^{228} , Po^{216} , etc. Hazards are due to the ionizing radiation released by the various members of the Th^{232} decay chain, causing a delay in cell division. Chronic radiation injury involved is cancer of the lung and bone. The hazard is there, however, only at doses so high as to be unimportant in the context of thorium (or thoria) exposures in industry. Industrial hygiene regulations have been established. The maximum permissible air concentration of Th^{232} is $10^{-11} \mu\text{C}/\text{cm}^3$ with respect to the lung and $2 \times 10^{-12} \mu\text{C}/\text{cm}^3$ with respect to the bone. Similar concentrations are established as maximum permissible for members of the Th^{232} decay chain.

The reaction of thoria with metals and its wetting by metals is of interest when considering metallizing and brazing of thoria (and yttria-stabilized zirconia) in combination with Cr, Mo, W, Mn, and Re was investigated by Manning and Stoops

(ref. 44). Thermodynamic calculations were made to predict stability up to 2500°K in vacuum and to 2750°K in helium. The Mo-40 wt. % Re alloy, Re, and W were stable in contact with the oxides to 2450°K, while the other metals were not. The thermodynamics of the reactions between Ag, Cu, Ni, Mo, and Nb with thoria (and zirconia) were also evaluated (ref. 45). In a study of high temperatures cermets, the wetting between thoria (and zirconia) and molten Cr, V, Pt, Rh, Mo, and Mo-Re alloy was measured at temperatures up to 2800°K in helium (ref. 46). Little wetting occurred between these metals and the oxides.

Zirconium Diboride. - In the earlier work to develop the diborides for use as high temperature oxidation resistant materials (ref. 11), it was found that fabrication of crack-free solid bodies of pure zirconium diboride (ZrB_2) was extremely difficult and fully dense bodies had rather extensive grain growth. Various combinations of silicon carbide and graphite additives were used to alleviate the cracking problems. The most important combinations were found to be $ZrB_2 + 14$ v/o SiC + 30 v/o C, and $ZrB_2 + 20$ v/o SiC.

It is stated that ceramic bodies of the SiC and/or C modified diborides have the strength, thermal stress resistance and oxidation and corrosion resistance for use as nose cones, leading edges, and as hardware in gas turbine and rocket motors. Rectangular and cylindrical shapes of these diborides are available commercially.

The principal fabrication technique for these diborides was conventional hot pressing, which could produce cylindrical and bar or prism-shaped billets of theoretical density and dimensions to several inches. Hot pressing of tubes of 4-6 inches O.D. by 3-5 inches I.D. by 4-6 inches high appeared feasible. The amount of SiC addition varied from 5-30 volume percent and of C from 10-50 volume percent.

Hot pressing temperatures varied from 1975-2575°K pressures from 17,200-55,200 kN/m². (2500-8000 psi) and time at temperature from 40-440 min., depending upon material, additions, and geometry of mold. Induction heating was used with graphite dies lined with pyrolytic graphite and boron nitride. Hot pressing apparently took place in air since a relatively large amount of CO₂ evolved from the graphite dies to ensure a neutral atmosphere.

It should be remarked that high pressure hot pressing of HfB₂ to 100% density with no addition of SiC and/or C has been done at somewhat lower temperatures (2120-2175°K), but required pressures of 790,000 kN/m² (115,000 psi) (refs. 47 and 48).

Microstructure of HfB₂ and ZrB₂ with SiC and/or C additions (refs. 11 and 12): Limitations imposed by present powder production technology for hot pressing purposes result in the presence of 0.5-1.5% nonmetallic impurities in the starting powder, principally oxygen and carbon. There is some Zr in HfB₂ and some Hf in ZrB₂. Other metallic impurities are all below 0.1%.

The addition of SiC and/or C enhances hot pressing characteristics such as lowering the needed hot pressing temperature for the achievement of full densification controls the grain growth, and improves the physical integrity of the material (incidence of cracking virtually eliminated).

Grain sizes varying from 2-10 μ in as-pressed material, densities at or close to 100%, and porosities less than 1% are achieved.

The chief effect of the addition of SiC was an improvement in oxidation resistance; that of C a decrease in the bulk elastic modulus, with an accompanying increase in thermal stress resistance.

Young's modulus as a function of temperature to 1875°K is presented in fig. 5 for 100% dense ZrB₂ containing 20% SiC. Residual porosity or the addition of carbon markedly reduce the modulus values. Young's modulus decreases slightly from room temperature to 1675°K. Increased plasticity encountered above 1675°K rendered accurate measurement of Young's modulus difficult.

Transverse bend strength of the diboride compositions varied from 310,000 - 620,000 kN/m² (45,000-90,000 psi) at temperatures to 1075°K and from 138,000 - 276,000 kN/m² (20,000-40,000 psi) to 2175°K. Below 1675°K all compositions and microstructures displayed brittle fracture. At 1675°K and higher varying degrees of plasticity were observed. Macroscopic deformation was observed above 1975°K for a dense 4 μ grain size ZrB₂ containing SiC and C.

Limited stress rupture testing at 1315°K in air indicated a 100-hour stress rupture strength of 100,000 kN/m² (15,000 psi) for a dense ZrB₂ composition containing SiC. Again, no information is available for the low stress levels, endurance stress and creep, required for resistojet design; i.e., 100 kN/m² (15 psi).

The presence of carbon in amounts of 10-30 volume percent produced strength anisotropy. Materials cut perpendicular to the hot pressing direction had bend strengths greater than those cut parallel to it. Also, the presence of carbon as agglomerates or perhaps discrete particles could effect a crack arrestment phenomenon at elevated temperatures.

The electrical resistivity of ZrB₂ with SiC and/or C additions is low even at room temperature. Its dependence on temperature was measured only to 1275°K for 100% dense ZrB₂ + 20% SiC. The room temperature value 1.02×10^{-7} ohm-m and at 1275°K 5.45×10^{-7} ohm-m. The temperature coefficient is positive. These materials can be used as electrical conductors both at room and high temperatures. The characteristic is typical of metal conductors (fig. 4).

Hot pressed diboride compositions with additives of SiC and/or C were evaluated in low pressure cold air/hot sample, isothermal furnace tests for times of several hundred hours at 1575°K to 90 min. at 2475°K (ref. 12). As an example, the time dependence for the oxidation process was found to be logarithmic for the composition ZrB₂ + 20% SiC for times up to 236 hours at 1575°K. Protective oxide formation persisted to 2375°K for all ZrB₂ compositions. The addition of SiC and/or C improved the adherence of the oxide to the diboride and prevented oxide spalling after a considerable number of thermal cyclings.

High and low pressure hot gas/cold sample tests were conducted with oxidizing and corrosive gases (air, O₂, CH₄, NO) at one to four atmospheres and arc plasma at 0.01 to 1.0 atmospheres, as well as at high stagnation pressures. Stability was reduced at high stagnation pressures if sufficient gas dynamic shear forces developed to remove the protective oxides and expose unprotected diboride material.

Ranking of Materials

Resistojet experience has shown that the long duration effects govern the design. The endurance type criteria in the main are used here then as a basis for ranking the candidate materials. The scope of the study did not permit an exhaustive investigation of all of the effects but only those judged as most important in the opinion of the authors. Those effects not surveyed are noted.

The effects compared against resistojets design needs are:

- (1) Chemical compatibility with propellant species
- (2) Sublimation.
- (3) Creep
- (4) Endurance stress
- (5) Thermal stress resistance

Effects which may be important but not treated are:

- (1) Thermal cycling endurance
- (2) Grain growth
- (3) Electrical property stability

Compatibility with propellant species. - A number of physical-chemical interactions between biowaste gases and the ceramic resistojets tube materials ZrO_2 , ThO_2 and modified ZrB_2 must be taken into account for resistojets design above $\sim 2000^\circ K$. The most important is high temperature chemical reaction and corrosion. An example is the formation of ZrN in the reaction between zirconia and nitrogen at temperatures much greater than $2000^\circ K$; the exact value of which has not been reported. Another effect to consider is the diffusion and permeation of gases into the oxide ceramic. For example, ZrO_2 acts as a solid-state electrolyte for the diffusion of oxygen at temperatures as low as $650^\circ K$. The oxide may also act as a catalyst for reactions between the gas species. Thoria is notable in this respect; catalyzing the oxidation of CO.

Any reaction between a hot gas and resistojets material is, of course, detrimental to the operation of the resistojets. Any gaseous reaction products would result in mass change of the material, resulting in ultimate consumption of the material or that portion of it subject to reaction with time, to the point that the operating characteristics would change. Solid reaction products in the form of particles could be swept away by the flow of gases and similarly result in mass losses.

The mass losses are a function of reaction rate kinetics and perhaps whether scales are formed through which gaseous reaction products have to penetrate. The reaction rate kinetics between the ceramics and gas species in question are not known generally and design criteria involving factors such as wall thickness requirements depend on the completion of an endurance type experimental program.

The stability of scales depends on their adherence to the tube wall. It is likely, however, that even scales would be eroded away by the high-velocity flowing gases, exposing the wall to new attack.

It is well to bear in mind that reaction and corrosive attack of the tube wall is a strong function of temperature and, therefore, any mass loss, scale formation, etc., will vary locally along the tube. Increased partial pressure of the gas will also tend to increase reaction rate. Flow velocity is another parameter to consider. Increased axial flow velocity of the gas does not necessarily mean increased mass flow of gas to the surface. In fact, increased gas flow means less residence time and possibly less likelihood for reaction. The erosive effect of the gas increases, however, with increased axial flow velocity. Design criteria, must therefore, be based on the situation at the critical (generally the hottest) section of the tube where the attack is most severe.

Fortunately, for many of the biowaste gas species and temperature levels as described in Table IV reproduced from the studies of reference 49, the reaction/corrosion between the gases and candidate oxide ceramics is not found to be significant so far.

The data contained in Table V, based upon a literature search, should indicate safe temperature ranges (where available) of physical and chemical processes that may effect preliminary design and guide long-term experimental verification testing.

Table V gives an overall review of the chemical interactions between gas species and solid carbon and the ceramics ZrO_2 , ThO_2 , and ZrB_2 . Diffusion/permeation, catalytic action, erosion, and adsorption/desorption are not included in the table.

ZrO_2 compatibility with biowaste gases: The resistance of ZrO_2 to high temperature steam has been studied in Russia by Bunikov (ref. 50). Water absorption and porosity were stated to have increased while specific gravity and structural flexure strength decreased with length and severity of exposure, resulting in the formation of hydroxides and in decreased stability. Unfortunately, the details were lacking and no temperature references were given in the available abstract.

Experimental results reported herein on H_2O exposure run at a material temperature of $1895^\circ K$, for 49 hours showed only partially stabilized zirconia by x-ray diffraction analysis. No H_2O related failure was involved in this test.

No known references were found on the interaction of CO_2 and ZrO_2 and the tests reported herein, for 44 hours at $1910^\circ K$, showed no apparent reaction. If any reactions are to occur, much longer times and higher temperatures are required. It is unlikely that CO_2 will react chemically below $2200^\circ K$.

The stability of zirconia in hydrogen was studied by Trostel up to temperatures between $2760^\circ K$ and $3030^\circ K$ (ref. 51) and by May, et al., at temperatures between $2475^\circ K$ and $2760^\circ K$ (ref. 52). The ZrO_2 in reference 53 contained SiO_2 and TiO_2 as impurities besides CaO as a stabilizer. SiO_2 and TiO_2 were reduced to suboxides and metals and were lost by volatilization below $1775^\circ K$. The CaO is quite difficult to reduce and will not volatilize below $2275^\circ K$ in dry hydrogen.

TABLE IV. - CHEMICAL SPECIES PRESENT IN TYPICAL BIOWASTE PROPELLANTS IN MOLE FRACTIONS

Propellant		Initial Composition ^a						
Case	Rationale	Temp. °K	CO ₂	H ₂ O	N ₂	O ₂	CH ₄	
CO ₂	Molecular sieve waste output	2000	9.84·10 ⁻¹	.	1.2·10 ⁻²	4·10 ⁻³	.	
CH ₄	Sabatier waste output	1000	5.4·10 ⁻²	1.5·10 ⁻²	1.4·10 ⁻²	.	9.17·10 ⁻¹	
H ₂ O	Water recovery	2000	1	
CO ₂ & CH ₄	Stoichiometric mixture	1000	4.88·10 ⁻¹	8·10 ⁻³	1.2·10 ⁻²	4·10 ⁻³	4.88·10 ⁻¹	
H ₂ O & CH ₄	Stoichiometric mixture	1000	2.8·10 ⁻²	4.85·10 ⁻¹	7·10 ⁻³	.	4.85·10 ⁻¹	

NOTES

- a Neglects trace contaminants
 - b Two chemical kinetic models used are Finite Chemical Kinetics (FCX) and Equilibrium
 - c Program excludes solid carbon existence
 - d Solution not available
 - e CH₃ was less than 10⁻⁵ in all cases
- Mole fracture < 10⁻⁵ denoted by .

		Final Composition ^b										Species ^e		
Case	Solution	CO ₂	CO	O	O ₂	N ₂	NO	CH ₄	H ₂ O	OH	H	H ₂	C _{so1}	NH ₃
CO ₂	FCX Equil.	9.9·10 ⁻¹	2.9·10 ⁻⁴	2.0·10 ⁻⁴	4.1·10 ⁻³	1.2·10 ⁻²	2.0·10 ⁻⁷
		9.54·10 ⁻¹	8.5·10 ⁻³	3.7·10 ⁻⁵	7.6·10 ⁻³	1.2·10 ⁻²	1.8·10 ⁻²
CH ₄	FCX Equil.	5.4·10 ⁻²	.	.	.	1.4·10 ⁻²	.	9.17·10 ⁻¹	1.5·10 ⁻²	.	.	5.3·10 ⁻¹	(c)	.
		1.5·10 ⁻³	.	.	.	6.0·10 ⁻³	.	1.3·10 ⁻¹	2.1·10 ⁻²	.	.	2.5·10 ⁻³	2.8·10 ⁻¹	6.7·10 ⁻⁵
H ₂ O	FCX Equil.	.	.	.	1·10 ⁻³	.	.	.	9.97·10 ⁻¹	9.0·10 ⁻⁴	2.0·10 ⁻⁵	2.5·10 ⁻³	.	.
		.	.	1.8·10 ⁻⁵	1.7·10 ⁻³	.	.	.	9.92·10 ⁻¹	1.6·10 ⁻³	6.6·10 ⁻⁵	4.3·10 ⁻³	.	.
CO ₂ & CH ₄	FCX ^d Equil.	1·10 ⁻¹	.	.	.	6.6·10 ⁻³	.	4.7·10 ⁻²	1.2·10 ⁻¹	.	.	2.8·10 ⁻¹	(c)	.
		7·10 ⁻³	.	4.83·10 ⁻¹	4.83·10 ⁻¹	.	.	1.6·10 ⁻¹	1.6·10 ⁻¹	3.3·10 ⁻⁵
H ₂ O & CH ₄	FCX Equil.	2.8·10 ⁻²	.	.	.	3.9·10 ⁻³	.	1.1·10 ⁻¹	1.1·10 ⁻¹	.	.	5.4·10 ⁻¹	(c)	.
		5.4·10 ⁻²	1.6·10 ⁻¹	1.1·10 ⁻¹	.	.	5.4·10 ⁻¹	3.0·10 ⁻²	4.3·10 ⁻⁵

TABLE V. - CHEMICAL REACTIONS BETWEEN GASES AND ZrO_2 , ThO_2 AND ZrB_2 - LITERATURE SURVEY

Gas Species	Zirconium dioxide, ZrO_2 (Reference)	Thorium dioxide, ThO_2 (Reference)	Zirconium diboride, ZrB_2 (Reference)
H_2O	Data unclear. H_2O absorption. Increased porosity. Decreased flexure strength. Hydroxide formation. But no temperature reported (ref. 50).	No known references.	Corrosion above 1500°K. (ref. 62)
CO_2	No known references.	No known references.	Corrosion above 1500°K. Oxidation at high temperature. (ref. 62)
CH_4	No known references.	No known references.	No known references.
H_2	Reacts to a measurable extent at 2475°K. (ref. 52). Also see refs. 51 and 53	No known references.	Corrosion above 1500°K. (ref. 62)
NH_3	Reacts to form oxynitrides and then nitrides at higher temps. Temp. ranges studied: 1075-1575°K, 2275-3275°K (refs. 54,55 and 56)	No known references.	No known references.
N_2	Forms ZrN from N plasma jet of very high mass temp. (ref. 57)	No known references.	Corrosion above 1500°K. (ref. 62)
O_2	Surface exchange reaction only. (ref. 58)	Surface exchange reaction only. (ref. 58)	Oxidation resistance improved by addition of SiC and C to ZrB_2 . (refs. 63 and 16)
O	No known refs., but situation should be similar to O_2 .	No known references.	No known references but situation should be similar to O_2 .
OH	No known references.	No known references.	No known references.
H	No known references but situation should be similar to H_2 .	No known references.	No known references, but situation should be similar to H_2 .
C solid	Forms eutectics & carbides at high temperatures (ref. 59)	Forms eutectics & carbides at high temperatures (ref. 61)	Can be incorporated in the ZrB_2 lattice or as mechanical mixture. (ref. 63)

This ZrO_2 was, therefore, stable to this temperature. The reaction of ZrO_2 with H_2 was slight in the range 2760° to $3030^\circ K$.

Tests here at $1810^\circ K$ for 90 hours on pure H_2 showed only partially stabilized ZrO_2 . An unexplained darkening did occur. The reduction of ZrO_2 by H_2 is believed to be serious only at temperatures much higher than $2200^\circ K$. If an insignificant amount of reduction occurs below this temperature, the suboxide ZrO would first form at the surface, followed by possible reduction to metal.

The reaction between ZrO_2 and NH_3 was studied by Collouges, et al., at $1075-1575^\circ K$ and $2275-3275^\circ K$ (ref. 54) and by Gilles, et al., at the same temperature ranges (refs. 55 and 56). Reaction between ZrO_2 and NH_3 results in the formation of oxynitrides at the surface, of which two or three modifications occur. This is followed by reaction to the complete nitride, ZrN , at high temperature. Zirconium oxynitrides and ZrN were formed. Ammonia totally dissociates at higher temperature to H_2 and N_2 . The non-equilibrium effects though (short residence time in the reactor) can permit the brief presence of NH_3 at this temperature. Only trace amounts of NH_3 are found in biowaste gases. The purpose for study was primarily considering use with a separately-supplied supplementary propellant during lean biowaste availability periods.

Matsumoto studied the nitridation of ZrO_2 by a nitrogen plasma jet (ref. 57). The N_2 flow rate was 1.5-4.1 l/min. at a power input of 3-8 kW. ZrN was formed. The plasma jet was directed vertically on pelletized mixtures of ZrO_2 and graphite. The high mass flow rates here are different from the conditions of an N_2 stream along the ZrO_2 tube wall. The temperature of the ZrO_2 was not given.

Tests here on N_2 for 122 hours at $1805^\circ K$ showed no obvious reaction products only partially stabilized ZrO_2 .

Oxygen does not react with ZrO_2 . It does diffuse through ionically. Winters studied the exchange reaction between O_2 and ZrO_2 and ThO_2 (ref. 58). The exchange reactions occur by a dissociative atomic mechanism confined to the surface layer of O atoms. The slow stage is the desorption of oxygen. This exchange reaction is not expected to influence the integrity of the tube.

Diffusion and permeation data are only known in the case of oxygen for ZrO_2 and ThO_2 and in the case of N_2 and "combustion gases" for ZrB_2 . The diffusion rates are apparently low and of no consequence to the resistojet tube itself, since dissolution of the gases is not indicated. The only concern for design purposes would be the reaction of the gases with materials outside the resistojet tube. That could be a metal heater structure (indirect heater concept) and/or insulation. Metal could be attacked by O_2 in the long run even if diffusion was low if the materials and design temperatures (during operation) were not properly chosen. This consideration rules out use of a primary wire heater in the resistojet design.

No references were found on the reaction between ZrO_2 and CO_2 , CO , O , OH , and H , the products of high temperature dissociation. These effects are undoubtedly covered in high temperature tests on the primary gases, themselves, providing residence time is properly simulated to produce these species.

The reaction between solid carbon and zirconia takes place at high temperatures forming eutectics and carbides. The reaction between carbon and ZrO_2 occurs according to Elyutin, et al., (ref. 59) at temperatures above $2200^\circ K$ forming ZrC .

ThO₂ compatibility with biowaste gases: No references were found on the reaction between ThO₂ and the species listed in Table V, except the unimportant exchange reaction with O₂. It is not unreasonable to expect similar reaction characteristics as for ZrO₂. If any differences should exist, they would be expected to take place at even higher temperatures because of the more refractory character of ThO₂.

The catalytic action of ThO₂ (ref. 60) in the oxidation of CO to CO₂ may effect the specific impulse to a trivial extent and would be of little concern in resistojet design.

In the single test conducted with ThO₂ and CO₂ for 47 hours at 1790°K, some as yet unidentified reaction occurred, perhaps an anomaly. See Table XIV in the section entitled "Analysis of Data."

ThO₂ may form ThC₂ at a temperature as low as 1375°K but only when ThO₂ and C are in intimate contact as when mixed together as powders (ref. 61).

ZrB₂ compatibility with biowaste gases: References on reactions between the gas species and ZrB₂ are also meager. Peters has examined ZrB₂ as a rocket liner material subjected to propellant species at temperatures from 1500-4000°K (ref. 62). He finds that H₂O, CO₂, H₂ and N₂ corrode ZrB₂ above 1500°K. Clougherty, et al., (ref. 63) reports SiC and C improve oxidation resistance of ZrB₂ considerably.

Below ~1400°K, a protective B₂O₃ glass layer forms from oxidation of the ZrB₂ surface. At higher temperatures, a SiC modifier is needed because of the evaporation of the B₂O₃. Then a SiO₂ glass phase formed from the SiC modifier provides similar protection over an intermediate ZrO₂ layer. Short-term loss rate, measured over four hours at 1775°K in an atmosphere of 250 Torr O₂, were ~5 x 10⁻¹⁰m/s which is promising. This would suggest longer term tests on the biowaste gases.

No reference was found on possible reaction between NH₃ and ZrB₂. Carbon is not considered a serious reactant in the case of ZrB₂ since indeed carbon is used as a modifier to improve the properties of the material.

Tests of CO₂ and ZrB₂ were not possible within the scope of this test program. The primary reason was lack of joining technology to propellant feed tubes of the current facility or the immediate availability of a high current power supply of the order of 500 amperes to directly heat the tubes in an atmospheric pressure (CO₂ environment) where improvised fittings could be used. Such future tests are warranted if modified ZrB₂ is to be used in propulsion programs where CO₂, H₂O, O₂, N₂, the combustion gases are involved.

CH₄ pyrolysis: For the remaining biowaste gases reactions do occur. While no references were found on any direct reaction between CH₄ and the present oxides, it is known that decomposition of CH₄ by pyrolysis in platinum alloy resistojet may result in ultimate clogging of the tube by solid carbon (above 1080°K), a situation which might reasonably be expected to occur for ceramic resistojets (ref. 5). Reactions between this carbon and the oxide have been previously noted.

With respect to compatibility with propellant species, ZrO₂ is ranked as the most desirable tube material. From available data it appears reasonable to expect that stabilized ZrO₂ can be used as a resistojet material for extended periods at high temperature in flowing gases of CO₂, H₂, N₂, and O₂ even if these gases con-

tain small amounts of O, H, and OH but not NH₃ and CH₄. It is also possible that H₂O can be used as propellant provided the hydroxide formation as mentioned in reference 53 is insignificant below the design temperature. Extended experimental tests, with regard to chemistry interaction encompassing 10,000 hours, are required to establish precise temperature limits.

It is believed that ThO₂ will behave similarly to ZrO₂ to the above gas species and that, therefore, this material merits use under the same conditions. On the basis of sketchy information (ref. 62) ZrB₂ would appear to be uncertain as a material for all these gas species under the required service conditions and requires further experimental study for confirmation of this preliminary conclusion.

Sublimation. - Sublimation is the change in phase of a material directly from a solid to a gas, thus generally causing its surface to recess. This important process can be the controlling factor in determining the permissible life of a device operating at a given high temperature. The mass flux evaporation rate is the highest in a vacuum environment. It is greatly suppressed by adding a static inert gas. As is well known, this latter fact was utilized by Langmuir in the invention and development of the gas filled tungsten filament lamp. Motion of this gas cover increases the rate over that of the static case.

For design purposes, the useful form for comparing candidate materials is surface recession as a function of surface temperature: (a) in a vacuum and (b) in a non-reacting gas atmosphere over a range of pressures and velocities. Data under vacuum conditions is available for the candidate materials from several investigators. Little experimental data is available under inert atmospheres particularly under forced convective conditions.

In a vacuum: Sublimation data generally come about from high temperature thermodynamic data determinations, specifically vapor pressure. This technique measures directly the evaporation rate, G, from a heated wire or its equivalent the effusion rate from a Knudsen cell. The vapor pressure, P_v, is calculated from this rate from the kinetic theory of gases (ref. 64 or 65):

$$P_v = G \sqrt{2\pi RT/M} \quad (1)$$

Surface recession rates, $\dot{\delta}$, due to sublimation, are calculated here by use of the original measured evaporation rate data and the mass continuity equation:

$$\dot{\delta} = \frac{G}{\rho} \quad (2)$$

In the original vapor pressure determination work considerable effort was made to identify the species vaporizing. There is much discussion on this subject in the original literature this being essential to the proper choice of molecular weight in equation (1). Does thorium dioxide, for instance, evaporate undissociated or in part as ThO? If the measurements are not influenced by external materials effects like Knudsen cell materials for instance (such as tantalum as was the case of ref. 66), then the evaporation rates are correct for the purposes of this section. The only remaining question would be chemical stability if there is dissociation at temperature.

The evaporation rates of materials of interest, in a vacuum, are shown summarized on fig. 12. The metals, rhenium (not biowaste resistant), platinum and iridium are shown only for reference purposes from ref. 65 these materials having been used extensively in previous resistojets. Rhenium has been demonstrated in resistojets (ref. 4), using non-oxidizing propellants, both hydrogen and ammonia, to temperatures of 2200°K for over 8000 hours without sublimation being of consequence. With oxidizing or biowaste propellants, platinum alloys generally with iridium are currently being used up to temperature of 1550°K (ref. 5) and tested up to 250 hours to date.

The evaporation rate for zirconia, shown in fig. 12, is that recommended by Thermophysical Properties Research Center from their survey (ref. 39). This data corresponds closely to the work of ref. 67. There a double slit mass spectrometer was used in combination with the Knudsen effusion cell to detect the molecular species in the vapor. The presence of Zr or Ta (the cell material) metal reduced zirconia (ZrO_2) to ZrO beginning around 1975°K. The literature is not clear whether ZrO_2 by itself dissociates before vaporizing.

Thoria evaporation rate, G, shown in fig. 12 from ref. 39 is somewhat higher than that of zirconia. On a recession rate, δ , basis they are essentially the same (see fig. 13).

Zirconium diboride, (ref. 39) unmodified is somewhat lower in evaporation and recession rates than either ZrO_2 or ThO_2 . Zirconium diboride has been modified by additives to improve its oxidation resistance (ref. 63). Two compositions considered here are one containing 20 volume percent Si, and containing 30 and 14 volume percent of C and SiC respectively. The sublimation rate data of carbon alone is thus shown in fig. 12 and is less than ZrB_2 . Data for SiC was not found. No statement can be made then relative to the modified form since the integrity of the total system must be considered.

For the same given (design) recession rate, δ , the corresponding temperatures to produce these rates are within approximately 140°K for the candidates. This is not of major significance.

Graphite has been shown for reference as it was used as the test heater to indirectly heat the ceramic. Difficulties were experienced in its surface regression which later was determined to be oxidation due either to insufficient vacuum ($\sim 10^{-2}$ torr) or test gas diffusion.

The data of fig. 13 is useful in the design of high temperature dewars such as those used in some efficient resistojet designs (ref. 3). It must be borne in mind that this surface may not be the most critical one in a given design relative to sublimation as is described further.

Under conditions of a flowing gas: As expected in any heat exchanger the maximum wall temperature requirements occur in contact with the heated (expellant) gas. The influence of gas properties, velocity and pressure on evaporation rates of the specific designs must be determined. Reference 68 treats the subject with regard to metals but not the candidate materials, for vacuum and forced convection with helium at 1 atmosphere and 100 feet per second velocity conversion factors for other gases are given.

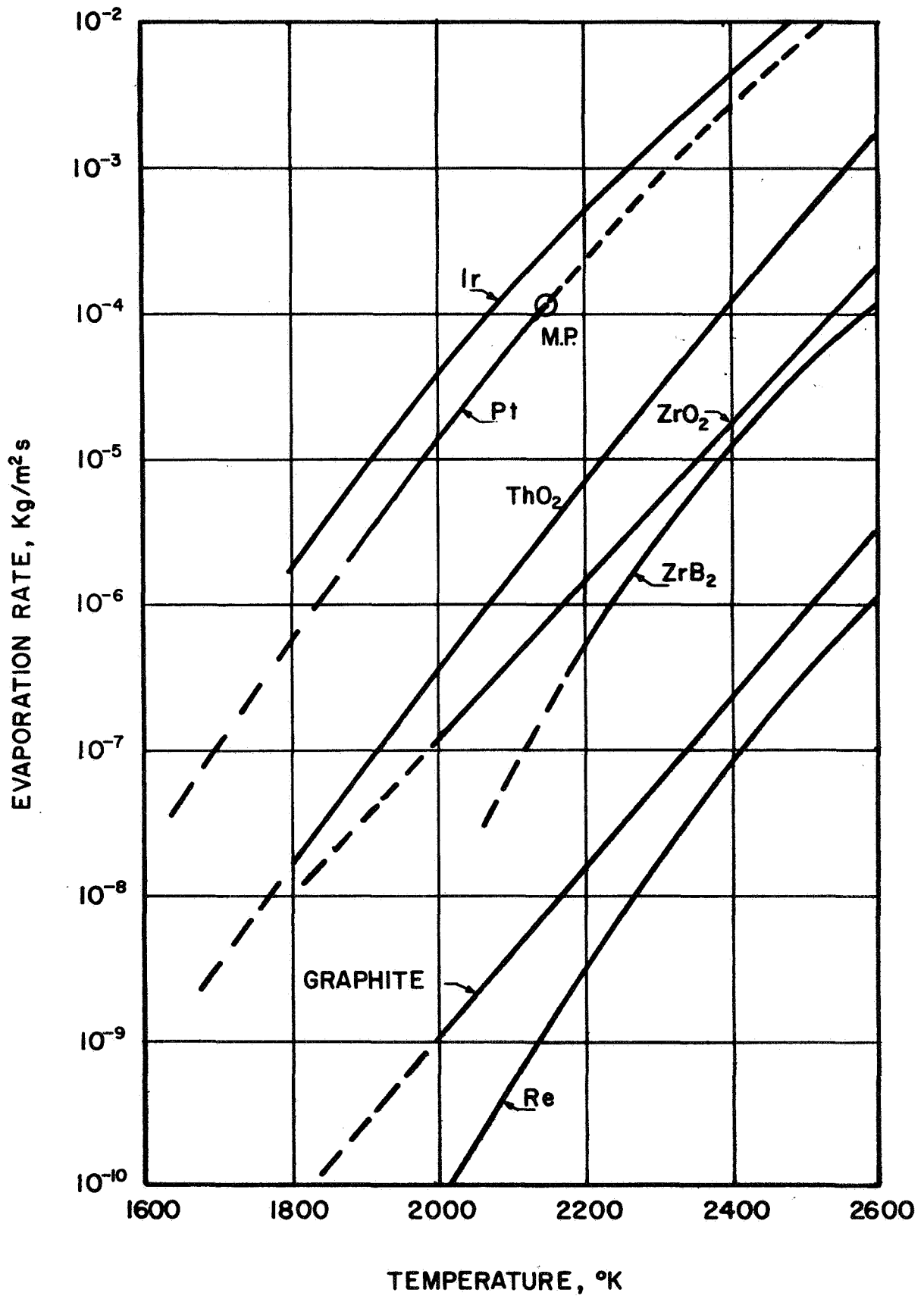


Figure 12.- Surface sublimation rates of biowaste resistant materials in a vacuum compared to rhenium.

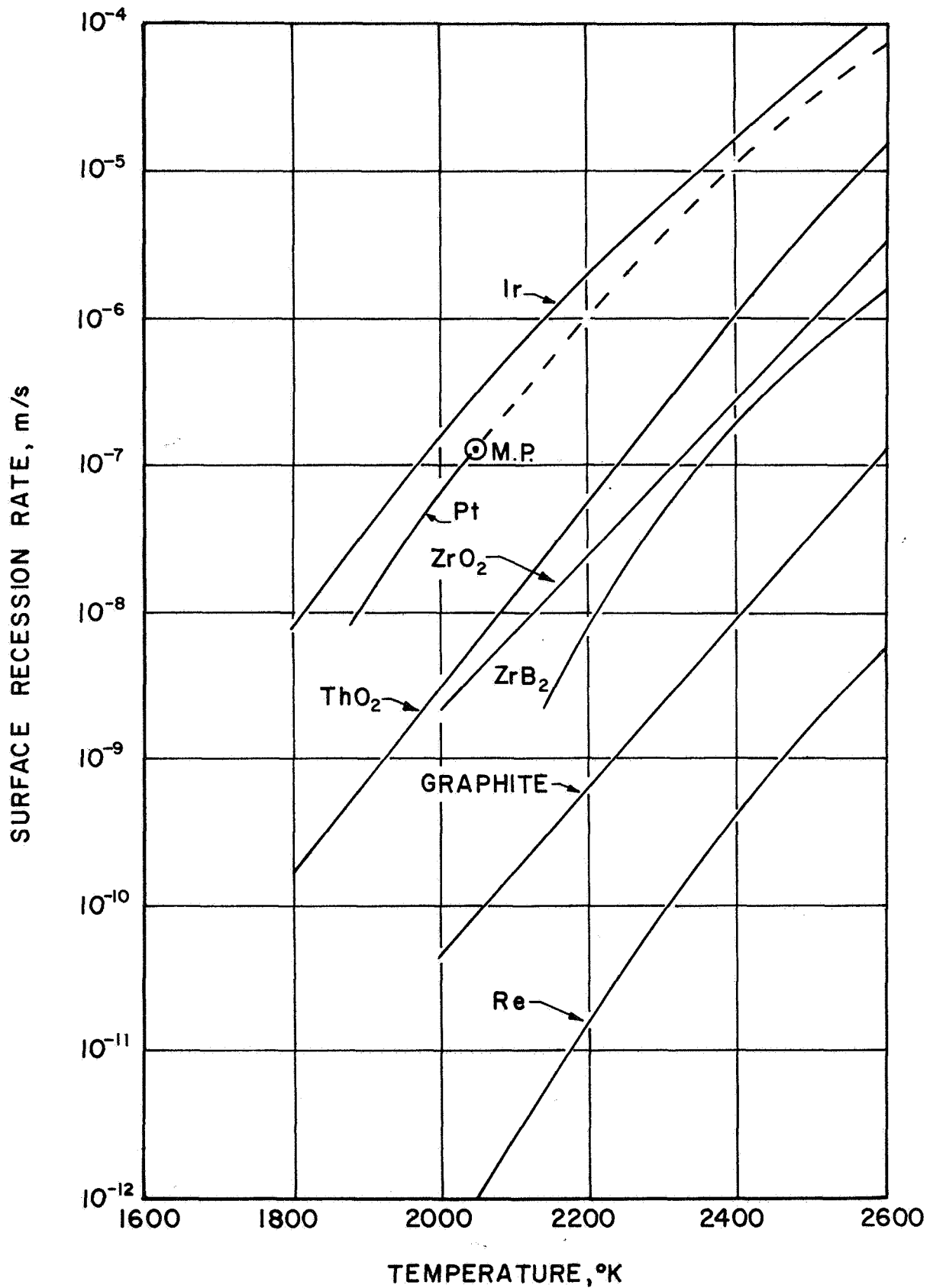


Figure 13.- Surface recession rates due to sublimation of biowaste resistant materials in a vacuum compared to rhenium.

Since according to ref. 68 mass, G , and thickness loss rates, δ , are inversely proportional to the square root of the pressure and directly proportional to velocity, pressure and velocity effects can be found from the 1 atmosphere, 100 feet per second data by applying the following equation:

$$G_{P, T_1} = G_{1, 100} \cdot \left\{ \frac{P_1}{P} \cdot \frac{V}{V_{100}} \right\}^{0.5} \quad (3)$$

As an example of the suppressing effect of pressure even under conditions of 100 feet per second flows, for the tubular geometries of Zima, the recession rate for rhenium, at 2500°K, is reduced by a factor of 100 over that in a vacuum. This increases the permissible use temperature of the materials by ~300K over those indicated by fig. 13 when the influence of pressure is considered.

The above generalizations are useful for preliminary selection purposes. Calculations of the specific geometry, material, gas and conditions are recommended in each instance prior to design.

Based on the above data, the maximum permissible temperature based on sublimation rates will be of the order of 2000°K for a design life of one year. Further, the temperatures of any surfaces exposed to a vacuum such as dewars must be limited to 1700°K. The ranking of the candidates is close: zirconia, thoria with no decision for zirconium diboride because of the unavailability of data on the modified form primarily the silicon carbide phase.

Creep deformation. - The permanent or plastic deformation of a material with time under conditions of constant load and constant temperature is an important engineering property commonly known as creep. Creep may be due to compressive, tensile, or shear loads or combinations of these.

The critical parts in the resistojet subjected to long-term, high temperature, stressed conditions, hence creep, are the last passes of the heat exchanger at the center of the thruster just prior to the thrust nozzle. Depending upon design, these parts which are generally tubular may be subject to compressive or tensile loading due to (1) pressure loading and/or (2) restrained differential thermal expansion.

The stress levels due to pressure loading, hoop stress, are small being of the order of 100 kN/m² (15 psi) because of the low design total pressure in the chamber (<3 atm). Stresses due to restrained thermal expansion through improper design can be large. This could be brought about, for instance, during the greater axial expansion of the hotter inner element relative to the outer case if there is an improperly designed pressure balancing-expansion compensator system.

This compensator system which must be included in the design is described for one design in ref. 3. It is located in the low temperature region of the engine to relieve these thermally induced axial stresses, as well as longitudinal stresses caused by pressure forces. This compensation system also may accommodate the small inevitable creep due to mismatching in the system design itself.

Creep can cause two effects which cannot be compensated and must be accommodated in the design. First, the parts may change shape to the extent that surfaces

of a different electrical potential may touch causing short-circuiting. Second, they may creep to failure. The design must be adequate to withstand these during the thruster lifetime.

Summary experimental data in the literature are generally presented in terms of creep rate versus reciprocal temperature with stress level as a parameter or creep rate versus pressure with temperature as a parameter as shown, for example, in fig. 14 for thoria (ref. 69). For the designer, however, this data is more usefully presented in terms of allowable working stress versus design life based upon a given allowable total percentage strain.

Experimental creep rate data associated with the low values of stress encountered in resistojet designs of say less than 100 psi, both compressive and tensile on high temperature parts, are generally not found in the literature for the temperatures of interest, 1600-2100°K. Since ceramic parts are generally designed to take advantage of their great compressive strength, virtually all creep data are compressive. There were no tensile data found in the literature survey conducted here. Hence, design curves must rely on an extrapolation from the typical 4000 psi or more compressive creep rate data (occurring over a period of a few days) to stresses approximately two orders of magnitude smaller (involving years of application). Part of the experimental problem is the long period of time necessary and the associated difficulties to gather low stress-creep rate data. This information is important, nevertheless, as the long operating periods required of resistojets, the order of years, causes them to gradually deform and could impose side effect problems; sometimes serious if not properly anticipated.

An understanding of the fundamental mechanisms of deformation at high temperatures is necessary then before the long time-low stress performance of these can be meaningfully projected from available data.

Tensile creep can only be guestimated based at present upon the ratio of ultimate tensile to compressive stress.

Until recently there was little information available on the creep behavior of stabilized zirconia apart from the limited data from Stavrolakis and Norton's measurements on calcia-stabilized zirconia in torsion (ref. 70). Recent work on yttria and scandia stabilized zirconia by Evans (ref. 71) and yttria rare earth stabilized zirconia by Fehrenbacher, et al., (ref. 72) is briefly summarized in fig. 15. The description of physical properties, etc., of the specimens is treated in Table VI.

The compressive creep rate of thoria was measured by Poteat and Yust, (ref. 69) so as to show the stress dependence of strain rates over a range of temperatures from 1700°K to 2060°K. These data are summarized in fig. 14. Table VI compares the properties with those of zirconia referred to previously.

There are three regimes of creep. The secondary represents a uniform minimum creep rate (MCR). This was used in the zirconia investigations surveyed. Thoria used the average, a higher rate.

The mechanical properties of materials are very structure sensitive; consequently, consistency of purity and density of the specimens as well as other

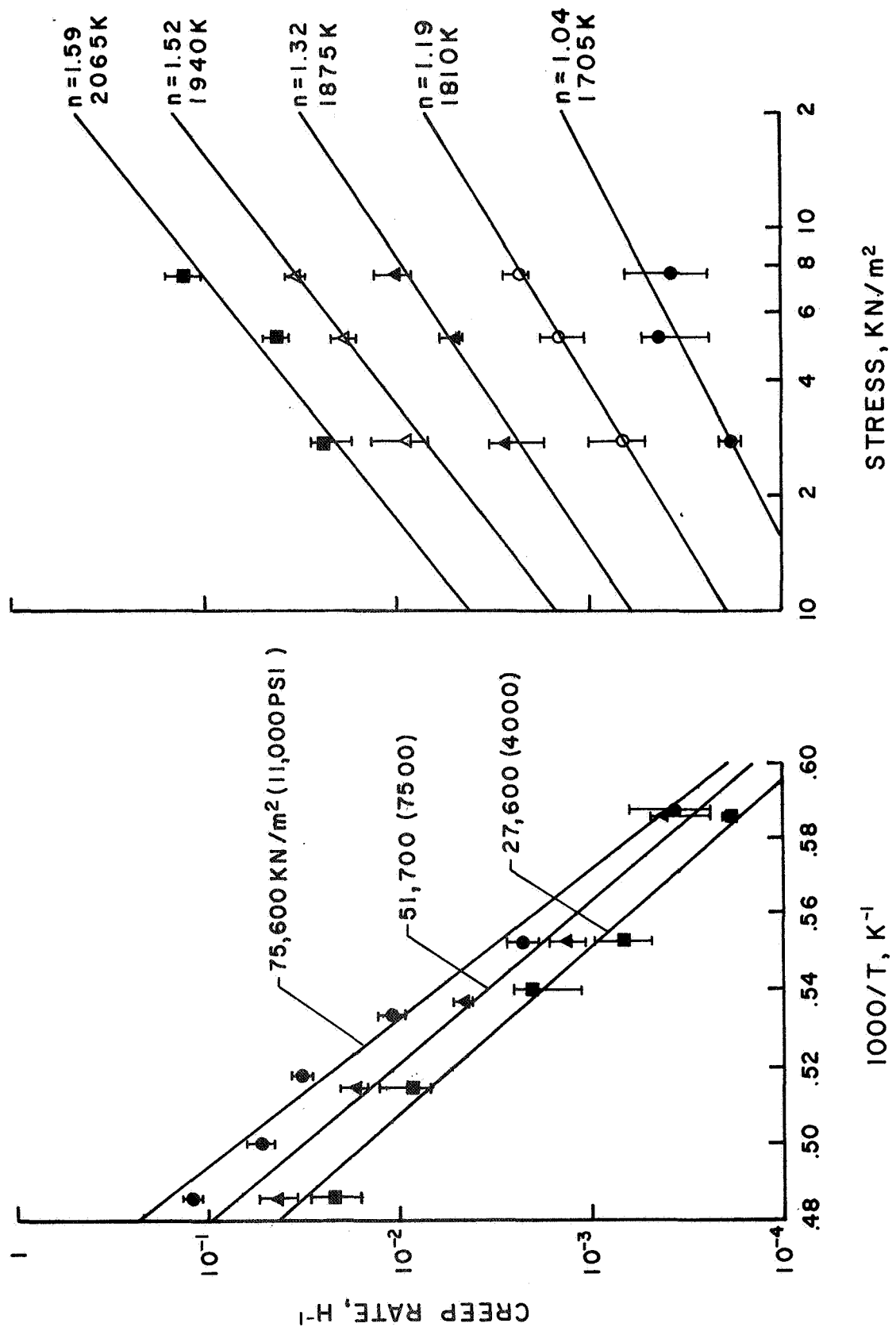


Figure 14.- Summary of compressive creep data for thoria showing dependence on temperature and stress.

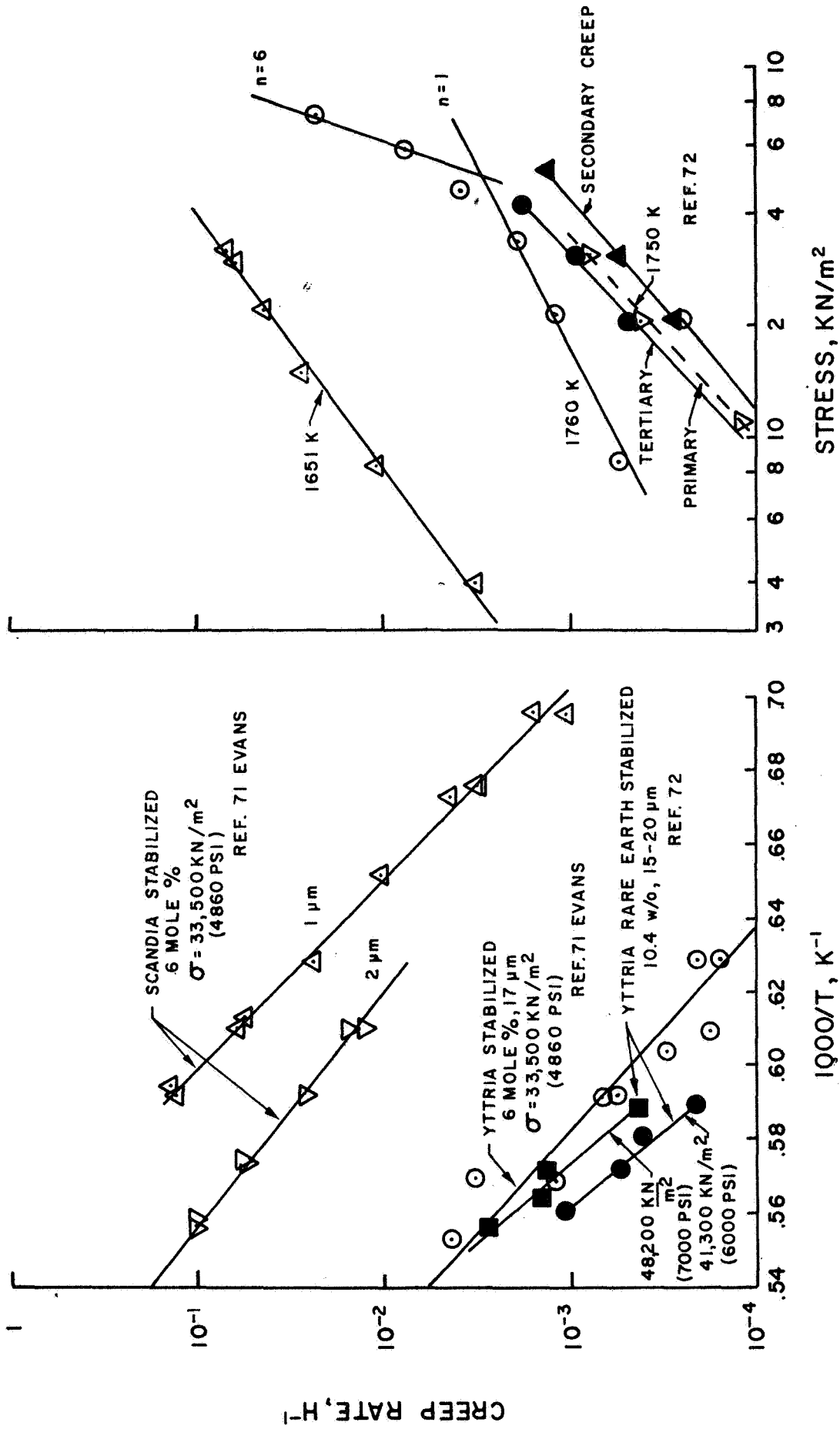


Figure 15.- Summary of compressive creep data for stabilized zirconia.

TABLE VI. - SPECIMEN SUMMARY OF COMPRESSIVE CREEP INVESTIGATIONS

Description	Thoria	Zirconia	Zirconia	Zirconia ^b	Zirconia
Stabilizer	None	Yttria	Scandia	Scandia	Yttria, rare earth
Material	None	6 mol % (or 10.47 w/o)	6 mol % (or 6.68 w/o)	6 mol % (or 6.68 w/o)	10.4 w/o
Amount	Poteat and Yust	Evans	Evans	Evans	Fehrenbacher, et al.
Investigator	69	71	71	71	72
Reference	99.99	99.99	99.99	99.99	99.39
Purity, %					
Range of Study	27,600; 51,700; 75,800	8,270 - 71,000	4100 - 35,100	4100 - 35,100	5500 - 51,700
Stress, KN/m ²	(4,000; 7,500; 11,000)	(1200 - 10,300)	(600 - 4800)	(600 - 4800)	(800 - 7500)
Temperature, K	1675 - 2075	1590 - 1808	1440 - 1795	1440 - 1795	1670 - 1810
Maximum deformation, %	10%				~5
Density					
Theoretical		6.1	5.9	5.9	6.01
Measured, g cm ⁻³		5.60	5.58	5.58	5.68 - 5.70
% theoretical	97.5	91.8	94.6	94.6	94.7
Fabrication Process	Isostatically pressed	Hot pressed	Hot pressed	Hot pressed	Isostatically pressed
Pressure KN/m ² (psi)	(35,000)	(5,985)	(4,865)	(4,865)	a
Firing temperature, K	2075 (in air)	1775	1775	1775	a
Time at temperature, min.	120	115	40	40	a
Grain diameter, μ m	10	17	1	2	15 - 20
Particle size, μ m	0.5	(a)	(a)	(a)	(a)
Porosity, %	<1.0	(a)	(a)	(a)	(a)
Specimen size		(a)	(a)	(a)	(a)
Length, mm	7.6	5.1	5.1	5.1	(a)
Diameter, mm	4.3	2.5	2.5	2.5	(a)
L/D	1.76	2	2	2	3, 6
Heating elements	Molybdenum disilicide	Silicon carbide	Silicon carbide	Silicon carbide	Platinum - Rhodium
Carbon resistor <1875K	Carbon resistor <1875K	-	-	-	-
Arrhenius equation const.					
Stress dependence					
Exponent, n	1.04	1	1.48	(a)	1.65
Applicable stress range (psi)	(4000-11,000) @ 1700K	(1200-6000) @ 1760K	(600-5000) @ 1650K	(a)	(1500-7500) @ 1760K
Exponent, n	1.59	6 (possibly 7)	-	-	-
Applicable stress range (psi)	(4000-11,000) @ 2060K	(6000-10,500) @ 1760K	-	-	-
Activation energy, Q, KCal/mole	112 \pm 7	86	89	74	110
Creep rate basis	Average	MCR	MCR	MCR	Secondary creep (MCR)

^a Not reported.

^b Heat treated in air for 48 hours at 1800K to promote grain growth.

^c Linear intercept method

factors such as grain size, substructure, pore shape, and pore distribution are of the utmost importance for reproducible results.

The source materials of the studies of refs. 71 and 69 were of high purity by preparation from chemical compounds. In the case of thoria, the maximum impurities were carbon (40 ppm) and calcium (25 ppm). For the zirconia, Evans used the method described by ref. 73. The yttria and scandia powder used were 99.99% and 99.75% pure. The principle impurities determined in the stabilizer spectrographically were Si 0.1, Al 0.03, V 0.03, Y 0.02, Yb 0.02, Ca .02 and Er 0.02%.

In the case of Fehrenbacher, et al., (ref. 72) significant additions of "C" rare earths were added in addition to the yttria (9.1 weight percent). These were the yttria rare earth oxide stabilizer consisting of 90% yttrium sesquioxide with the balance being the other heavy type "C" rare earth oxides. By spectrographic analyses, mass and x-ray, the additives were Y 9.2 and RE 0.9%, the impurities 0.6%. The principal impurities were Na 0.02, Mg 0.03, Al 0.03, Si 0.05, K 0.015, Ca 0.05, Fe 0.1 and Hf 0.3%. The purity then was 99.39%.

The mechanism of creep in these materials is discussed in some detail in refs. 71, 72 and 69 and is not repeated here. In brief, the plastic deformation of polycrystalline single-phase ceramic bodies occurs in general by one or more of the following mechanisms: (a) dislocation motion, (b) diffusion processes, and (c) grain-boundary shearing. It is apparent that several mechanisms exist by which deformation in ceramics can be described. Under any given set of conditions, each mechanism may make some contribution to the total shape change of the body. The principal mechanism at any time depends on the conditions imposed. Which mechanism is rate controlling can be sensed from microstructural evidence and dependence of strain rate on stress; namely, the exponent, n .

The steady-state creep rate, $\dot{\epsilon}$, can be expressed by means of an Arrhenius equation in the form:

$$\dot{\epsilon} = (S\sigma^n/d^m) \exp (-Q/RT) \quad (4)$$

note that n , the stress exponent, is a function of applied stress, σ , temperature, and structure.

The data surveyed here indicate that the dominant mechanism of creep under the conditions of these studies involves a diffusion transport of material since the deformation rate is very nearly proportional to the stress, and that the mechanism includes the sliding of grains and the concurrent creation of grain-boundary voids. In cases of thoria and zirconia, analysis of the creep data indicated that the dominant material transport mechanism was Nabarro-Herring creep.

The mathematical description of diffusion coefficient, D , for uniaxial compressive creep by the Nabarro-Herring mechanism is,

$$D = \frac{3}{40} \frac{\epsilon k T d^2}{\Omega \sigma} \quad (5)$$

If diffusion transport of material is responsible for deformation, the strain rate will be directly proportional to the stress or $n = 1$ as suggested by equation (5) above.

A stress exponent, n , of 1.5 was found by Evans for the scandia-doped zirconia and two regimes with $n = 1$ and 6, were found for the yttria-doped zirconia. These data, supported by microstructural evidence, are interpreted by him as showing that $n = 1$ is associated with cation diffusion control of creep, $n = 6$ with local propagation of intercrystalline cracks, and $n = 1.5$ with a transition region.

Evans found, for the stress of 4860 psi and temperature of 1675K investigated, that creep rates are linearly proportional to the inverse square of the grain size of the zirconia regardless of stabilizer. That is, $m = 2$ in equation (4). The N-H mechanism equation (5) suggests this $\dot{\epsilon}$ dependence on d^2 . The cause of the inherently larger grain size of yttria stabilized compared to scandia stabilized zirconia was unknown. It is suggested that the different creep rates are in general caused by the different grain sizes of the zirconia.

The design working stress curve for zirconia based on the extrapolation of the available data is shown in fig. 16. The extrapolation is based on equation (4) and not account for structural changes with time such as grain growth or second phase disappearance for instance. It is conservative in that these factors will improve (lower the creep rate) the allowable working stress otherwise. The temperature effect can only be skeletally accounted for by the temperature dependence curve of Evans shown noted. The stress exponent, n , is unknown for these temperature levels.

The effect of grain size and additives appears to be dramatic. The upper two (2) sets of time extrapolated curves represent approximately 17 micron diameter grain size; the lower one (1) micron. The upper curve appears to be significantly improved over the zirconia of Evans. The reason for this is unknown. The upper curve does include some rare earth additives.

The working stress curve, fig. 17, for thoria is much better defined in terms of temperature dependence based on the data of ref. 69. For design purposes, this curve is conservative relative to zirconia for the reasons of creep rate interpretation and the fact that the elongation of 3% represents a smaller percentage of the failure elongation (~10%) than zirconia (~5%).

Based upon the data extrapolated in time, both thoria and yttria rare earth stabilized zirconia possess acceptable working stresses on the basis of creep elongation. This extrapolation does not take into account the beneficial effects of the larger grain size (growth) with time.

The development of large grain materials, according to the data of ref. 74, significantly improve the working stress based upon elongation under low stress-high temperature conditions over those shown in figs. 16 and 17.

Modified zirconium diboride creep data are meagre limited to that of ref. 14, typically 25,000 psi with times less than one hour. Insufficient data were available to make any design estimations similar to those of fig. 16 and 17.

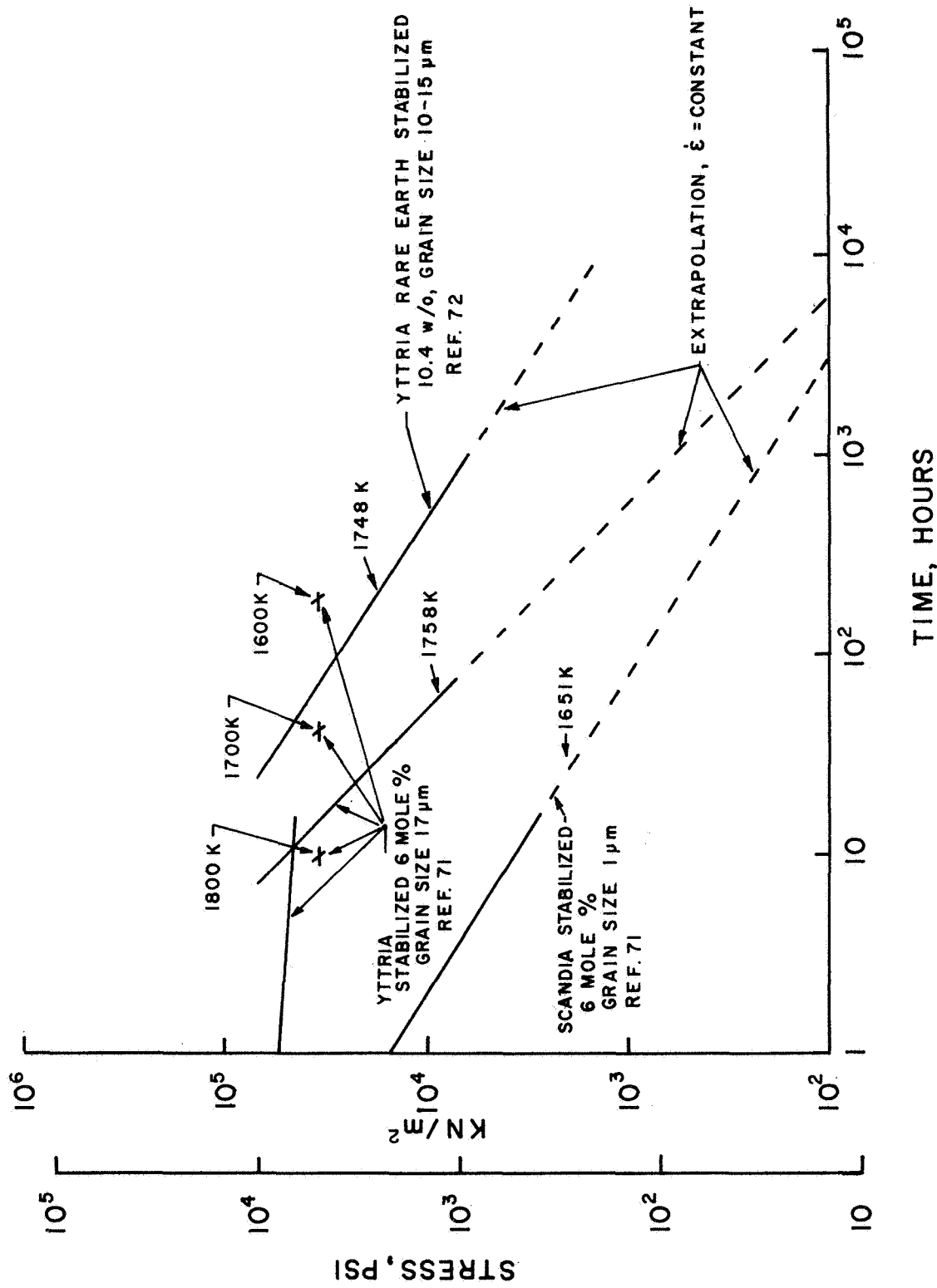


Figure 16.- Extrapolation of compressive creep data (for 3% total creep) to determine service life expectancy or working stress for various forms of stabilized zirconia.

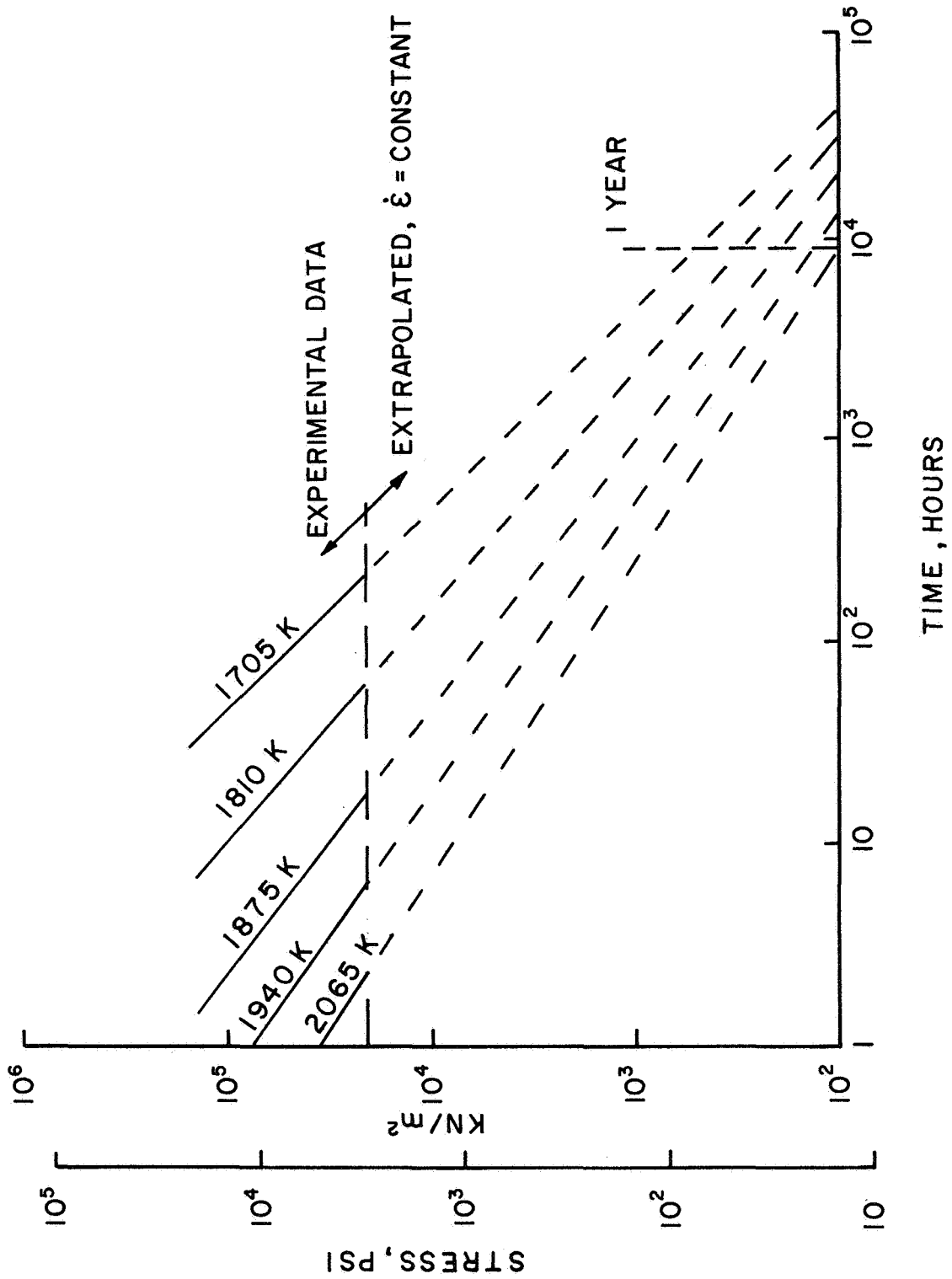


Figure 17.- Extrapolation of compressive creep data (for 3% total creep) to determine service life expectancy or working stress for thorium for a range of temperature.

The ranking of materials relative to creep is difficult because of the absence of any low stress, long duration compressive data let alone any tensile creep data. Based upon considerable extrapolation, but done conservatively, tensile creep poses a serious design problem. Resistojets using ceramics must be very carefully designed with respect to pressure drop such that all members of any temperature in excess of $\sim 1300^{\circ}\text{K}$ must be in compression but within the limits of figs. 16 and 17. Preliminary design shows this to be entirely feasible. While tensile creep data is valuable, a design rule avoiding any tensile stresses is paramount.

Endurance stress. - The stress that produces creep elongation to failure in a material at elevated temperature in a given time is known as the endurance stress.

Such failure in most resistojet parts connotes engine failure such as breaching of a high pressure vessel wall for example.

Like creep deformation, no data to failure at the low stress levels and high temperatures required for resistojet design is available. However, useful interim working stress curves can be generated based upon creep deformation data described in the previous section. In zirconia, Fehrenbacher (ref. 72) noted that total elongation to failure was approximately 5%. The working stresses shown in fig. 16 represent 3% permissible. An interim preliminary endurance stress as a function of time may be found from fig. 16 by increasing the time for each stress given in the ratio of 5 to 3%.

Poteat and Yust noted elongations of 10% in thoria; hence, the working stress curve for creep elongation may be used for endurance stress by increasing the times in the ratio of 10% to 3%. The above is suggested for compressive failure only. Tensile endurance can only be guesstimated at this time in the ratio of the ultimate stresses as suggested under creep deformation.

Thermal stress resistance. - Thermal stresses originate in a body when differences in thermal expansion of its various elements cannot proceed freely. This condition can arise in a number of ways.

If a body is heated uniformly, no stresses arise providing the body is homogeneous, isotropic, and unrestrained (free to expand). Thermal stress, as used here to compare candidate resistojet materials, is defined as a stress caused by: (1) a constraint of system members from free expansion and (2) a temperature gradient either steady-state or transient.

The susceptibility of ceramic materials to thermal stresses has long been recognized and studied. It is an important consideration with regard to their potential for use in resistojet thrusters where high heat flux rates and temperature gradients can exist in some designs.

Kingery (ref. 75) shows the various analytical descriptions which have been developed for the conditions to initiate fracture of a brittle material considering simple shapes in a variety of thermal stressing situations. Based upon these analyses, no single parameter or test value is a suitable index to rate a material's resistance for all conditions of thermal stressing.

The material properties which affect thermal stress resistance are elasticity, strength, coefficient of expansion, Poisson's ratio, and in some cases, thermal conductivity, diffusivity or emissivity.

Analyses for different conditions result in the following three parameters that can be used to rate the thermal stress resistance of material under conditions where plastic strain is insignificant:

$$R_1 = \frac{\sigma_f (1 - \mu)}{E\alpha} \quad (6)$$

$$R_2 = \frac{\sigma_f k(1 - \mu)}{E\alpha} \quad (7)$$

$$R_3 = \frac{\sigma_f a(1 - \mu)}{E\alpha} \quad (8)$$

where σ_f is either tensile or shear fracture stress whichever is significant to the problem.

For ceramics, the most dangerous thermal stresses are tensile. Since the compressive strength is generally four to eight times the tensile strength, failure from compressive stresses is relatively unimportant. Shear strengths for ceramics are always greater than or equal to the tensile strengths.

Conceptually, the critical condition for fracture, f , is defined by the product $f = R \times S$. Where R is the appropriate material parameter; R_1 , R_2 , or R_3 , and S is a corresponding parameter dependent only on specimen geometry and size. R_1 can apply when fracture results from an extreme thermal shock, in which case f is the instantaneous surface temperature change, ΔT_f , of an object, initially at one temperature, suddenly heated or cooled, a situation which is generally referred to as thermal shock. R_2 can apply under conditions of steady-state heat flow, q_{\max} , that will cause a sufficient temperature gradient to induce fracture. R_3 can apply to the minimum constant rate of surface temperature change, ϕ_f , that will cause fracture.

In summary, it should be emphasized that the use of these factors would be exact only to a homogeneous isotropic body whose physical properties are substantially independent of temperature. These relations do not cover all possible conditions but are representative of the factors comprising thermal stress resistance.

$$\Delta T_f = R_1 S \quad (9)$$

$$q_{\max} = R_2 S \quad (10)$$

$$\phi_f = R_3 S \quad (11)$$

Reference 76 notes these relations only apply when plastic strain does not occur. Plasticity causes a sharp increase in thermal stress resistance. These factors do not cover all possible conditions. For example, in the case of a shape at a uniform temperature immersed suddenly in a medium at a lower temperature, the

relation $\Delta T_f = R_1 S$ holds only when Biot's modulus, β , is greater than about 20. This is the case where fluid surface heat transfer is excellent compared to that of a relatively thick ceramic part or one of poor conductivity. If Biot's modulus is very small, equation (12) is applicable and R_2 is the basis for material comparison.

$$\Delta T_f = R_2 S \quad (12)$$

Or stated another way, poor fluid-to-surface heat transfer or thin highly conductive ceramic parts is involved. For intermediate values of β , ΔT_f is not directly proportional to any of the three material parameters. Manson (ref. 77) has developed an expression, however, for ΔT_f in terms of R_1 , R_2 and $r_m h$ for all values of β .

Kingery (refs. 75 and 78) gives shape factors for certain simple geometries and thermal stressing conditions.

The size and shape of a ceramic part greatly influences its resistance to thermal stresses. In particular, for moderate rates of temperature change, thermal stress resistance of a part is inversely proportional to specimen dimensions. For very high rates of change, this size effect is only important for small dimensions. In general, shapes having sharp corners or edges are to be avoided as are parts having both thick and thin sections together.

For complex shapes or materials which are subject to plastic flow, experimental measurements are the only reliable method for measuring thermal stress resistance of the specific system.

Table VII presents the calculated values of the thermal stress resistance factors for the prime candidate materials on the basis of properties at the temperatures noted. The higher the resistance factor, the more resistant is the material to weakening or thermal fracture from thermal stress. These factors should be taken only as relative.

From a thermal stress viewpoint, ZrB_2 is seen to be clearly superior with regard to R_2 and R_3 factors. ZrO_2 and ThO_2 are seen to be roughly comparable on the basis of thermal stress resistance although the literature, in general, ranks ThO_2 lower than ZrO_2 .

In resistojet design, the Biot modulus is very small primarily because of the physical sizes involved. Thermal shock is valued on the basis of R_2 as discussed above regarding equation (12) rather than R_1 or equation (9). It will be shown later that the thermal stressing requirement due to heat transfer functions in the resistojet design including transient ones are not severe and ZrO_2 and ThO_2 can amply qualify as candidates providing certain situations are avoided as is discussed in the following section.

TABLE VII.- CALCULATED THERMAL STRESS RESISTANCE FACTORS

Factor	Temperature °K	ThO ₂	ZrO ₂	ZrB ₂
R ₁ (°K)	298	50.4	69.7	63.9
	1200	37.5	56.7	69.3
	1600	-	66.2	67.1
R ₂ (W/m)	298	726	122	5530
	1200	112	107	5430
	1600	-	132	5060
R ₂ (m ² °K/s) x 10 ⁶	298	313	47.5	2400
	1200	37.5	28.4	1370
	1600	-	31.1	1200

THRUSTOR DESIGN PHILOSOPHY

Objective

The purposes of a preliminary conceptual design of an advanced biowaste resistojet are: To define the environmental conditions which must be met by the associated materials and to verify the availability of the techniques required to fabricate the resistojet parts from the selected materials.

There are no known preceding resistojets, constructed with ceramics, upon which to base an initial concept. Related technology is found, through, this along with the experimental experience herein and that of Halbach, et al. (ref. 79) on a subsequent program, involving conducting-ceramic-heat-exchanger initial experiments, allow formulating a rudimentary set of design principles. It is considered beyond the scope of this phase of the study and too early to present a detailed preliminary design. The design considerations here are based upon the use of Y_2O_3 stabilized ZrO_2 and possibly ThO_2 for the highest temperature parts.

Modified ZrB_2 is not being considered further for the design primarily because of its high current-low voltage characteristic and the associated power adaptation required. There was some uncertainty also about its long-term chemical compatibility.

The design objectives are to achieve the highest specific impulse compatibility consistent with a service life of $\sim 10,000$ hours. This is primarily a temperature limit set by one of the material considerations as described in the previous sections. Which one of the material considerations is limiting depends upon the design chosen. The second part of the design problem; namely, to minimize the electric power requirement for a given thrust is not considered critically at this time.

Table VIII itemizes the expected design goals of a thruster which is to be operable on the propellants shown and delivering a thrust of 0.111N (25-mlb). The projection is based upon the semi-empirical analysis of Halbach and applied to biowaste propellants in ref. 49 which takes into account the optimization of the viscous, divergence, expansion ratio, and frozen flow effects of a laminar nozzle. The temperature of $2000^\circ K$ can be achieved based upon the materials criteria reviewed herein being the important and limiting ones. Operation on CH_4 is shown limited to $1000^\circ K$ by the carbon deposition problem. Reasonable, achievable heater efficiency goals are projected based upon previous experience; specifically at the $2000^\circ K$ level. The power lost to the surroundings is estimated at 45W.

Figure 18 schematically describes the thruster configuration functionally. The design is three-pass and regenerative.

Design Principles

The following represents the recommended direction for the design of a ceramic thruster:

TABLE VIII. - ADVANCED RESISTOJET DESIGN GOALS
THRUST, 0.111 N (25mlb)

Parameter	Propellant, nominal				
	CO ₂ ^a	CH ₄ ^a	H ₂ O ^a	H ₂	NH ₃ ^b
Gas temperature, T ₄ , °K	2000	1000	2000	2000	2000
Chamber pressure, P ₄ , atm.	1	1	1.1	1	1
Mass flow, m, Kg/s x 10 ⁵	5.85	5.31	4.18	1.67	3.37
Specific impulse, I _{sp} , s	194	214	271	679	336
Total electrical power, W	171	121	320	487	347
Efficiencies: ^c					
Heater efficiency, η _H	0.754	0.940	0.869	0.919	.877
Nozzle efficiency, η _N	0.769	0.803	0.493	0.723	0.569
Overall power eff. η _o	0.580	0.756	0.428	0.664	0.498
Overall electrical eff. η _o *	0.629	0.965	0.460	0.760	0.527
Nozzle frozen flow eff. η _F	0.97	0.97	0.65	1.00	0.77

^a See Table IV for initial and final reactant species composition at temperature of propellants and rationale.

^b Chemical compatibility with ceramics is uncertain.

^c See Appendix B for definitions of efficiencies.

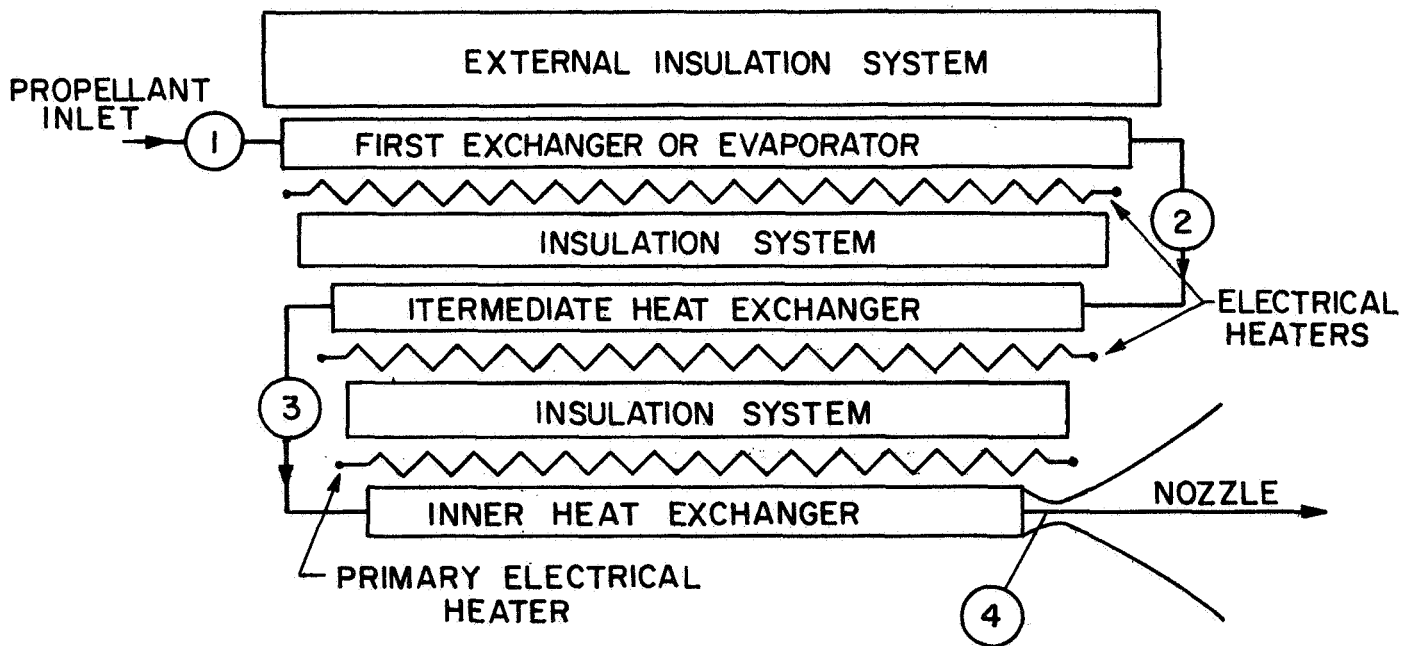


Figure 18.- Functional schematic of an advanced resistojet configuration.

(1) The ceramics considered must be ohmically heated directly if they are to take advantage of their superior temperature capability ($>2000^{\circ}\text{K}$) over the platinum alloys ($\sim 1500^{\circ}\text{K}$). There are two reasons for this recommendation based upon the experience with indirect high temperature heating of ceramics on this program.

- (a) Close coupling of heater and ceramics required for efficient heat transfer promotes touching resulting in thermal shock failure of the ceramic. Indirect heating by metal conductors at the design condition requires substantially higher wire temperatures. The R_1 factor on Table VII indicates the ΔT , required between heater and ceramic to transfer the power, will cause such failure. Over 70% of the test terminations on this experimental program were for this cause.
- (b) Indirect heaters if not biowaste gas resistant at use temperature are quickly consumed. The graphite test heater life, for example, was less than 100 hours even though located in a vacuum environment. In particular, the primary refractory metal heater would have to be protected from exposure to the propellant at high temperature as the inability of metals to withstand this sort of environment is the very reason for the use of ceramics in this application. If protected in an inert zone, the wire would soon succumb to oxidation by the inevitable diffusion of gases through walls. ZrO_2 , as discussed earlier, ionically transports O_2 as a solid-state electrolyte when an electric field is applied. Even metals can develop leakage paths over the life of operation which do not seriously influence performance (ref. 4) but could pose material's problems elsewhere due to oxidation. The primary electrical heater and inner heat exchanger, in figure 18, then are one and the same.

(2) The ceramic inner element must be started by an auxiliary means. The heating of the inner exchanger would take place in two ways mainly by warm propellant from the intermediate exchanger (~ 10 seconds) and secondarily by transient conduction through the inner insulation system (~ 100 seconds alone).

- (a) An electrical heater may be used. The heater material, a wire, selected must be resistant to biowaste gases to about 1300°K , its operating temperature, and located next to intermediate heat exchanger as shown in figure 18.
- (b) There is a possible future alternative; namely, the addition of "doping" materials to make the ceramic conduct at low temperature. In many respects this choice is better but reports of early attempts have

indicated a tendency to return to the more resistant state with gradual loss of the doping material. More work in this area is needed to determine if this approach can be made practical in the future.

- (3) Tensile stresses are to be avoided. An all compressive design is possible by careful choice of the configuration and the pressure drop from the thruster inlet, station 1, through to the nozzle exit, 4. Limiting compressive stress levels to the order of 100 kN/M^2 ($\sim 15 \text{ psi}$) are estimated to allow a 10^4 hours ($\sim 1 \text{ yr}$) life at a temperature of 2000°K .
- (4) The use of vacuum dewars in areas greater than 1700°K must be avoided because sublimation effects, on vacuum side, could limit life. Further, such vacuum jackets cause undesirable tensile stresses. Preliminary heat transfer calculations show that they may not be necessary in ceramic designs at the 25-milipound thrust level.
- (5) Platinum to ZrO_2 or ThO_2 for metal-to-ceramic seals are recommended to be considered. These show good expansion capability but may be made further more compatible by the use of graded joints.
- (6) The metals platinum-rhodium or thoria-dispersed platinum are recommended to fabricate members for temperature service for temperatures below approximately 1200°K . Thoria-dispersed nickel is preferred for parts below approximately 800°K .
- (7) The conducting ceramics because of a negative electrical resistance characteristic with temperature must have an electrical resistance in series as a ballast for stability. The inlet stage electric heaters are to be used for this ballast thus utilizing the power, otherwise lost, for propellant heating.

Based upon principles outlined, the design to meet the goals of Table VIII is made somewhat more definite and is briefly outlined below. The geometric throat diameter is 0.89 mm for all propellants shown. The ceramic inner element will range from 2 to 4 cm long, depending upon terminal voltage selected. Maximum wall temperature will be less than 50°K above gas temperature in the worst case. The inner element process, from stations 3 to 4, with proper heat transfer design, should make the major power input contribution to the gas, the maximum temperature to occur at station 4. Only the inner element and its associated supports and heater system need have the high temperature capability; hence, be fabricated of ceramics. The chamber pressure should be selected around one atmosphere for reasons of minimizing creep loads. Less than 6 seconds in specific impulse is lost by this choice say over a 3-atmosphere design. The throat size is very reasonable as a result making it less sensitive percentage-wise to any small changes that may occur in surface dimension. The power to evaporate the water is 110W of the 320W shown in Table VIII. The low temperature of 1000°K for CH_4 was chosen to avoid the carbon formation by pyrolysis. The ceramic heater would not be activated for this case and the resistojet would be run on the starter heaters alone. The terminal voltage will be directly matchable to space station power systems and will be alternating current.

A thorough design of this thruster is in process on NASA Contract NAS1-10934. A preliminary report of this later study is given by Halbach in reference 79.

Fabrication Techniques

The resistojet demands little in quantity of its material but much in quality. This small quantity permits quality fabrication methods for parts which otherwise would be uneconomical in larger quantity applications. The principal problem is specifying the exact additive composition to achieve all the desired properties in an advanced resistojet for lives of the order of 10^4 hours. It is an important conclusion that the method must be able to control purity and permit controlled additions of desired additives.

ZrO_2 and ThO_2 parts have been made by well known methods of slip casting, extrusion, and cold pressing followed by sintering (ref. 78). More recently they have been made by conventional and isostatic hot pressing. The "Zyttrite" process (ref. 18) has been discussed earlier as compared to hot pressing as a low temperature hot pressing technique producing a fine grain reported to be relatively shock resistant ceramic. High purity techniques are described by Henderson (ref. 73) for zirconia and hafnia. The isostatic hot pressing technique by Coors promises a fabrication technique for high quality heat exchanger parts of the shapes desired. Reference 72 describes creep tests on this material the resistance to creep being high. Parts ordered for this program, but unfortunately untested in depth, had low porosity.

Dense bodies of thoria have been prepared by cold pressing disks followed by sintering in a molybdenum resistance furnace in a hydrogen atmosphere at $2275^\circ K$ - $2575^\circ K$, according to reference 80. The addition of a 2 mole % CaO to the ThO_2 inhibited discontinuous grain growth and allowed sintering to proceed to theoretical density. It should be possible to hot press cylindrical and bar-shaped specimens with corresponding additions of CaO at considerably lower temperatures to achieve theoretical density.

The use of ultra-fine oxide particles is a well-known method to produce high density bodies by hot pressing. Submicron hafnia powders have been prepared by hydrolytic decomposition of alkoxides (ref. 81).

Joining Techniques

There are two type joints of interest in the design: ceramic-to-ceramic and metal-to-ceramic.

Ceramics may be joined to themselves. According to a recent report from Naval Research Laboratory, ZrB_2 , ZrO_2 , and MgO have been welded by high temperature solid-state diffusion and/or reaction and by fusion welding (ref. 82).

A great deal of work on the ceramic-to-metal seal problem has been done. See ref. 83 for such a summary. However, most of the available information and standard processes apply to the joint of metals to alumina and other ceramics in more widespread use than ZrO_2 and ThO_2 . Although the technology generally may be

adaptable to the latter materials, the exact processes have not been developed to nearly the same extent as those for Al_2O_3 , etc.

Hermetically tight seals suitable for electrical apparatus at all low and high temperatures are reported to be formed by Buyers (ref. 84) between any stabilized ceramic containing at least 10 mole % ZrO_2 including mixtures with ThO_2 with Ta and its alloys with W, Re, Nb, Mo., etc., by contacting the ceramic and metallic members together, heating to 2200-2500°K by any method and cooling to room temperature. Seals are reported to withstand immersion in liquid N_2 , prolonged heating at 2300°K and repeat 1-2 minute cycles between 2200°K and room temperature. If this process works with Pt then a viable seal or electrode may be achieved. The following compounds were identified by x-ray diffraction patterns: Ta zirconate, Y tantalate, Ta silicide, etc. The biowaste resistance of these joints must be established.

Research to evaluate the active metal process for joining zirconia ceramics is discussed in reference 85. Filler alloys with 10% Ti produced the best results. Also investigated was the Ag-Zr system for joining ZrO_2 and Al_2O_3 ceramics. Good wetting and bonding were obtained when the tests were conducted in a vacuum.

The platinum-zirconium graded joint applied by ion plating with subsequent brazing to the platinum alloy members appears attractive.

THRUSTOR ELEMENT FABRICATION AND TEST

Based upon the results of the materials properties evaluation, yttria stabilized zirconia, thoria and modified zirconium diboride were chosen for experimental evaluation in the form of representative thruster elements. The purposes of these tests were to determine the compatibility of these materials with the potential propellants carbon dioxide, water, methane, ammonia and hydrogen to the most severe conditions expected in a thruster design and to determine their maximum temperature capabilities. CO_2 was used as a screening test and the most suitable materials were then to be tested on the balance of the above propellants. ZrB_2 was not tested as described later.

The major emphasis of the test was the exposure of the materials to the high temperature candidate gases to see if there were any obvious interaction. Other effects to which a simulated resistojet heat exchanger may be exposed were attempted to gain design experience. An external vacuum jacket was simulated (10^{-2} to 10^{-5} torr.) so as to subject the specimen to sublimation on its exterior and its walls to tensile creep effects for periods of the order of 10^2 hours. External heater techniques were studied, as the original thruster design concept indicated this approach. The test program gave valuable data to indicate otherwise. A subsequent program has confirmed that direct ohmic heating approach was superior and times demonstrated to the order of 10^3 hours at higher temperatures than reported here (ref. 79). The thruster design section herein takes the later results into account.

It was not the original intent of this program to develop the high temperature ceramic-to-metal seal technology which would ultimately be required in fabricating thrusters of ceramic materials. The materials test program, however, under the indirect heating concept required that such joints be made on each test item to protect the heater from oxidation.

The type of joint required was found not to be a standard, easily accomplished thing but instead is apparently right at the edge of currently available technology. It was, therefore, necessary to devote a major part of the program to the development of a workable high temperature ceramic-metal seal assembly for the test program. This is reported herein.

Element Fabrication

It was found that sophisticated or even special parts fabricated from these materials were not readily available in terms of both cost and delivery time. Tubes of zirconia and thoria in a commercial grade, porous but impervious to gas leakage, could be ordered either from stock or in special lots. The diameters of these tubes varied but in general the smallest available sizes were one-eighth to one-quarter inch. Slip cast one-eighth inch O.D. CaO stabilized ZrO_2 , one-quarter inch Y_2O_3 stabilized ZrO_2 and one-eighth O.D. ThO_2 tubes were ordered from Zircoa, Solon, Ohio. The CaO stabilized tubes were later dropped from the candidate list in favor of the Y_2O_3 stabilized ones. One-quarter inch O.D. tubes of isostatically pressed fully and partially Y_2O_3 stabilized zirconia were ordered from Coors, Golden, Colorado. Hot pressed tubes of ZrB_2 with SiC and SiC + C additives were specially ordered from ManLabs, Cambridge, Massachusetts. The complete matrix of test samples is shown in Table IX.

TABLE IX. - TEST MATRIX

Sample type	Basic material	Stabilizer a or additive	Source	Density % ^b	Grain size (μ)	Fabrication technique	Initial dimensions		
							Length cm	O.D. mm	I.D. mm
A	ZrO ₂	8 w/o Y ₂ O ₃	Zirconia Solon, Ohio	95	25	Slip cast, then sinter	30.5	6.18 6.25	4.62
B	ZrO ₂	3.0 w/o CaO	"	95	25	"	15	3.30	1.60
C	ZrO ₂	12 w/o Y ₂ O ₃	Coors Golden, Colo.	95	17	Cold isostatic pressed then sint.	15	7.16 7.34	4.45
D	ZrO ₂	8.4 w/o Y ₂ O ₃	"	95	17	"	15	7.29 7.37	4.45
E	ThO ₂	None	Zirconia Solon, Ohio	95	25	Extruded sintered	15	3.50	1.60
F	ThO ₂	None	"	95	25	Slip cast & sint.	30.5	6.20	4.62
G	ZrB ₂	20 v/o SiC	ManLabs, Cambridge, Mass.	~100	2-10	Hot pressed	12.8	4.88	3.33
H	ZrB ₂	14 w/o SiC + 30 v/o C	"	~100	2-10	"	12.8	4.95	3.43

^a See text for impurity details. Purity >99+%

^b Manufacturer quote (typical)

Since the simulated resistojet heat exchanger elements were to be tested in the presence of various flowing propellants and since the graphite and refractory metal heaters could not be used in the presence of most of these propellants, it became necessary to attach the test samples to propellant inlet and exit tubes. Initially there appeared to be several possible approaches to this attachment problem and the easiest of these were attempted first since the object of the program was the testing of ceramic materials and not the development of joining techniques.

The simplest method involved the use of long tubes (12 inches) and metal Swagelok fittings with teflon ferrules. The heated test section was located closer to the cooled inlet end with the long exhaust section serving to cool the gas adequately before encountering the exhaust fitting. Early tests revealed, however, that the end was too high in temperature for teflon over long testing periods because of its creep.

The basic approach was the brazing of Kovar fittings to ceramic tubes with metal coated ends. The original geometry would then have attached the Kovar fittings as shown in figure 19 for easy removal, however, the sensitivity of the tubes to the torque necessary to seal the fittings caused this technique to be abandoned in favor of attachment by torch brazing the Kovar to the propellant tubes.

The first coating method explored was vapor deposition of a tungsten film (also to be used as a heater) approximately .01 mm (.0004 inch) thick, shown in figure 19. The coating thickness was determined by the heater requirement and not the brazing requirement. First attempts at brazing these samples to Kovar end fittings met with some success in producing leak tight joints but it was also obvious that the braze alloy attacked and dissolved the thin tungsten coating. Interaction of the alloy and coating material is a necessary condition for brazing but the thickness of the coating must be sufficient to prevent its total loss during the time that the alloy melts and flows. When W was abandoned as a heater material, as discussed later, it was also discontinued as a joint coating. It is, in fact, not entirely suitable since it would suffer from long-term exposure to the oxygen component of the propellant ionically diffusion through the ceramic wall.

The next approach, pursued concurrently with the tungsten film deposition, was the application of Liquid Bright Platinum No. 6857 obtained from the Hanovia Liquid Gold Division of Engelhard Industries. This method was described in reference 83 as being successfully used. This is a fine suspension of platinum and proprietary flux materials in an organic solution. It is applied to the ceramic surface with a brush and heated in air to 670°K with good ventilation to burn off the organic matter. Heating is then continued to 1050-1100°K for fifteen minutes or more to bond the metal film to the ceramic.

Brazing of Kovar end fittings to platinum coatings prepared as above was accomplished as follows: The Kovar and platinum surfaces were cleaned with trichloroethylene (vapor degreasing). 82% gold - 18% nickel alloy wire was applied to the fitted joint and the parts heated in three hours to 1280°K, in a hydrogen furnace, and cooled immediately to below the melting point of the alloy (1220°K). The parts were then cooled to room temperature in three hours.

Early results using this technique were successful. There were problems, however. The initial Pt coatings were less than .01 mm thick and were subject to

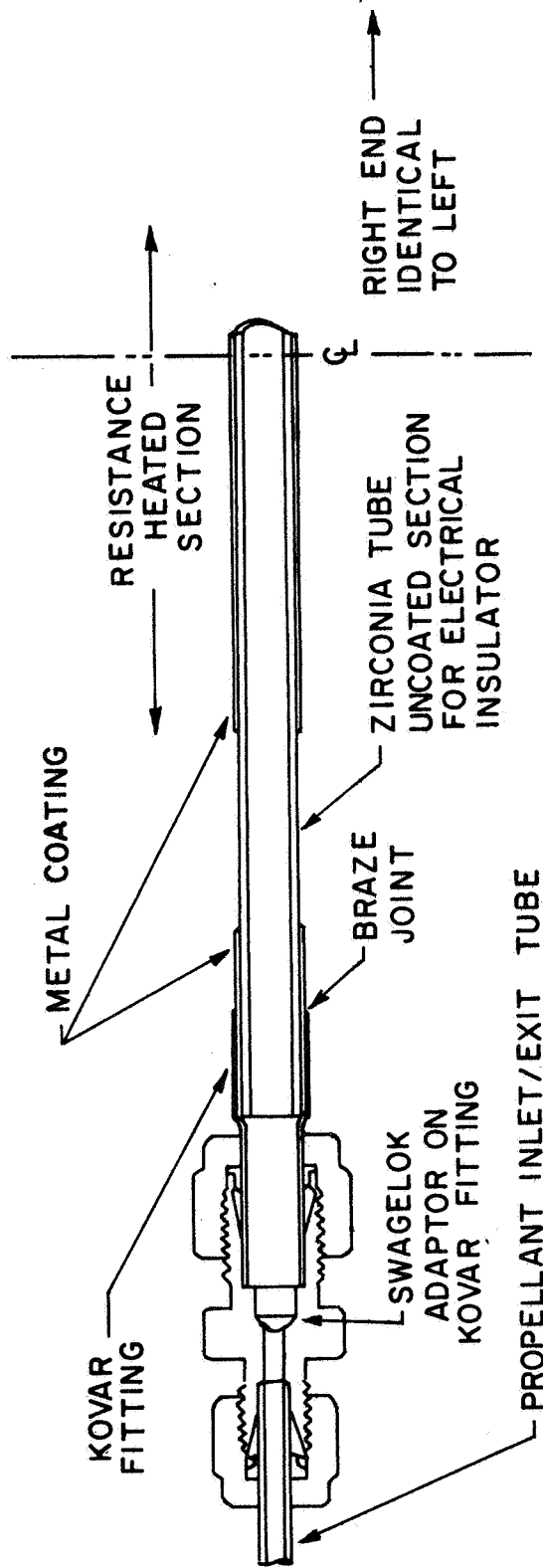


Figure 19.- Test sample configuration.

attack by the filler alloy during brazing. Two steps were taken to eliminate this problem. (1) The braze cycle was changed so that the maximum temperature reached of 1250°K was just above the melting point (1220°K) of the 82 Au- 18 Ni alloy and this temperature was held only for the order of seconds to allow the alloy to melt and flow where previously it had been held at a higher temperature for several minutes. (2) The initial Pt coating was electroplated to produce a thicker metal jacket so that the material could not be completely removed by the alloy.

Two types of electroplating, gold and nickel were initially contemplated. There were reservations about the gold plating because its melting point is close to that of the Au-Ni alloy and nickel was attempted first. Samples of Pt coated ThO₂ and ZrO₂ were plated with Ni to a thickness of .07 mm (.0027 inch) and then brazed to Kovar fittings by the procedure in (1) above.

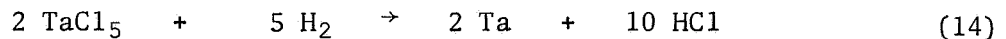
Due, apparently to problems of thermal expansion, the plated metal coatings separated from the ceramic during the braze cycle. At this point it was determined metallographically that the Pt coatings were not forming a good bond to the ceramic and were nearly always removed by a heating and cooling cycle sufficient for brazing. The procedure was abandoned in favor of the tantalum coating process.

Tantalum coating process. - Vapor deposited tantalum coatings were applied to the tube samples by Ultramet, Pacoima, California, using a proprietary process. The essential details of this process are as follows:

The tantalum metal in the form of powder, briquette, or sheet clippings is reacted with chlorine gas to form tantalum pentachloride by the reaction:



The metal chloride is mixed with hydrogen and passes through a reaction chamber. The object to be coated is placed in the reaction chamber and heated to a suitable temperature by induction heating (fig. 20). With the proper gas flow and temperature, found by experimentation, the following reaction takes place:



The tantalum is deposited as a solid coating on all surfaces heated to the appropriate temperature. Surfaces on which a coating is not desired are masked with graphite which is removed at the conclusion. The samples prepared for the subject program were 0.635 cm dia. ceramic tubes with .07 cm walls. The coatings were .005 to .008 cm thick applied over a 2 to 3 cm length on both ends of the 15 to 23 cm long tubes.

Surface defects in the tubes are to be avoided since these can cause cracks in the ceramic during heating.

The coatings produced in this manner have relatively good mechanical adherence to the ceramics but do occasionally separate at elevated temperatures under stress.

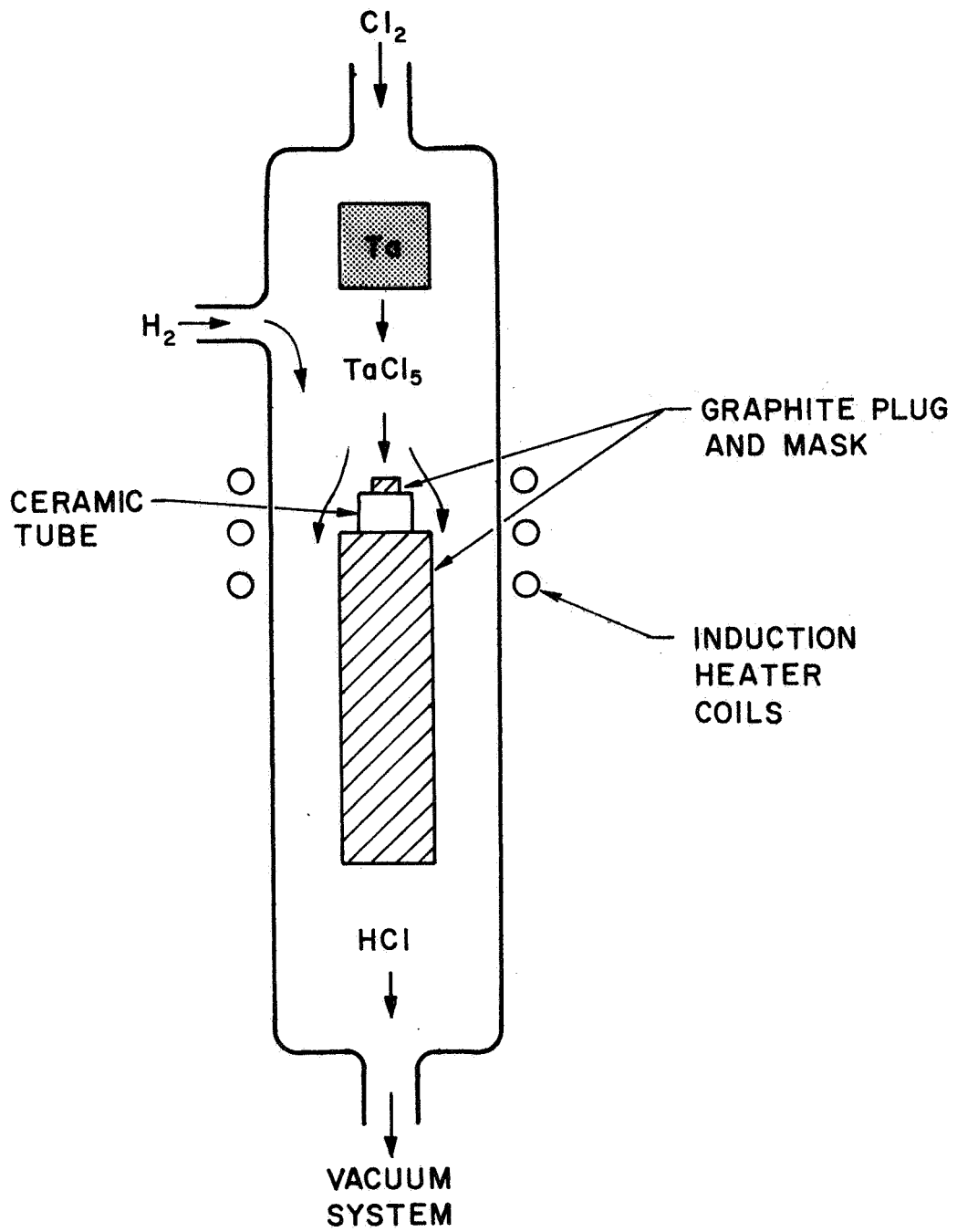


Figure 20.- Vapor deposition process schematic.

Brazing. - To prevent undue stresses the materials involved should have similar thermal expansion characteristics, as shown in figure 21, and should be applied in relatively thin sections. Figure 22 shows the dimensions found to be generally successful.

Kovar fittings were fabricated to fit each individual tantalum coated tube end with .003 to .008 cm radial clearance. Larger clearances were also successful however. The tubes and fittings were cleaned with acetone and assembled. Later samples were cleaned with an Alconox detergent solution in an ultrasonic cleaner and rinsed with acetone. The vacuum tube grade 82% gold - 18% nickel alloy was applied either in the form of wire rings (one ring of .064 cm diameter wire) or slurry. Best results were obtained with the wire. In some cases two rings of wire were applied but this resulted in an excess of alloy which formed a "run" and this sometimes caused a non-uniform stress during cooling or later during the test resulting in separation of the tantalum coating from the ceramic.

The assembly was heated in a vacuum furnace, at 10^{-5} torr, to 1142°K just below the melting point, 1223°K of the alloy over a period of 1 hour and 50 minutes and held 30 minutes. The temperature was then increased to 1256°K and remained above the melt temperature for 5 minutes. Melting was observed through a window in the furnace to insure adequate time for brazing. The furnace temperature was then reduced to 700°K in a period of two and one-half hours. The cooling rate was accelerated over the next 40 minutes to room temperature. A typical braze joint is shown in figure 23.

A number of joints were sectioned and examined to determine the flow of and wetting of the metal surfaces by the braze alloy. These sections also indicated that the tantalum coating formed a physical rather than a chemical bond with the ceramic surface. A typical section photograph is shown in figure 24. Wetting of both tantalum and Kovar surfaces by the alloy is evident.

Samples fabricated by this process and tested for periods of about 100 hours in the presence of nitrogen, hydrogen, CO₂ and steam with joint temperatures of about 600°K have shown no evidence of chemical attack or physical degradation except for the occasional separation traceable to the imposition of non-uniform thermal stresses.

The above process have been used to produce reasonably reliable ceramic-metal seals between Kovar and either thoria or zirconia tubes. These seals can be considered useful to temperatures of at least 600°K.

Improved quality and reliability of these seals and, probably, higher useful temperature can be achieved through greater attention to the quality of the ceramic, better surface preparation such as roughening and cleaning, and optimization of braze geometry and time at temperature. These efforts were not within the scope of the present program.

Other metallizing processes, resulting in physical or chemical bonds to the ceramics, may result in joints that are more dependable when exposed to cyclic thermal stresses, such as those expected in resistojet thrusters, or to higher temperatures. Such processes are currently under investigation.

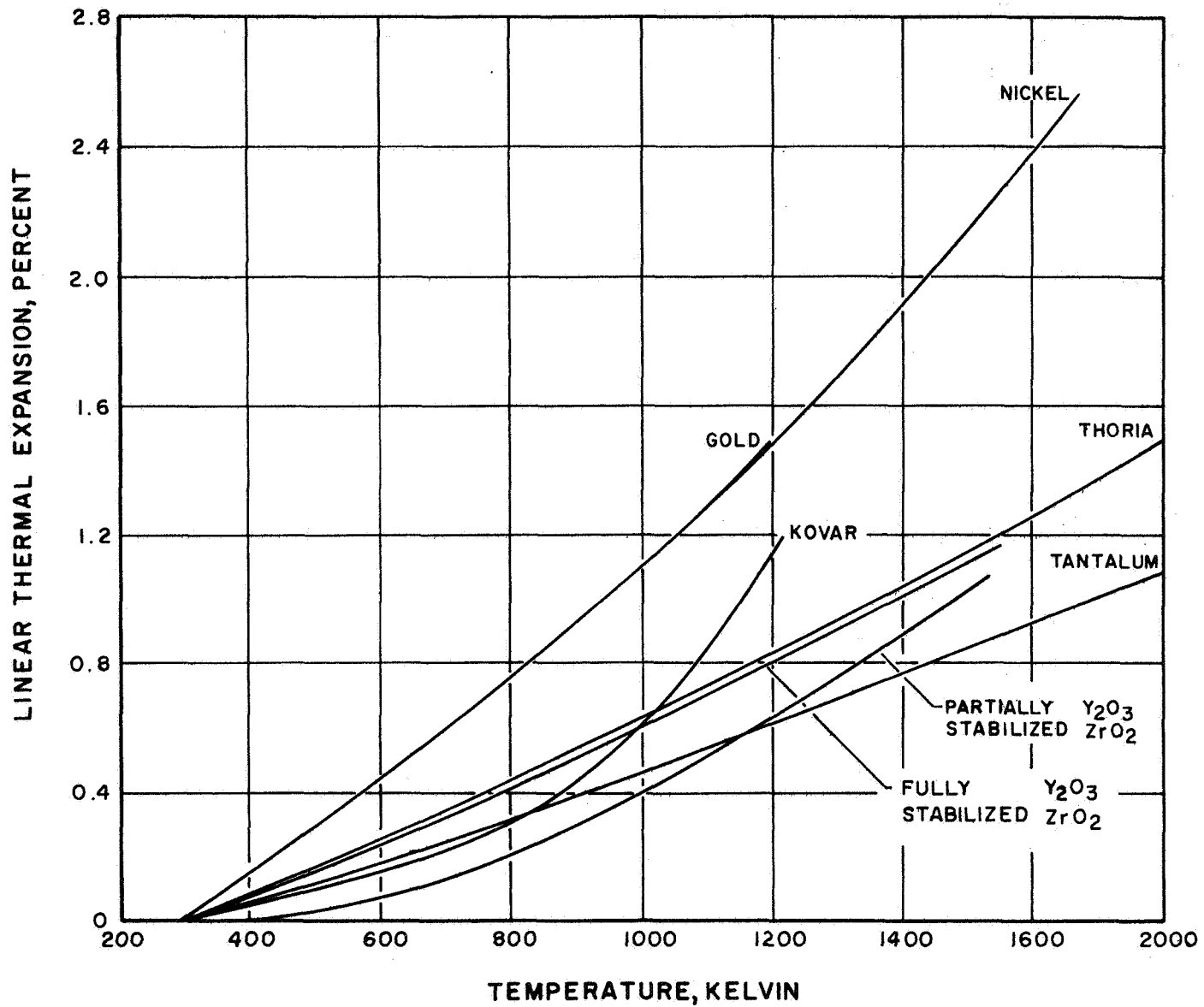


Figure 21.- Thermal expansion comparison of materials used in ceramic-to-metal seals.

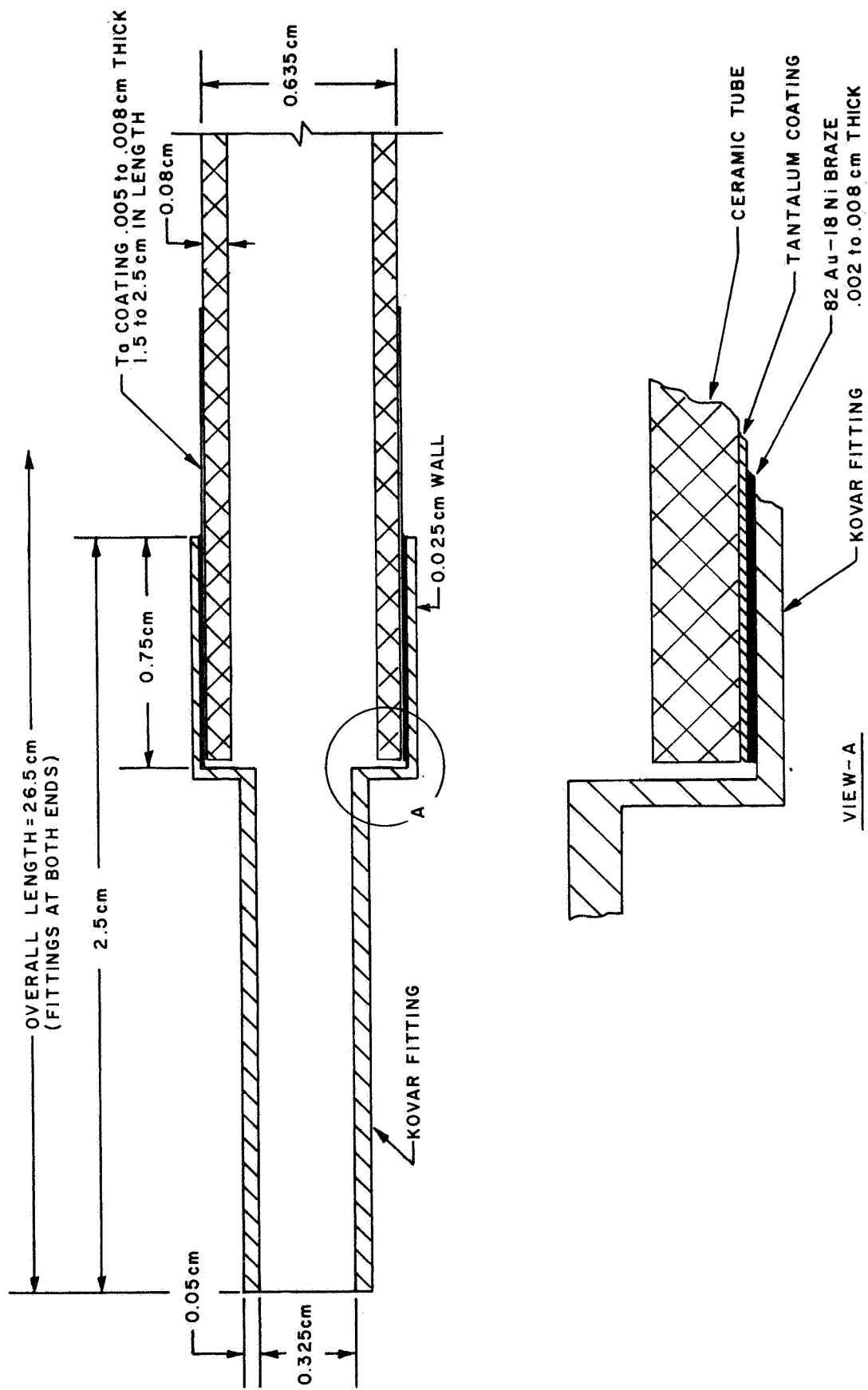


Figure 22.- Seal geometry.

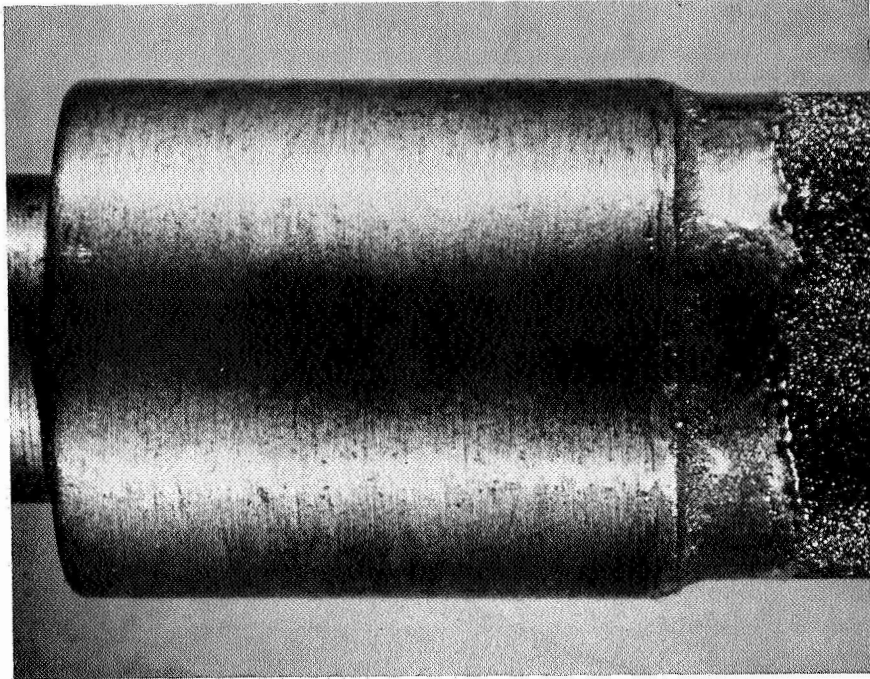


Figure 23.- Kovar to zirconia seal (5.5x).

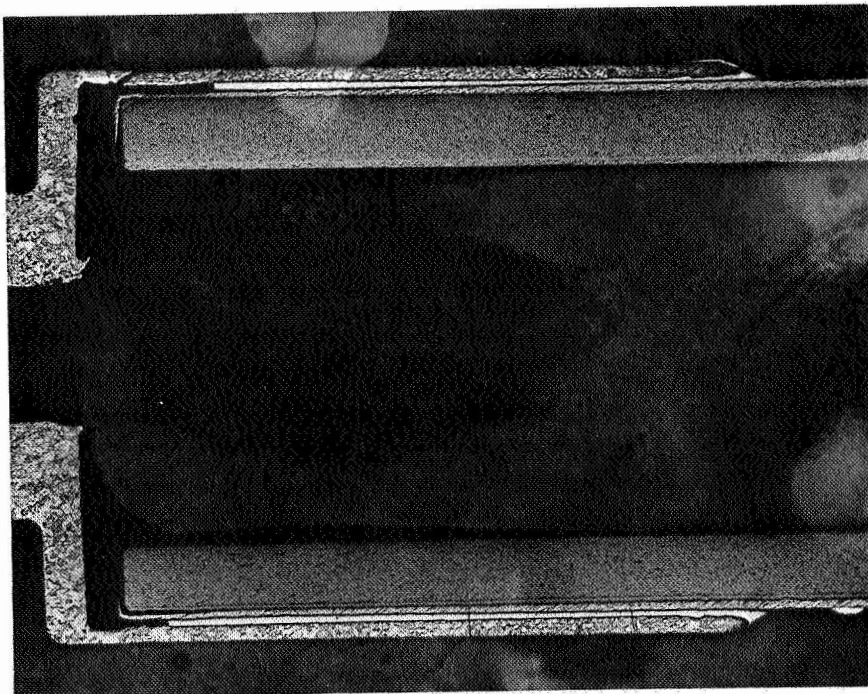


Figure 24.- Kovar to zirconia seal - longitudinal section (11x)

Material Test Apparatus

Vacuum station. - The bell jar vacuum system used for the materials tests is shown in figure 25. The pumping station is a Bendix CVC Model PAS41C capable of producing a vacuum in the 10^{-7} Torr. range. Initial tests were run with the mechanical pump only at a pressure in the 1 to 10 micron range as was the practice of contemporary resistojet material testing. Later tests were run in the 10^{-5} Torr. range in an attempt to get longer graphite test heater life. The propellant enters the system through the baseplate, passes through the tube sample, and exits through the baseplate. Thus, no flow handling capacity is required in the vacuum system and the region of greatest interest is the interior surface of the tube sample.

Instrumentation. - The most important information obtained from the tests was the net ability of the material to withstand exposure to a typical resistojet operating environment. This meant that the environmental conditions during the tests must be known and their effects on the material determined by observation before, during, and after the tests, mainly by microstructural analysis of as-received and post-test samples. The most important parameter to be measured then is the maximum temperature of the test item.

Sample temperature: All of these temperature measurements were made with a Pyrometer Instrument Company Micro Optical Pyrometer, Model 95. Measurements made with this instrument are based on black body radiation and were corrected for the conditions of the experiment according to the analysis presented in Appendix A. For temperature differences of less than 60°C between heater and sample, the indicated sample temperature is very close to the true temperature.

Propellant flow rate: Propellant flows were measured with a Brooks Model 1214-1560 laboratory flowmeter system. This is a conventional glass tube rotameter with interchangeable tubes and floats for various propellants and flow rates. Accuracy of this type of meter is in the ± 1 to 2 percent range, more than sufficient for these tests.

Propellant pressure: Pressure measurements were made with a bourdon tube gage with 1 percent accuracy.

Bell jar vacuum: A conventional thermocouple gage was used. (HVEC model G-91-1.)

Heater voltage and current: A Honeywell model 333R Digital Voltmeter with a calibrated shunt was used for the electrical power parameters.

Temperature: Lower temperatures on the test items, fittings, and fixtures were measured with chromel-alumel thermocouples indicated on the digital voltmeter or a Leeds & Northrup K-3 Potentiometer.

Test fixture and heater geometries. - The general test schematic is shown in figure 26. The problem of heating small samples of the type used in this program is considerably more difficult than it first appears. Small metallic tubes are easily heated resistively to $\sim 1600^{\circ}\text{K}$. The problem is compounded by the requirement, imposed by the initial ground rules, of indirectly heating the ordinarily non-conductive ceramic materials in addition to the much higher temper-

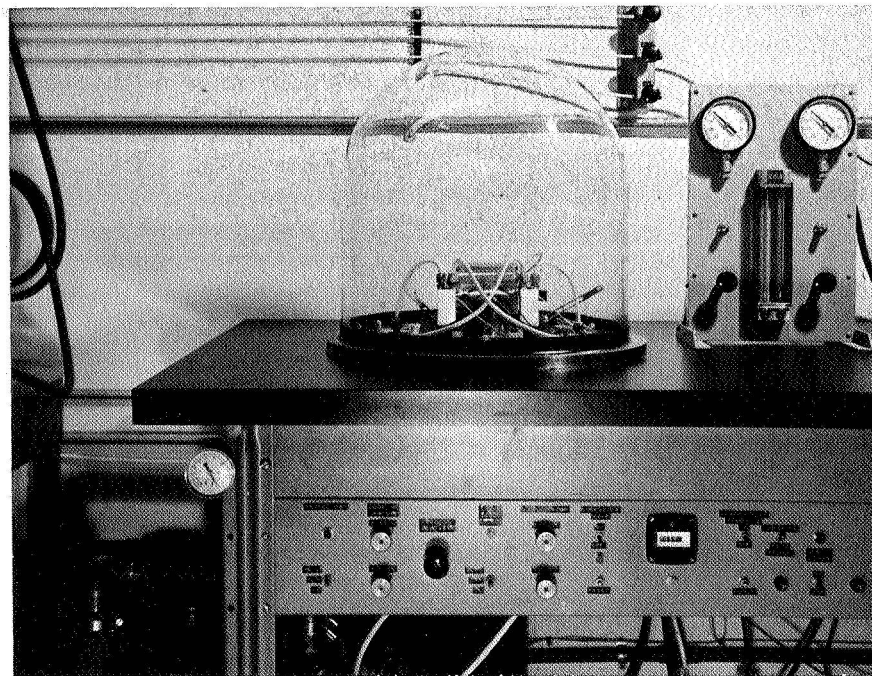
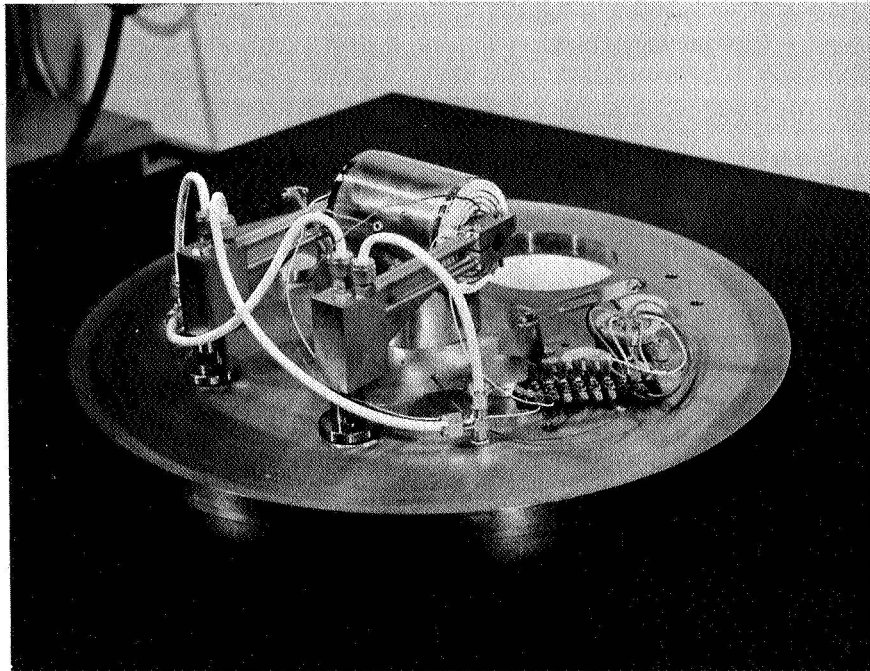


Figure 25. - Material test apparatus.

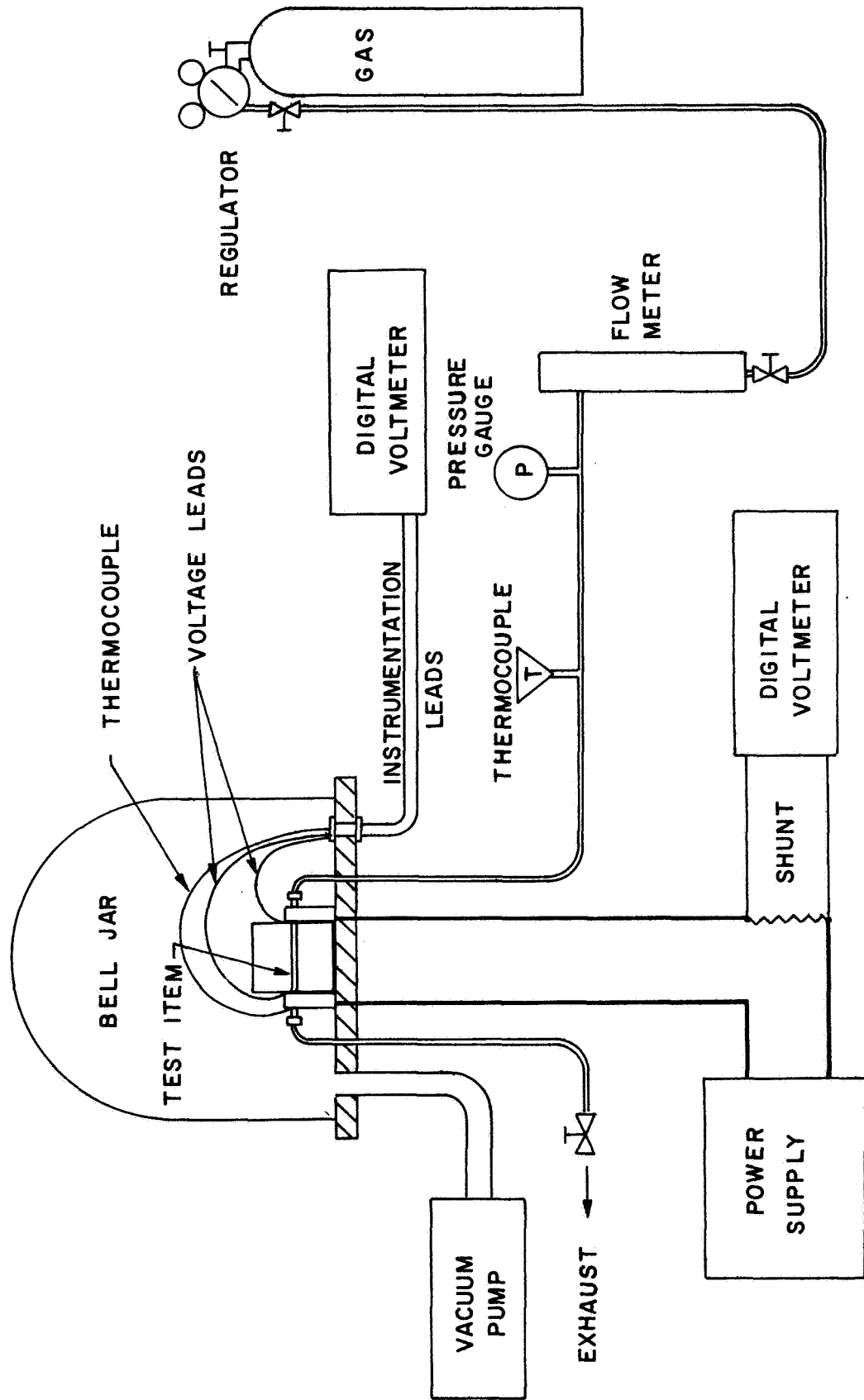


Figure 26.- Test schematic.

atures desired. The auxiliary heater transfers the heat to the test sample with a lower efficiency resulting in a greater loss than in the case of direct heating. A number of heater configurations were considered and several attempted before a workable system was found. These are briefly discussed below.

An induction heater was considered but rejected because most of the samples are non-conductive (at low temperatures) and a graphite susceptor would have been required and this could have been more easily heated resistively. Also, the high frequency power inputs would have resulted in other problems. Auxiliary resistance heating was selected as the simplest and most efficient method.

The first resistance heater was a slotted graphite cylinder designed to accept a relatively low current, since a straight cylinder would have required a prohibitively high current of several hundred amps. This first heater was used to reach test item temperatures of the order of 1600°K using a Perkin Model MR1040-30B to supply heater power. Losses to the surrounding equipment were high, however, due to the relatively large external radiating surface of this heater.

The second method attempted was a vapor deposited coating of tungsten, less than 0.01 mm thick, described earlier and shown in figure 19, forming a resistance heater in direct contact with the material sample. The tungsten coatings were chosen for chemical compatibility with the ceramics, temperature capability, and relative ease of deposition. The electrical characteristics of this configuration were favorable, giving 11 volts and 10 amps at the peak power. However, the film began to break down at 1338°K, as evidenced by the formation of a local hot spot and the local temperature gradient in the tube caused it to fracture at that point. This failure could be caused by one or more of the following:

1. Differential expansion: Thermal stresses in the W could have caused it to separate locally and overheat because of the lack of thermal conduction to the ZrO₂.
2. Instability: ZrO₂ becomes an effective electrical conductor at these temperatures. It was physically in parallel with the film heater with no ballast resistor in series. Without ballast, high electrical current locally on the circumference may have occurred.
3. Chemical attack on heater: The ZrO₂ wall could have become an oxygen transporter from the O₂ species present in the flowing dissociated CO₂ gas causing oxidation attack on the W.

The next heater geometry employed was a coil of W-26 Re wire wound tightly around the ceramic tube to give as much efficiency in heat transfer as possible. The heated section was approximately 5 cm in length, consisting of 25 coils. From the corresponding measurements of the wire and tube, the temperature difference was found to be small. Specifically, for a tube temperature of 1670°K, the heater coil temperature was 1730°K for a difference of approximately 60°K. Unfortunately, in the test vacuum evaporation of metal from the heater coil was sufficient to permit the deposition of a thin metal film on the surface of the ceramic tube in the matter of a few hours. This resulted in an intermittent short circuit of the heater coils with arcing between the coils and the deposited metal film. Use of such heater coils at these temperatures could possibly be encapsulated but not bonded to the ceramic in an attempt to prevent this short-circuit problem from

occurring. However, the thermal shock problem cannot be avoided. Figure 27 shows sample and wire temperature for Test 4, as a function of power input, representing the case of the coil in near contact. A ΔT of some 200°K is required. A maximum sample temperature of 1745°K was reached.

A series of tests were then run in an unsuccessful attempt at suppressing this deposition by adding an inert atmosphere (argon) at various pressure levels and reducing the required ΔT between heater and ceramic. The inert atmosphere tended to suppress the deposition but not to the extent necessary. The high temperature heater wire coil was abandoned.

The slotted graphite cylinder, originally dropped in favor of the two previously mentioned "easier" approaches, was reconsidered at this point. Careful redesign of the heater with a smaller heated section and much less external area for radiation resulted in more efficient heating of the test item (figure 28). The addition of better insulating structures, water cooling for the heater power clamps, and a water cooled shroud to protect the bell jar from overheating resulted in a workable test system capable of temperatures up to 2500°K. The final design of the test apparatus is shown schematically in figure 29.

Test description. - The following describes briefly the tests conducted:

The samples used for each test are listed in Table IX and an array of sample types is shown in figure 30. The tests are summarized in Table X. Included are heater and seal development tests as well as those for propellant compatibility. All fittings were made of Kovar and attached to the metallized samples with 82% gold - 18% nickel braze alloy. Details of the metallizing processes and the braze cycle were described earlier.

The tests, in the main, were not terminated by failure of the sample but by test equipment causes. Thermally induced movement of the components of the apparatus permitted the sample to contact the closely coupled graphite heater resulting immediately in a crack in the sample allowing gas leakage. The other tests in this last group were usually terminated when the heater had been eroded to the point where it could no longer effectively transfer heat to the sample or by heater breakage near this point of ineffectiveness.

The cause of this erosion may be minute leaks allowing CO₂ to escape into the bell jar and remove the heater material by oxidation or O₂ background level in the bell jar. It is also felt that the transmission of oxygen through the walls of the tube might be the reason. The problem occurred, however, with no gas flow, with nitrogen flow, and also when the system was known to be tight.

The cause was then thought to be the background level of oxygen in the 10⁻² torr. vacuum. Tests with hydrogen flow reduced the heater degradation to zero. Whether leaking from the flow system or through the tube walls, the hydrogen certainly, by its presence, prevented the removal of heater material. At the time, it was thought that longer heater life might have been due to somewhat lower pressures in the bell jar during the H₂ tests. It was later discovered in tests at 10⁻⁵ torr., however, that heater deterioration was as rapid as at the higher pressures. Either the background oxygen level is still a problem or some other mechanism is responsible.

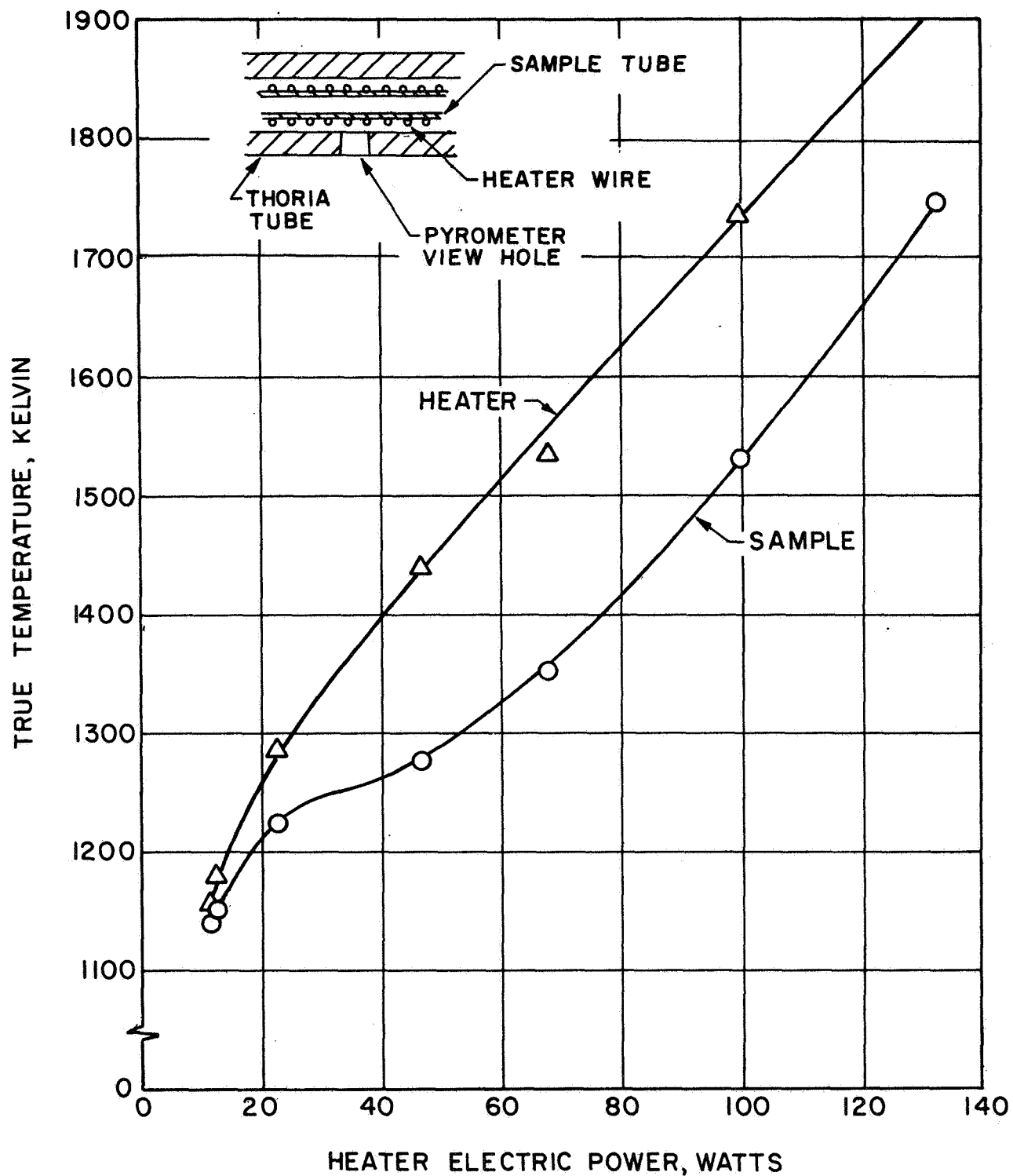
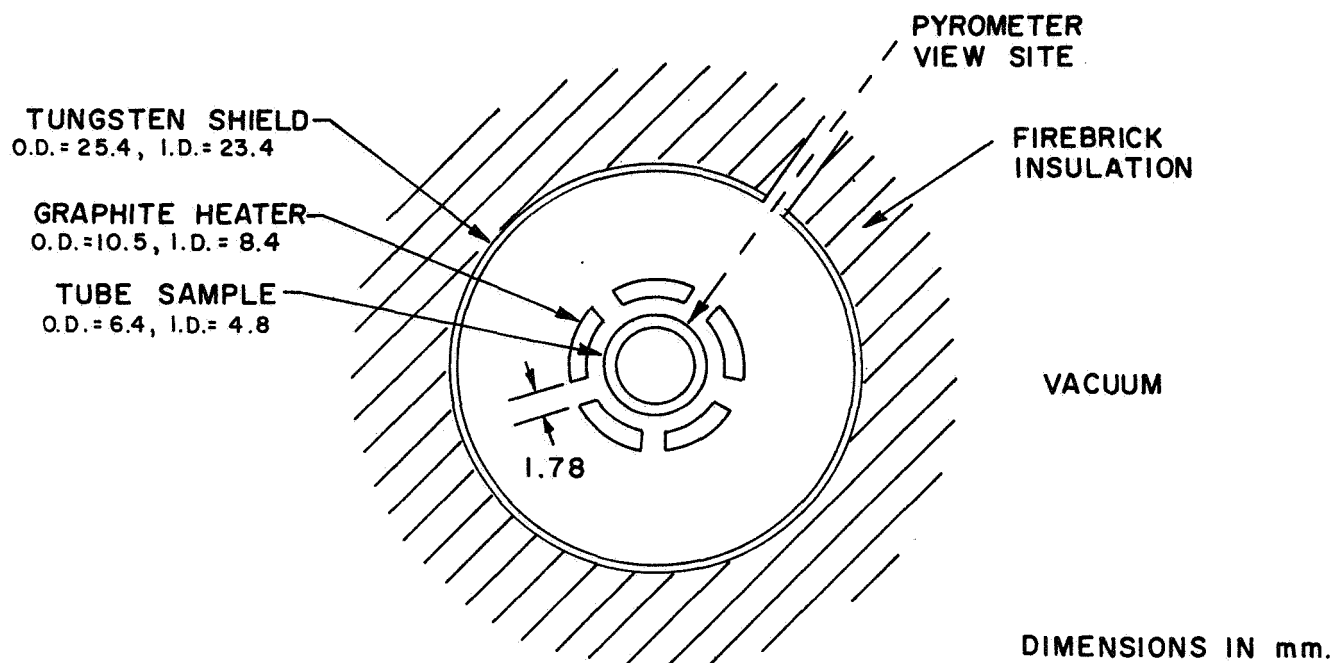
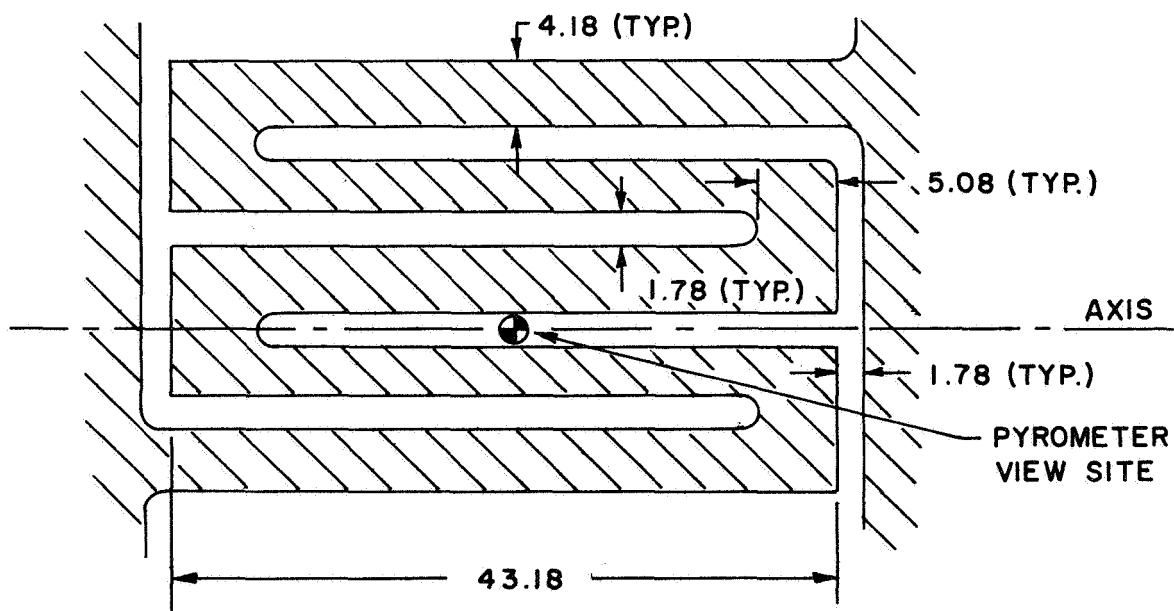


Figure 27.- Coil heater - sample temperature difference vs electric power - Test #4.



(a) Cross section



(b) Rolled-out view of heater pitchline

Figure 28.- Test heater - sample geometry.

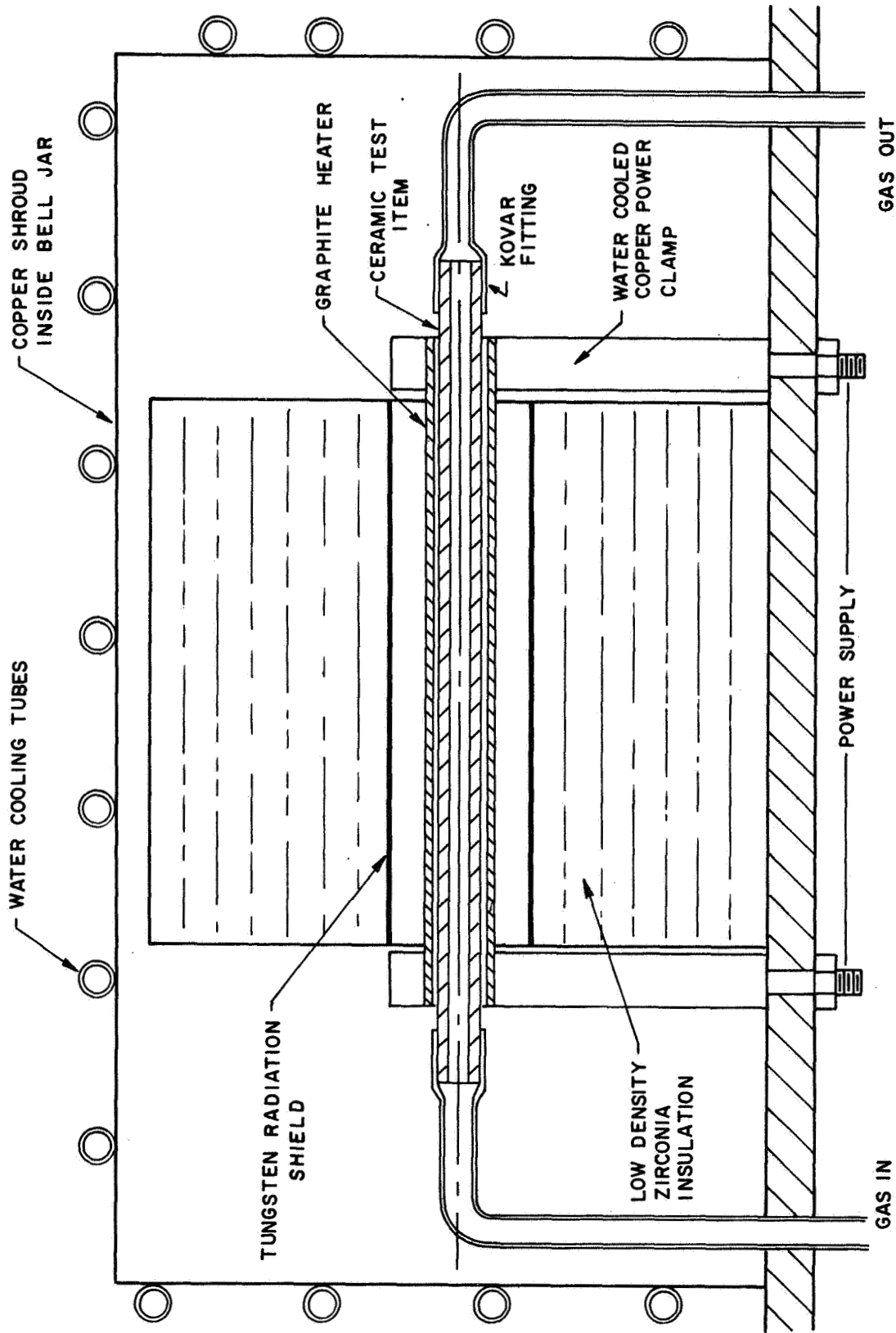


Figure 29.- Longitudinal cross-section of experimental apparatus.

TABLE X. - SUMMARY OF TESTS

Test	Mat'l	Sample type ^a	Test sample length cm	Gas	Flow g/s	Pressure atm.	Sample temp. °K	Test duration hr	Heater type	Metal-lizing	Test objective	Reason for test term.
1	ZrO ₂	A	15	CO ₂	.01	1.7	1338	2	(b)	W	(g)	(l)
2			15	None	-	-	1574	2	(c)	-	(g)	(m)
3			15	CO ₂	.01	1.7	1133	1	(c)	(f)	(g)(i)	(n)
4			30	CO ₂	.01	1.7	1745	1	(c)	(f)	(g)	(o)
5	ZrO ₂	B	15	None	-	-	-	1	(c)	-	(h)	(o)
6	ZrO ₂	A	15	None	-	-	2003	2	(d)	-	(g)	(m)
7	ThO ₂	E	15	CO ₂	.01	1.7	2098	1	(d)	Pt	(g)(i)	(p)
8							1023	-			(g)	(p)
9							1603	-			(g)	(n)
10	ZrO ₂	D	15	CO ₂	.01	1.7	2103	2	(e)	Pt	(g)	(p)
11							-	-			(g)	(n)
12	ZrO ₂	A	15	CO ₂	.01	1.7	1833	22	(e)	Ta	(j)(i)	(n)
13	ThO ₂	F	15	CO ₂	.01	1.7	1833	47	(e)	Ta	(j)	(p)
14	ZrO ₂	A	20	CO ₂	.01	1.7	1188	-	(e)	Ta	(j)	(l)
15			23	CO ₂	.01	1.7	1835	24				(l)
16			23	H ₂	.001	1.15	1856	90				(q)
17			23	N ₂	.02	1.7	1848	122 ^r				(m)
18			23	CO ₂	.01	1.7	1950	44				(l)
19	ZrO ₂	A	17	None	-	-	2049	-	(e)	Ta	(k)	(m)
20	ZrO ₂	A	15	H ₂ O	.01	1.2	1888	1	(e)	Ta	(j)	(n)
21			23				1938	49				(l)

NOTES

- a See Table IX for sample description
- b W film
- c Coil of 0.05 cm diam. W-26 Re wire
- d Graphite heater
- e Graphite heater (figure 28)
- f Nylon fitting
- g Heater development
- h Attempt to suppress vaporization w/Ar atmosphere
- i Propellant fitting development
- j Chemical compatibility test
- k See Appendix A
- l Heater failure causing sample failure
- m Voluntary
- n Fitting failure
- o Heater shorted by deposited film
- p Heater failure
- q Tube failure, leak
- r Additional 10 hrs with no flow, 2006°K

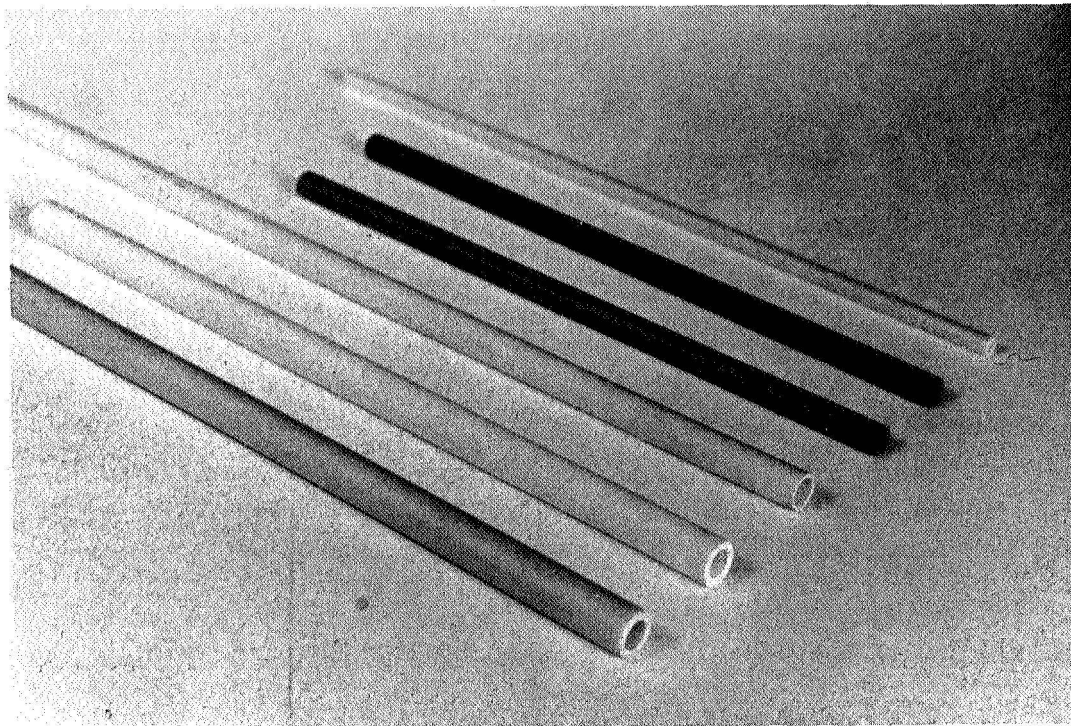


Figure 30.- Array of sample types.

ANALYSIS OF DATA

The search for high temperature chemical reactions of propellant gases with the candidate ceramic walls employed the following techniques:

1. Visual inspection for gross effects.
2. X-ray diffraction for composition, possible reaction products, and purity.
3. X-ray fluorescence for elemental identification.
4. Optical micrography for grain size, porosity, new phases and any anomalies.

The samples microstructurally analyzed are listed in Table XI. There, the axial position of the heated section and the station of temperature measurement are noted. The micrographical sections, etc., are identified by the axial location on the same basis and thus may be related to the test. A section at the temperature measurement site was made in each case. The later site was not necessarily the hottest section on the sample but had the advantage that its temperature history was known.

Information on As-Received Tubes

The ZrO_2 tubes obtained from Zircoa, described in Table IX, were all slip-cast and partially stabilized with Y_2O_3 at about 8 weight percent. The ZrO_2 tube from Coors, Test 10, was isostatically cold-pressed and sintered and was also partially stabilized with Y_2O_3 at 8.4 weight percent. The manufacturer reported it as having a closed pore structure. The ThO_2 tube, Test 13, obtained from Zircoa, was slip-cast.

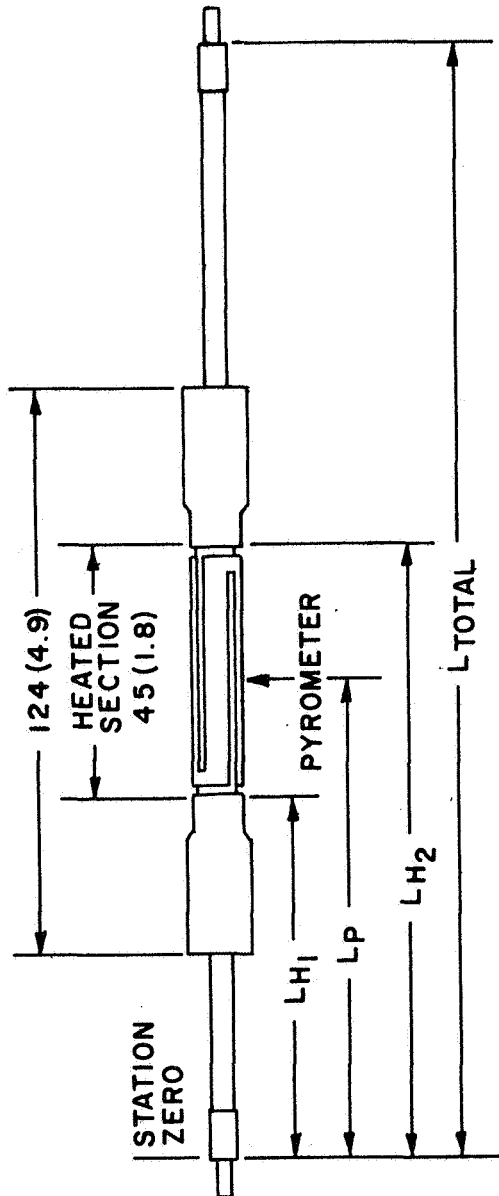
Aside from the stabilizer, all these tubes were reported by the manufacturer as having a purity of 99+%. In the case of ZrO_2 , the most important impurities are known to be SiO_2 , TiO_2 , MgO , Al_2O_3 , and Fe_2O_3 ; all adding up to less than 1% by weight. A minor impurity in the ThO_2 is HfO_2 .

In order to verify the purity and composition of the as-received tubes, one ZrO_2 and one ThO_2 tube were subjected to x-ray diffraction analysis. Table XII shows the d-distances obtained from the diffraction pattern for ZrO_2 in comparison with cards from the ASTM diffraction data file and Table XIII shows the same for ThO_2 .

From Table XII, it is seen that most of the diffraction pattern of the as-received tube agrees with the cubic, fully stabilized pattern while three low-angle peaks agree with the unstabilized, monoclinic pattern. This is to be expected for partially stabilized zirconia.

The diffraction pattern of the as-received ThO_2 is typical of that for cubic ThO_2 . Two very low intensity peaks were found in addition to those listed in Table XIII at $d = 2.87\text{\AA}$ and $d = 1.64\text{\AA}$. An explanation for their presence has not been found.

TABLE XI. - AXIAL POSITIONS OF KEY TESTS - mm (inches)



Test	Material	Gas	L_{H1}	L_P	L_{H2}	L_{total}
10	ZrO ₂	CO ₂	48 (1.9)	71 (2.8)	93 (3.7)	155 (6.1)
13	ThO ₂	CO ₂	46 (1.8)	69 (2.7)	91 (3.6)	155 (6.1)
16	ZrO ₂	H ₂	62 (2.4)	84 (3.3)	106 (4.2)	231 (9.1)
17	ZrO ₂	N ₂	76 (3.0)	99 (3.9)	121 (4.8)	231 (9.1)
18	ZrO ₂	CO ₂	76 (3.0)	99 (3.9)	121 (4.8)	203 (8.0)
21	ZrO ₂	H ₂ O	79 (3.1)	101 (4.0)	123 (4.9)	231 (9.1)

TABLE XII. - X-RAY DIFFRACTION DATA ON ZrO₂

Analysis of ZrO ₂ as-received tube, partially stabilized	Comparative data from ASTM file				
	Cubic ZrO ₂ , fully stabilized ^a		Monoclinic ZrO ₂ ^b		
	d-distances Å	d-distances Å	h k l	d-distances Å	k h l
3.67				5.05	100
3.15				3.69	011
2.94	2.92	111		3.63	110
2.84				3.16	111
2.55	2.53	200		2.84	111
1.81	1.80	220		etc.	etc.
1.54	1.53	311			
1.478	1.464	222			
1.274	1.267	400			
1.178	1.164	331			
1.146	1.133	420			
	etc.	etc.			

^a ASTM Card No. 7-337.

^b ASTM Card No. 7-343 (no stabilization)

TABLE XIII. - X-RAY DIFFRACTION DATA ON ThO₂

Analysis of ThO ₂ as-received tube	Comparative data from ASTM file	
	Cubic ThO ₂ ^a	
d-distances Å	d-distances Å	h k l
3.21	3.234	111
2.80	2.800	200
1.97	1.980	220
1.68	1.689	311
1.61	1.616	322
1.394	1.400	400
1.281	2.284	331
1.251	1.252	420
1.141	1.1432	422
	etc.	etc.

^a ASTM Card No. 4-0562.

From a cross sectional view of the as-received ZrO_2 tube, figure 31a, the particle size, was found to be about 25μ for most of the grains with some grains finer. The grains were brought out through etching with phosphoric acid at $520^\circ K$. For the as-received ThO_2 tube, shown in figure 31b, most of the grains again have a diameter of about 25μ .

Both the zirconia and the thoria tubes, types A and F in Table IX, are rated as "impervious" by their manufacturers. Figure 31 shows them both to be quite porous, particularly the ThO_2 . No gas leakage was experienced with these types of tubes. This is evidently not interconnected porosity.

Tested Tubes

Visual inspection. - Representative photographs of samples after test are shown in figure 32 for tests 16, 17, and 18. An obvious feature along sections of most tubes was the darkening and graying and in certain areas strong darkened bands and rings, whose color also could be tints of yellow, brown, and pink. In those cases where the graphite heater broke through wear and rested on the ceramic tube, pin holes or small cracks in the tube were observed.

The identity of the dark coating, bands, and rings of various tints is discussed in the following sections. Possible causes were thought to be (1) deposition and subsequent diffusion of metal oxide or carbon from the shield or heater, (2) contamination or deposition from other sources in the environment, or (3) migration of Ta from the metallized section or of Au (yellow tinted rings) or Ni from the brazing alloy. The deposition of C or oxides of W was thought to be the most likely cause.

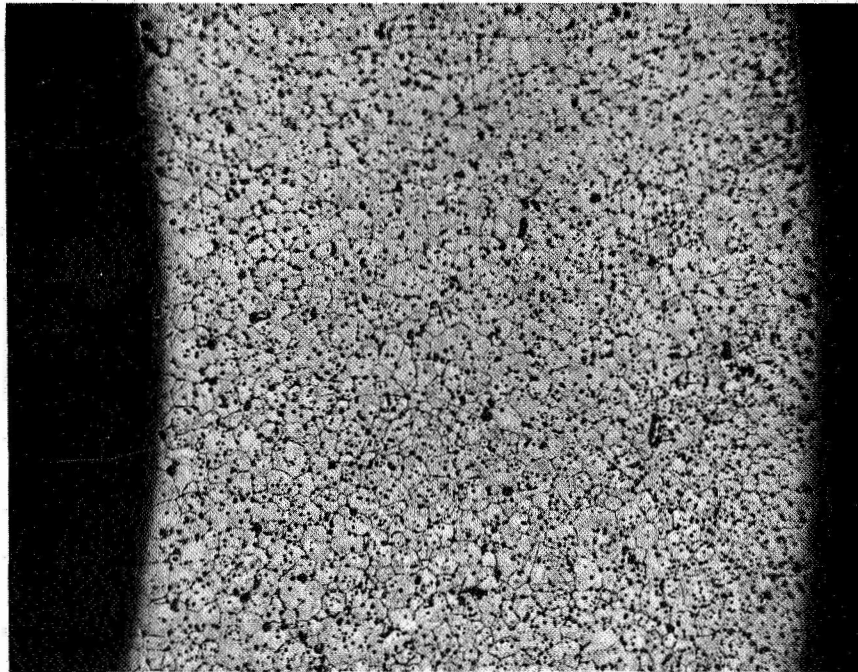
X-ray diffraction analysis. - This analysis was performed on a Norelco Diffractometer, Type No. 12045. The purpose of this analysis on selected samples was an attempt to identify the stained areas on the tubes, verify any changes in the composition of the tube, and identify any reaction product between tube and gas.

All measurements at the important temperature measurement sites for ZrO_2 showed only the partially stabilized zirconia, that is cubic plus some monoclinic phase and for ThO_2 the cubic pattern. These measurements were made on the internal surface of the tube.

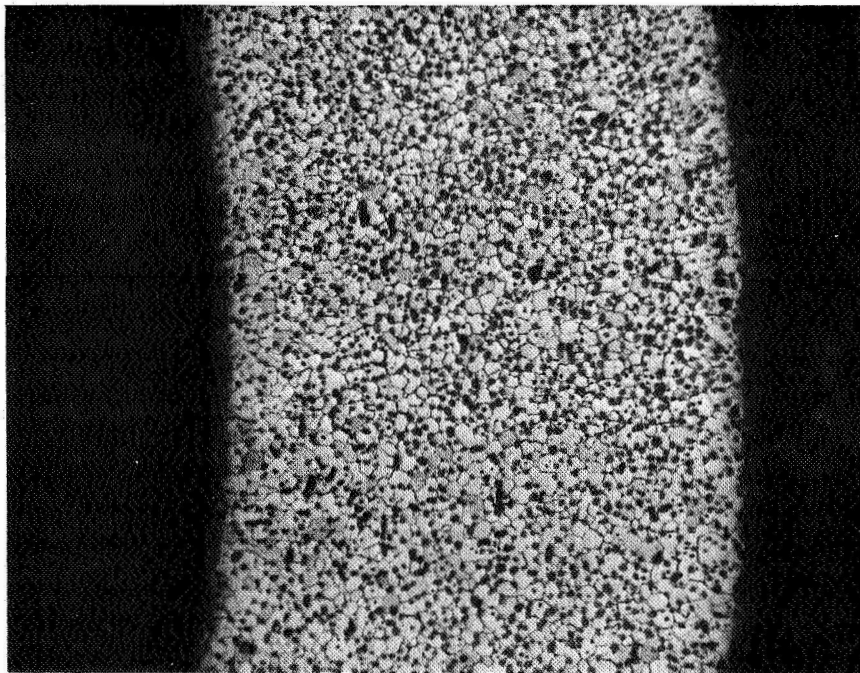
Table XIV shows the x-ray diffraction analysis on selected sites for stain identification purposes.

It should be remarked that x-ray diffraction analysis does not detect compounds in concentration below about 1%. It is, therefore, not surprising that no contamination was detected from the stained areas and rings on several of the samples in Table XIV since the coatings were extremely thin. In one case, however, Test 17, on N_2 graphite was indicated. This was the sample that had been subjected to the longest test run, 122 hours. It was found on the internal surface only downstream of the test section as a coating (station ~ 8 in.). The sample was also run 5 hours on CO_2 and 3 hours on H_2 as a check on gas type influence on graphite heater wear rate.

In a couple of samples unidentified peaks were found. Obviously, therefore, something other than graphite was present in the stained areas and rings. In an attempt to resolve this further, the presence of elements in these areas was examined by the more sensitive x-ray fluorescence technique discussed later.

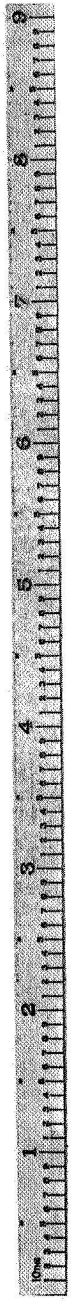


(a) ZrO_2 8 w/o Y_2O_3 (100x)

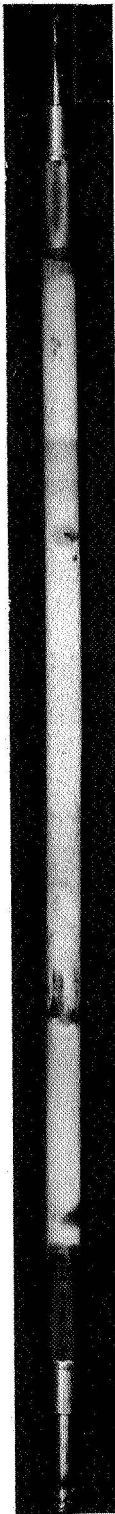


(b) ThO_2 (100x)

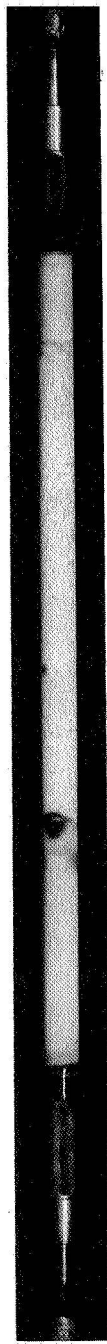
Figure 31.- Cross-sectional view of as-received Zircoa tubes.



(a) Test 16 (H_2)



(b) Test 17 (N_2)



(c) Test 18 (CO_2)

Figure 32.- After-test record photographs of representative ZrO_2 samples.

TABLE XIV.- X-RAY DIFFRACTION ANALYSIS OF SELECTED MATERIALS

Test No.	Area analyzed	Station (in.)	Results
10	Dark stained areas on external tube wall.	At 1 and 4.1	No graphite, carbon or Pt detected. Pattern of partially stabilized ZrO ₂ shown. Unidentified peak at $d = 2.56\text{\AA}$.
13	Dark stained area, yellow brown and pink rings at hot end of tube, external wall.	From 4.5 to 5.5	Shows typical cubic ThO ₂ pattern. Two unidentified peaks observed at $d = 2.87\text{\AA}$ and $d = 1.635\text{\AA}$.
16	Dark area of external tube wall towards hot end.	From 7.0 to 8.0	Shows partially stabilized ZrO ₂ Contaminated area below detection limit of x-ray diffraction method.
17	Dark area at internal tube wall. Adjacent to joint at hot end.	From 7.5 to 8.5	Small peak at $d = 3.36\text{\AA}$ agrees with strongest graphite reflection. Otherwise ZrO ₂ pattern shown.

According to reference 86, temperatures above 2200°K are apparently required before ZrO₂ reacts extensively with carbon to form ZrC. No ZrC was detected in any of the analyses performed here. The carbon (or graphite) found in the wall of the ceramic tube arrived there by diffusion. According to reference 87, however, the reaction $\text{ThO}_2 + \text{C} \rightarrow \text{ThC}_2$ may occur at a temperature as low as 1375°K if powders of ThO₂ and C are compacted together and, therefore, are in intimate contact. The two unidentified peaks found for the sample of Test 13 do not correspond to the x-ray diffraction pattern of ThC₂.

It should be explained that carbon (or graphite) would not be deliberately incorporated in a resistojet design. The interaction is discussed here to explain results observed.

In the literature survey presented earlier on the possible reactions between the gases CO₂, CO, H₂O, H₂, O₂, N₂, and NH₃ with ZrO₂, ThO₂ and ZrB₂, there are no known reactions to 2200°K except between NH₃ and ZrO₂ and possibly between H₂O and ZrO₂. This latter one, only, is of interest here. It is based on an abstract from a Russian article (ref. 50), but unfortunately, there is no mention of the temperature at which such reaction occurs. In any case, the test 21 was conducted in flowing H₂O gas to 1895°K and no zirconium hydroxide, if formed, was found at the internal wall of the ZrO₂ tube. All ZrO₂ and ThO₂ patterns found correspond to the pattern given for the phases in Tables XII and XIII.

X-ray fluorescence analysis. - The x-ray fluorescence analyses that were performed are shown in Table XV. The analyses were performed on a Norelco Vacuum Spectrograph, Type No. 52157-A.

The areas analyzed were generally stained. No unexpected elements were found except traces of iron. Some Ta appeared to have diffused through the tube wall underneath the Ta coating. Carbon is not detectable with this equipment except when using a sterate analyzing crystal, which was not available. Iron is present as an impurity in the zirconia tube material.

TABLE XV. - X-RAY FLUORESCENCE ANALYSIS OF SELECTED SAMPLES

Test No.	Area analyzed	Station (in.)	Results
10	Stained area	4.1	Spectral scan of all elements down to Mg, negative, except for those known to be present, such as Zr and Y.
12	(1) Tube section at Ta coating towards end, but outside joint. (2) Same but under Ta coating.	4.8	(1) Only Ta, plus Zr and Y indicated. Au, Ni and Fe absent. (2) Only Zr and Y indicated.
17	(1) Internal tube wall adjacent to joint.	8.5	(1) Besides Zr and Y, traces of Ta and Fe found.

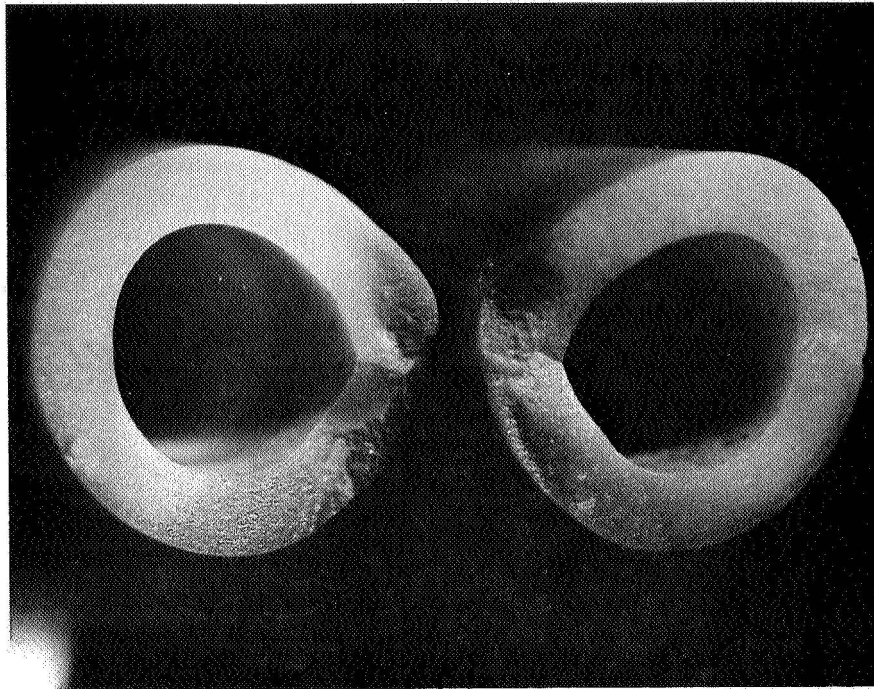
Optical micrography. - Photomicrographs were taken on some longitudinal and transverse cross sections on selective samples to observe the integrity of the tube with respect to stresses imposed and growth of grain size. The main purpose, in the joint area, was to examine the effectiveness of the bond in the metallized and brazed area. The work was carried out with a Leitz Model MM5 Research Metallograph. Table XV summarizes the findings.

Figure 33 is a typical example of a fractured or cracked ceramic tube wall caused by the failing or broken graphite heater resting on the ceramic tube. Referring to Table X, this type failure represented the major cause of test interruption (thermal shock) and clearly indicates the basic current emphasis on direct heating concept for advanced biowaste design which has solved this problem putting test times in 10^3 hour class, at present (ref. 79).

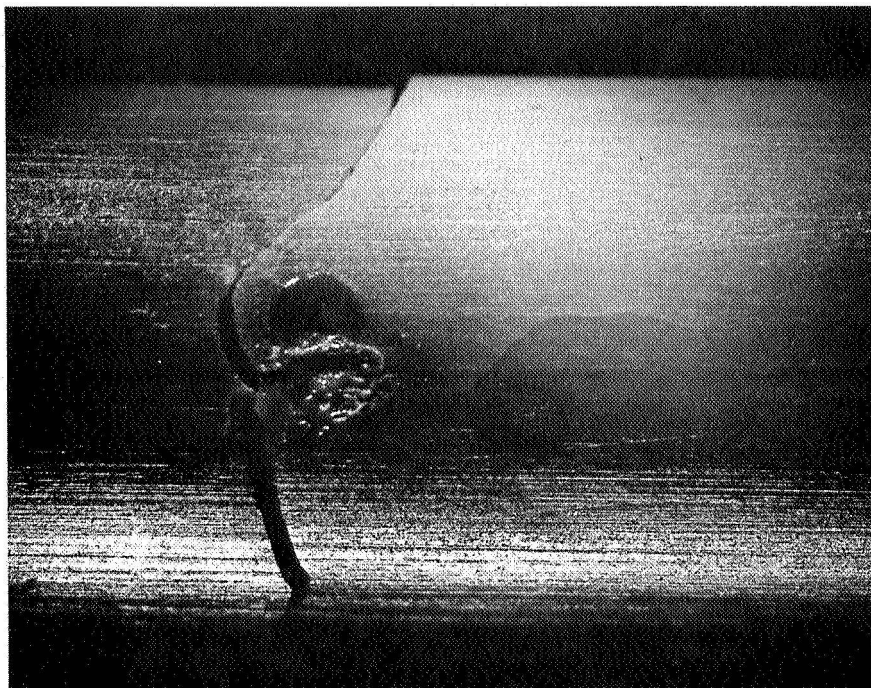
Figure 34 shows longitudinal and cross sectional view of the hot fitting for Test 13 (ThO_2 and CO_2 gas). The apparent poor bonding between Ta metallizing and ceramic and between niobium brazing alloy and the external Kovar tube after 47 hours is shown. No leakage was experienced during the test, however. A principal conclusion of these test runs is that the ceramic-to-metal bonding technology used is questionable for long-term, 10^4 hour, usage.

TABLE XVI. - OPTICAL MICROGRAPHY OF SELECTED MATERIALS

Test No.	Area analyzed	Observations and figure no.
10	(1) External macroview of the tube fractured near arc spot near Station 4.1 in.	(1) Shows tube fracture near arc-like spot, Figure 33. No component identification made.
13	(1) Longitudinal view through joint at hot end. (2) Cross sectional view through joint at hot end.	(1) Shows large void between Ta coating and Kovar tube, indicating insufficient flow of niobium braze alloy, Figure 33a. (2) Shows insufficient bonding between Ta coating and ThO ₂ and between niobium braze alloy and Kovar tube, Figure 33b. Joint was leak tight.
16	(1) Cross sectional view of tube at Station 3.3" at hot point of midsection where darkening had extended through wall 360° around circumference.	(1) Shows darkening through wall. Could be graphite or suboxide caused by H ₂ reduction. Microstructure of ZrO ₂ tube wall after 90 h in H ₂ at 1856°K.
17	(2) Cross sectional view at Station 7.5" where wall is light. (1) Cross section at Station 3.8". (2) Cross section at Station 7.5".	(2) Both sections show most grains with particle size about 25μ; some grains finer. (1) Shows grain boundary fracture at O.D., Figure 122 hours at 1.7 atm and 1848°K. (2) New phase indicated at I.D., Figure 35b.

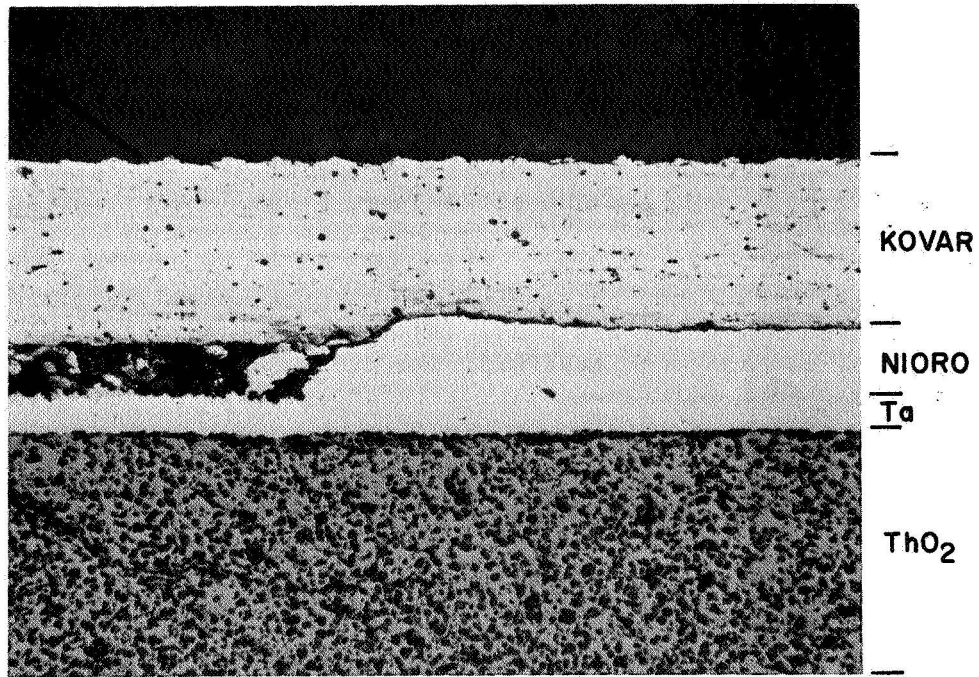


(a) End views

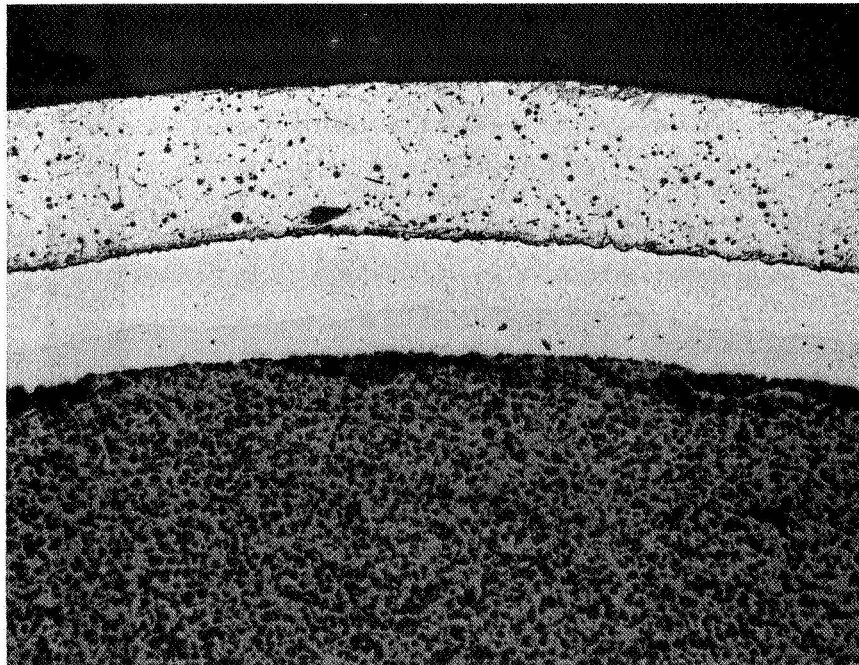


(b) Contact site

Figure 33.-Typical thermal shock fracture caused by contact with graphite test heater. Basis for recommendation of direct ohmic heating of ceramic.



(a) Longitudinal (100x)

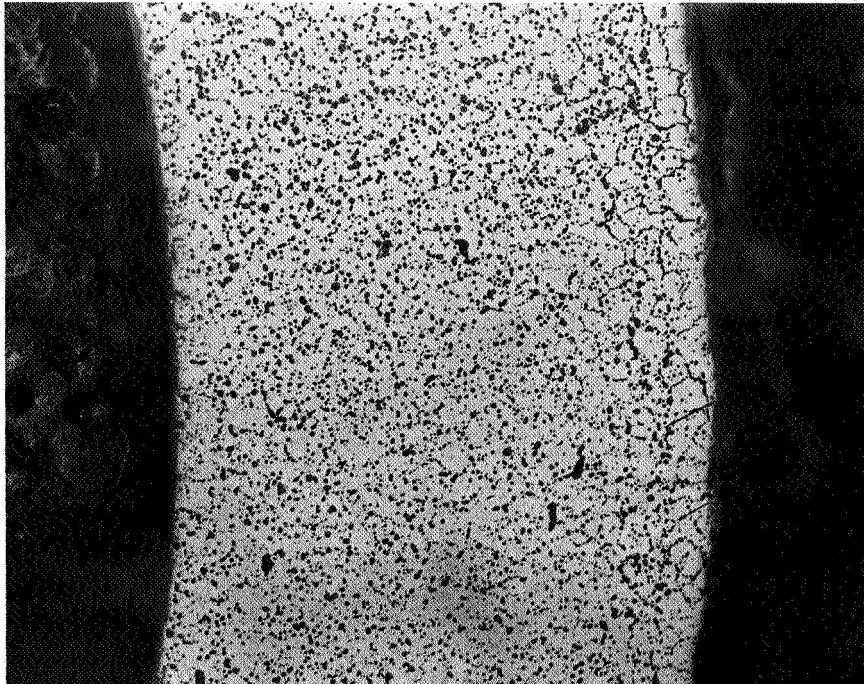


(b) Circumferential (100x)

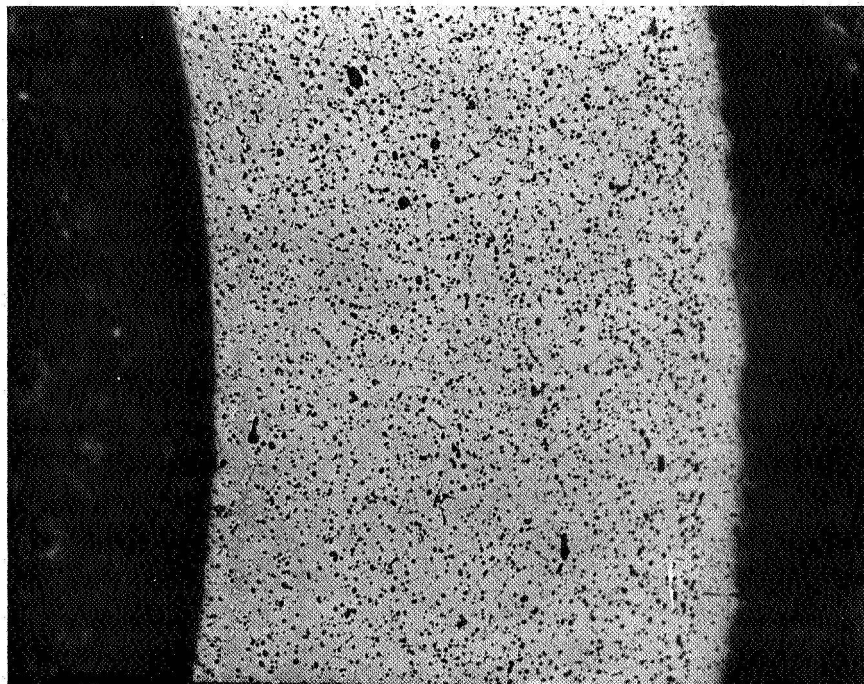
Figure 34.- Sectional view of metal-to-ceramic fitting (Station 5.9 in. Test 13).

Figure 35a is the first and only indication of a possible grain boundary fracture at the O.D. of the tube Station 3.9 inches of test 17. It demonstrates that endurance stress rupture under a tensile load of ~ 600 kN/m (85 psi) for periods of this test (~ 120 hours and 1850°K) is incipient. These data are roughly in agreement with fig. 16 and the supporting text given. All compressive stress type design as indicated.

Figure 35b indicates a new phase at the I.D. of the tube, Station 7.5 in. The gas used in this case was N. This phase has not been identified but Table XV indicated, by x-ray fluorescence analysis, the presence of Ta and Fe at the I.D. of Station 8.5 inches. From reference 57, the information of ZrN is possible at a high but not reported temperature.



(a) At station 99mm(3.9 in.) T=1848°K
showing incipient tensile creep
failure on O.D.



(b) At station 181mm (7.5 in.) T=585°K
showing unidentified phase at I.D.

Figure 35.-Cross sections of test 17, N₂ , 1.7 atmospheres, 122 hours.

CONCLUSIONS

In considering the data obtained and the facts learned from this program, the following conclusions are apparent. It is recommended that ceramics be studied further for ceramic biowaste resistojets.

1. Ceramic materials are the only possibility for oxidizing propellant resistojets operating above $\sim 2000^\circ\text{K}$ because of chemical compatibility. Compatibility to $\sim 10^2$ hours was demonstrated with no problem; 10^4 hours are required in service.

2. A ceramic heat exchanger heated by a separate refractory metal resistance heater is dubious because it requires the propellant to be completely separate from the heater. Because of diffusion mechanisms, this is difficult to achieve. It requires absolute physical separation of heater and ceramic or thermal shock due to their required temperature difference causes failure on contact. For this reason, a conducting ceramic is selected as the best choice for a design philosophy.

3. Y_2O_3 stabilized ZrO_2 is currently the best material choice for the conducting ceramic thrusters due to demonstrated high voltage-low current electrical properties at design. ThO_2 is second choice. They must be stably "doped" (as yet undeveloped) or used in conjunction with an auxiliary metal starter heater designed to not exceed 1300°K and biowaste gas resistant. The use of modified ZrB_2 is still uncertain.

4. The conducting ceramics cannot be used in tension but must be designed in compression if $\sim 10^4$ hours life is desired. A design chamber pressure of 1 atmosphere is feasible.

5. Substantial development of the metal-to-ceramic seal and electrode technology for ZrO_2 or ThO_2 is required for long life. Lives of $\sim 10^2$ hours are now demonstrated but $\sim 10^4$ hours are required. Such seal concepts are available but reliability must be demonstrated.

6. The fabrication and joining technology must be developed further for long-lived thrusters.

REFERENCES

1. Pisciotta, A., Jr., Eusanio, E. N., et al.: Definition of a Resistojet Control System for the Manned Orbital Research Laboratory. Final Report, Vol. I Summary, NASA CR-66600, 1968.
2. Greco, R. V.; and Charhut, D. E.: Resistojet Systems Studies Directed to the Space Station/Space Base. Summary Rept., NASA CR-111878, 1971.
3. Page, R. J.; and Short, R. A.: Definition of a Resistojet Control System for Manned Orbital Research Laboratory. Final Report, Vol. V, Resistojet Design and Development, NASA CR-66604, 1968.
4. Halbach, C. R.; Page, R. J.; Short, R. A., et al.: Resistojet Thruster Life Tests and High Vacuum Performance. NASA CR-66970, 1970.
5. Halbach, C. R.: 10 Mlb Biowaste Resistojet Performance. Preprint No. 71-687, Presented at AIAA 7th Propulsion Joint Specialist Conference (Salt Lake City), June, 1971.
6. Houghton, M. D., et al.: Test Report-Test Results Operational 90 Day Manned Test of a Regeneration Life Support System. NASA CR-111881, 1971.
7. Shaffer, Peter T. B.: Handbooks of High Temperature Materials, No. 1 - Materials Index. Plenum Press, 1964.
8. Anon.: Iridium. The International Nickel Company, Inc., 1965.
9. Kilpatrick, Martin; and Lott, Stanley K.: Reaction of Flowing Steam with Refractory Metals, II Rhenium (850°-1700°C). J. Electrochem. Society, vol. 113, no. 1, Jan. 1966, pp. 15-16.
10. Bradshaw, W. G. and Mathews, C. O.: Properties of Refractory Materials: Collected Data and References. LMSD --2466, June 24, 1958. Lockheed Aircraft Corp., Missile System Div., Sunnyvale, Calif.
11. Clougherty, E. V., et al.: Research and Development of Refractory Oxidation--Resistant Diborides. Part II, Vol. II, Processing and Characterization. AFML-TR-68-190, Jan. 1970.
12. Clougherty, E. V. and Peters, E. T.: Research and Development of Refractory Oxidation--Resistant Diborides. Part II, Vol. II, Processing and Characterization. AFML-TR-68-190, Jan. 1970.
13. Rhodes, W. H., et al.: Research and Development of Refractory Oxidation--Resistant Diborides. Part II, Vol. III, Thermochemical Stability Characterization. Part II, Vol. IV, Mechanical Properties. AFML-TR-68-190, Jan. 1970.
14. Clougherty, E. V., et al.: Research and Development of Refractory Oxidation--Resistant Diborides. Part II, Vol. V, Thermal Physical, Electrical and Optical Properties. AFML-TR-68-190, Nov. 1969.
15. Clougherty, E. V., et al.: Research and Development of Refractory Oxidation--Resistant Diborides. Part II, Vol. VI, Thermal Stress Resistance. AFML-TR-68-190, Dec. 1969.

16. Graham, H.C., Davis, H.H., Kvernes, I.A., and Tripp, W.C.: Microstructural Features of Oxide Scales Formed on Zirconium Diboride Materials. *Mat. Sci. Res.* Vol. 5, 1971, pp. 35-48.
17. Krochmal, J. J.: Fiber Reinforced Ceramics--A Review and Assessment of their Potential. AFML-TR-67-207, Oct. 1967.
18. Mazdiasni, K. S.; Lynch, C. T.; Smith, J. S.: Development of New Ceramic Materials (Zyttrite) by Thermal and Hydrolytic Decomposition of Metal Alcholates. AFML-TR-66-418, Dec. 1966.
19. Morgan, R. E. D. and Schaeffer, N. C.: Chemically Activated Pressure Sintering of Oxides. AFML-TR-66-356, Feb. 1967.
20. Scala, E., Schaeffer, N. C., Penty, R. A.: Chemically Activated Pressure Sintering of Oxides. AFML-TR-66-356. Part II, May 1968.
21. Penty, R. A.: Chemically Activated Pressure Sintering of Oxides. AFML-TR-66-356. Part III, April 1969.
22. Graves, G. A., Lynch, C. T., Mazdiasni, K. S.: Preparation and Mechanical Properties of Hot Pressed Zirconia-Zirconia Fabric Composites. *Am. Ceram. Soc. Bull.* 49(9), 1970, pp. 797-803.
23. Mazdiasni, K. S., Graves, G. A., Lynch, C. T.: SEM Studies of Fracture in Zirconia Fiber Reinforced-Zirconia Matrix Composites. *Proceedings of the 3rd Scanning Electron Microscopy Symposium.* Edited by Jahari et al, April 28-30, 1970.
24. Kieffer, R. and Benesovsky, F.: Metallic Heating Element Materials for High Temperature Furnaces. *Metallurgia* 58, Sept. 1958.
25. Grossman, L. N. and Kaznoff, A. I.: Insulators for Therionic Energy Converter Application. *Proceedings of the Conference on Nuclear Applications of Nonfissionable Ceramics,* (Washington, D. C.), May 1966.
26. Johnson, P. D.: Behavior of Refractory Oxides and Metals, Alone and in Combination in Vacuo at High Temperatures. *J. Am. Ceram. Soc.* 33(5), 1955, pp. 168-71.
27. Bruckart, W. K., Craighead, C. M., Jaffee, R. I.: Investigation of Molybdenum and Molybdenum-Base Alloys Made by Powder Metallurgy Techniques. Prepared under Contract Nr. AF 33(038)-12641, Battelle Memorial Institute, Columbus, Ohio. WADC TR-54-398, 1955.
28. Ruh, R. and Rockett, T. J.: Proposed Phase Diagram for the System ArO_2 . *J. Am. Ceram. Soc.*, Vol. 53, (6), 1970, pp. 360.
29. Yavorsky, P. J.: Properties and High Temperature Applications of Zirconium Oxide. *Ceramic Age*, June 1962.

30. Buckley, J.D. and Braski, N.: Elastic Modulus of Stabilized Zirconia. J. Am. Ceram. Soc. 50 (4) 1967, pp. 220-1.
31. Technical Data Sheet No. 6, May 1962. Zirconium Corp. of America, Cleveland, Ohio.
32. Dixon, J.M., et al.: Electrical Resistivity of Stabilized Zirconia at Elevated Temperatures. J. Electrochem. Soc. 110 (4), 1963, pp. 276-70.
33. Strickler, D.W. and Carlson, W.G.: J. Am. Ceram. Soc. 47 (3), 1964, pp. 122-7.
34. Anthony, Anne-Marie: Mesure de la conductibilite electrique de ZrO_2 stabilisee a 10^{10} b Y_2O_3 entre 1000 et 2400°K. C.R. Acad. Sc. Paris, t. 260, pp. 1936-1939, Feb. 15, 1965.
35. Fehrenbacher, L. and Wimmer, J.: (unpublished data), Aerospace Research Laboratories, U.S. Air Force, Wright-Patterson Air Force Base, Ohio.
36. Fehrenbacher, L.: Optimum Properties of Zirconia Ceramics for High Performance Storage Heaters, Vol. 5, Materials Science Research, Ceramics in Severe Environments, pp 105-123, Plenum Press, New York, 1971.
37. Pfeifer, W.H. (ed.): Advanced Materials for Aircraft Propulsion Systems Phase I: Investigation of Corrosion Resistant Coatings for Service at 3000°F and Above. Battelle Columbus Laboratories, Contract No. N00019-70-C-0337, Aug., 1970.
38. Mazdiyasi, K.; and Lurch, C.T.: Alkoxy - Based Single and Mixed Phase Refractor Oxide Particulates. C.R. Journees Etud. Solides. Finement Div., 1967 (Pub. 1969) pp. 9-28. Ed. by Ehretsmann, J., Dir. Doc. Fr. (Paris):
39. Touloukian, Y.S., ed.: Thermophysical Properties of High Temperature Solid Materials. Vol. 4, Oxides and Their Solutions and Mixtures. Part I, Simple Oxygen Compounds and Their Mixtures, pp. 421-38. Thermophysical Properties Research Center, Purdue University. The MacMillan Co., New York, 1967.
40. Lang, S.M.; and Geller, R.F.: The Construction and Operation of Thoria Resistor-Type Furnaces. J. Am. Ceram. Soc., Vol. 34, No. 7, 1951, pp. 193-200.
41. Imai, H.; and Hosaka, S.: Reaction of Pressed Mixtures. Zairyo 1968, 17 (177), 531-5 (Japan).
42. Smith, A.W., et al.: Permeability of Zirconia, Hafnia and Thoria to Oxygen, Thoria to Oxygen, J. Am. Ceram. Soc. 49(5), 1966, pp. 240-4.
43. Albert, R.E.: Thorium: Its Industrial Hygiene Aspects. Prepared under the direction of the American Industrial Hygiene Association for the Division of Technical Information, U.S. Atomic Energy Comm., New York. Academic Press, Inc., 1966.

44. Manning, C. R., Jr.; and Stoops, R. F.: High Temperature Cermets. I, Compatibility. J. Am. Ceram. Soc., 1968, 51(8), pp. 411-15.
45. Mozzhukhim, E. I.: Thermodynamic Evaluation of the Reaction of Dispersed Inclusions of Refractory Oxides with Hard Metals. Sb. Mosk. Inst. Stali Splavov, (Russia), 1968, No. 49, pp. 79-105.
46. Manning, C. R., Jr.; and Stoops, R. F.: High Temperature Cermets. II, Wetting and Fabrication. J. Am. Ceram. Soc., 1968, 51(8) pp. 415-19.
47. Kalish, D.; and Clougherty, E. V.: High Pressure Hot-Pressing Refractory Materials. Ceram. Bull., 48(5), 1969, pp. 570-8.
48. Kalish, D.; and Clougherty, E. V.: Densification Mechanisms in High Pressure Hot-Pressing of HfB_2 . J. Am. Ceram. Soc. 52(1), 1969, pp. 26-36.
49. Page, R. J.: Biowaste Propellants Performance and Power Goals-Space Station/ Base. ARTCOR Technical Bulletin, No. 16, Advanced Rocket Technology, Irvine, Ca., Oct. 1970.
50. Bunikov, P. P.; and Kharitonov, F. Ya.: Resistance of Calcium Oxide Stabilized Zirconia Ceramics Against High Temperature Steam. Epitanya E 21(10), (Hung.), 1969, pp. 375-7.
51. May, C. E.; and Hoekstra, P. D.: Stability of Refractory Compounds in Hydrogen Between 4500° and 5000°F. Lewis Research Center, Cleveland. NASA TN D-844, 1961, pp. 12.
52. May, C. E.; and et al.: Stability of Ceramics in Hydrogen Between 4000° and 4500°F. Lewis Research Center, Cleveland. NASA Memo 3-5-59E, 1959, pp. 13.
53. Trostel, L. J., Jr.: Stability of Alumina and Zirconia in Hydrogen. Am. Ceram. Soc. Bull. 44(12), 1965, pp. 950-52.
54. Collouges, R.: and et al.: Ammonia Action on Different Super-Refractory Oxides. Bull. Soc. Chim., 1962, (France) pp. 2113-17.
55. Gilles, J. C.; and Collouges, R.: Structure and Properties of Phases Obtained from Reaction of Zirconium Dioxide and Ammonia. Comp. Rend. 254, 1962, pp. 1084-6.
56. Gilles, J. C.; and et al.: Reaction of Ammonia with Various Super-Refractory Oxides. Corrosion Anticorrosion 12(3), 1964, pp. 99-107.
57. Matsumoto, O.: Chemical Reactions at High Temperatures. IX. Nitridation of Zirconium Oxide by a Nitrogen Plasma Jet. Denki Kaga Ku Oyobi Kogyo Butsuri KagaKu 36(12), (Japan) 1968, pp. 877-83.
58. Winter, E. R. S.: Exchange Reactions of Oxides. IX J. Chem. Soc. A(12), 1968, pp. 2889-902.

59. Elyutin, V. P.; and et al.: Reaction of ZrO_2 With Carbon. *Izv. Vyssh-Ucheb. Zaved. Chern. Met.* 1970, 13(1), 5-8 (Russia).
60. Beaumont, M. and et al.: Effect of Th-228 Incorporation on the Catalytic Properties of Thoria. *Ch. Acad. Sci. (Paris) Ser. C*(267(25), 1968, pp. 1648-50.
61. Imai, H.; and Hosaka, S.: Reaction of Pressed Mixtures. *Zairyo* 1968, (17(177), 531-5 (Japan).
62. Peters, D. L.: Chemical Corrosion of Rocket Liner Materials and Propellant Performance Studies. U. S. Dept. Comm. Office Tech. Serv. AD 425 888, 1963, pp. 79.
63. Clougherty, E. V.; and et al.: Research and Development of Refractory Oxidation-resistant Diborides. Part II, Vol. II. Processing and Characterization, AFML-TR-68-190. Jan. 1970.
64. Langmuir, I.: *Phys. Rev.*, 2, 329 (1913), and subsequent papers.
65. Dushman, S. and Lafferty, J. M., ed.: *Scientific Foundations of Vacuum Technique*. Second ed., John Wiley and Sons, 1962.
66. Hoch, M.; Nakata, M.; and Johnson, H. L.: *J. Am. Chem. Soc.*, 76, 2651-2.
67. Chupka, W.A. Berkerwitz, J. and Inghram. M. G. in cooperation with Argonne National Lab., sponsored by OOR, 1-14. AD 107 063.
68. Zima. G.E.: Vaporization of Advanced Power Plant Metals Under Vacuum and Forced Convection Conditions. Rept. UCRL-14274. Lawrence Radiation Laboratory, University of California, June 24, 1965.
69. Poteat, L.E.; and Yust, C.S.: Creep of Polycrystalline Thorium Diboride. *J. Am. Ceram. Soc.*, vol. 49, no. 8, Aug. 1966, pp 410-414.
70. Stavrolakis, J.A.; and Norton, F.H.: Measurement of Torsion Properties of Alumina and Zirconia at Elevated Temperatures. *J. Am. Ceram. Soc.*, 33 (9), 1950, pp 263-268.
71. Evans. P.E.: Creep in Yttria and Scandia-Stabilized Zirconia. *J. Am. Ceram. Soc.*, vol. 53, no. 7, July 1970, pp 365-9.
72. Fehrenbacher, L.L.; Bailey, F.P.; and McKinnon, N.A.: Compressive Creep of Yttria Rare Earth Stabilized Zirconia Storage Heater Refractories, *SAMPE Qtrly.*, Vol. 2, No. 3, July 1971. pp. 48-60.
73. Henderson, A.W.; and Higbie, K.B.: Improved Method for Obtaining High-Purity Zirconium and Hafnium Oxides. *J. Amer. Chem. Soc.*, 1954, pp. 5878-79.
74. Poteat, L.E.; and Yust., C.S.: Grain-Boundary Reactions During Deformation. *Ceram. Microstruct. Proc. Int. Mater. Symp. 3rd*, 1966 (Pub. 1968), Ed. by R.M. Fulbrath. John Wiley & Sons, Inc., New York. pp 464-56.

75. Kingery, W.D.: Factors Affecting Thermal Stress Resistance of Ceramic Materials. J. Am. Ceram. Soc., Vol. 38, 1955, pp 3.
76. Clougherty, E.V.; Niesz, D.E.; and Mistretta, A.L.: Research and Development of Refractory Oxidation - Resistant Diborides, Part II, Vol. VI, Thermal Stress Resistance. Part II, Vol. VI, AFML-TR-68-190, Dec. 1969.
77. Manson, S.S.: "Thermal Stresses and Thermal Shock," Mechanical Behavior of Materials at Elevated Temperature, McGraw-Hill Book Co., New York, John Dorn, Editor, 1961.
78. Kingery, W.D.: Introduction to Ceramics. John Wiley and Sons, Inc., 1960.
79. Halbach, C.R.; Page, R.J.; and Short, R.A.: High Temperature Biowaste Resistojets Using Electrically Conducting Ceramic Heaters, preprint 72-454, Am. Inst. Aeron. and Astronaut. April 1972.
80. Jorgensen, P.J.; and Schmidt, W.G.: Final Stage Sintering of Thoria. J. Am. Ceram. Soc., vol. 53 (1), 1970, pp 24-7.
81. Mazdiyasni, K.S.; and Brown, L.M.: Preparation and Characterization of Sub-micron Hafnium Oxide. J. Am. Ceram. Soc, vol. 53(1), 1970, pp 44-5.
82. Rice, Ray W.: Welding of Ceramics. Naval Research Laboratory, NRL Rept. 7085, July 1970. AD 710 359.
83. Pattee, H.E.; et al.: Joining Ceramics and Graphite to Other Materials, NASA SP-5052 (1968).
84. Buyers, A.G.; and Mohr, A.J.: Sealing Zirconia Ceramics to Tantalum and Its Alloys, U.S. Pat. 3,254,403, June 7, 1966.
85. Bender, H.: High Temperature Metal-Ceramic Seals. Ceramic Age. 63(4), 1954.
86. Elyutin, V.P., et al.: Reaction of ZrO with Carbon. Izv. Vyssh. Ucheb. Zaved., Cern. Met. 13(1) (Russ.) 1970.
87. Imai, H.; Hosaka, S.; Zairyo: Reaction of Pressed Mixtures, 17(177) (Japan), 1968, pp 531-5.

APPENDIX A
CORRECTIONS TO OPTICAL PYROMETER TEMPERATURE MEASUREMENTS OF
AN INDIRECTLY HEATED CERAMIC TUBE WHERE REFLECTION AND
TRANSMISSION TERMS MAY BE SIGNIFICANT

By Russell J. Page

SUMMARY

An analysis has been made of the pyrometer measurements problem for the advanced resistojet materials program. Both an analysis of a one-dimensional and a carefully considered two-dimensional model representing the sample heater system have shown that reflection and transmission terms in non-conductors heated by external heaters require careful pyrometer interpretation. An experiment reported confirms the fact that good temperature measurements may be made on the sample when the propellant flow rates are kept small enough to keep temperature differences between heater and sample less than 60°C. The simplified illustrative method gives close approximation to the apparent temperature expected.

INTRODUCTION

Normally, the chief problem in pyrometry is the lack of knowledge of the emissivity of the specimen being measured. In the current task, not only is the emissivity not precisely known, but the reflected power and transmitted power terms can cause significant temperature measurement errors when the surrounding surfaces are much hotter than the sample. This large temperature difference between sample and heater can be brought about by over-cooling the tube sample with the propellant gases. The question is what is the best flow rate of each propellant gas to be tested that: (1) will not seriously influence the pyrometry measurement, and (2) will simulate the chemistry influence on the ceramic samples. This analysis shall determine the temperature difference influence on pyrometry measurement to aid in answering the above important question.

The scope of this bulletin is to analyze and experimentally confirm the influence of these reflected and transmitted terms on the materials program data of a NASA study contract to evaluate high temperature materials for advanced resistojet designs. Analytically the problem is considered as two-dimensional, radiant heat transfer between the three members with all reflections diffuse. All members are to be treated as uniform within themselves in temperature. The emissivities of each surface are treated as constants about the experimental temperature of interest. The range of heater temperatures considered is from 1000 to 2200°K. A broad range of temperature differences between heater and tube sample are considered to study the reflective and transmissive influence. In the materials test

program itself, this temperature difference range may be adjusted by varying the propellant rate.

The method of analysis is believed new. The method is numerical. The power leaving each given surface, in turn, is distributed to all possible surfaces where they are eventually absorbed. The successive reflection process is continued to any degree of desired accuracy. The original temperature identification of the power is preserved so that its power contribution at the wavelength of the sensing optical pyrometer can be interpreted properly by Planck's law. The simplification of the method comes about by the bookkeeping system used. After each reflection (transaction) the power arriving by different paths is summed up at each surface to be distributed again to all surfaces.

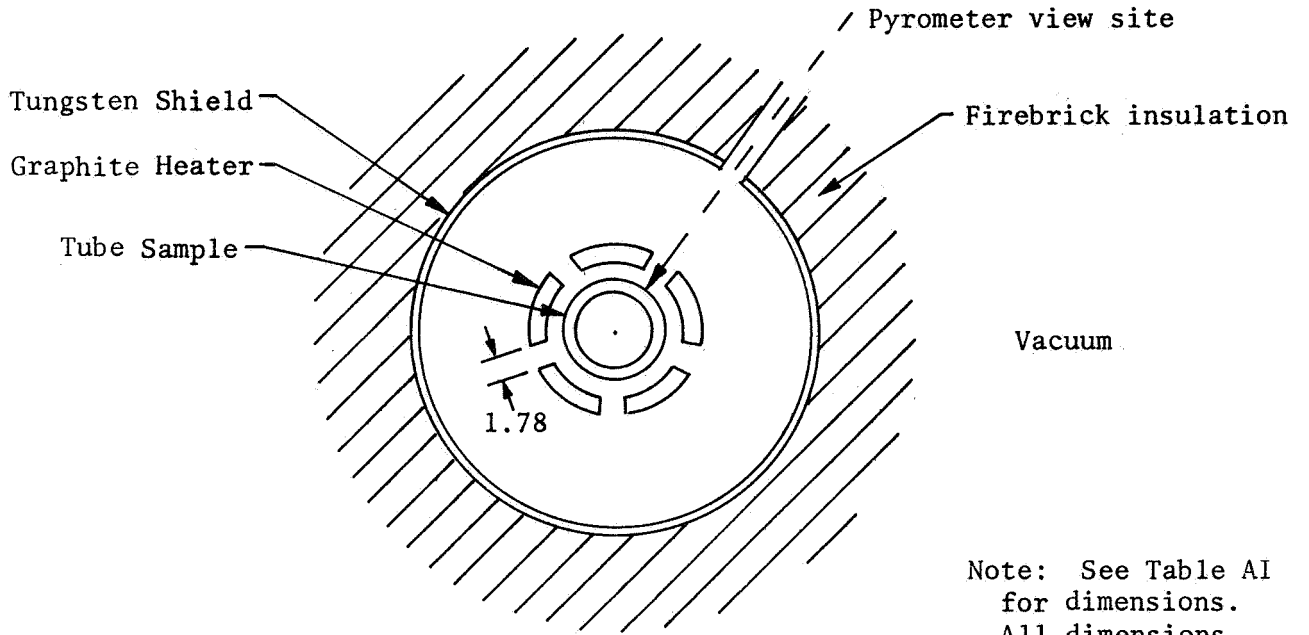
Experimentally the approach consisted of using an identical test sample in the setup with a 0.76 mm hole drilled into the sample wall next to the normal viewing site. Thus a black body ($\epsilon = 1$) was realized in the small opening, or hohlraum. Measurement of the sample was thus compared against the hohlraum or "true" temperature over a broad temperature range. This case represented minimum heat transfer to be expected between tube and heater (no propellant flow). It may be compared with the analysis only in the case of low temperature differences.

PHYSICAL DESCRIPTION

The physical problem described by Figure AI and Table AI is self-explanatory. The tube sample length varied from 15 to 23 cm. The active heater section was 4.67 cm in length. The pyrometer view site is centered on the heated section. Emissivities given in Table AI are nominal values corresponding to typical temperatures encountered.

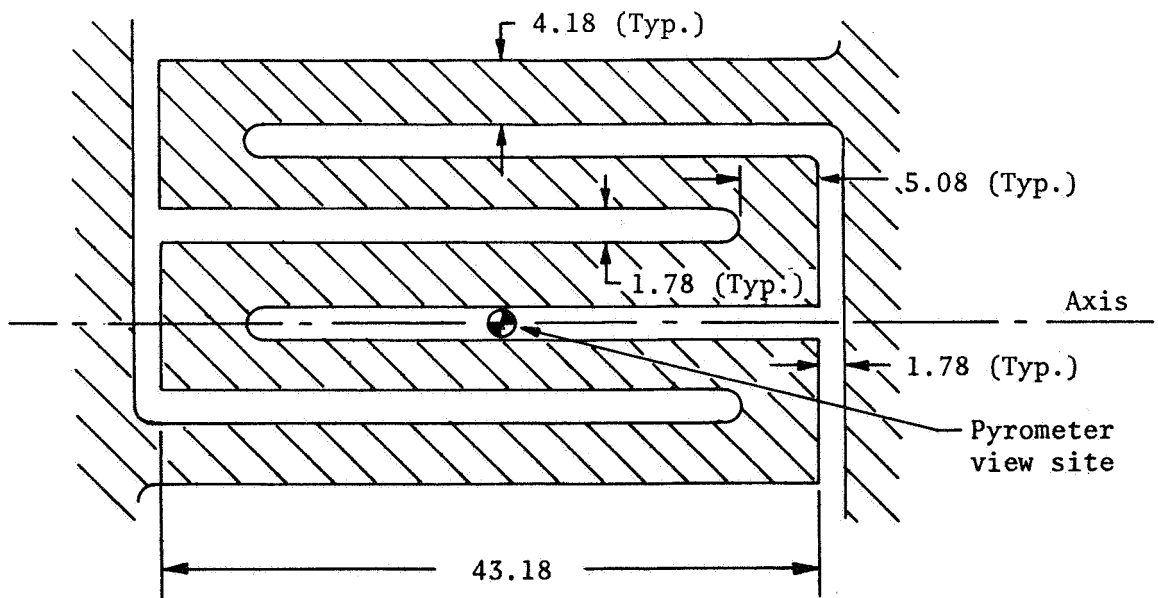
TABLE AI. - DIMENSIONS OF HEATER-SAMPLE SETUP

Part	Material	Emissivity, ϵ_λ at 0.65 μ	O.D. mm	I.D. mm
Shield	Tungsten	0.43	25.4	23.4
Heater	Graphite	0.80	10.52	8.41
Samples	Zirconia	0.50	6.35	4.83



Note: See Table AI for dimensions. All dimensions in mm.

a. Cross section



b. Rolled-out view of heater at pitchline

Figure A1. - Test heater-sample geometry.

THE MEASUREMENTS PROBLEM

Pyrometers measure temperature by comparison of the intensity of emitted radiation with a known source. When properly designed and applied, they are very accurate instruments. See Eckert and Drake (reference A1) for a description of such instruments.

Two classes of instruments are in existence. One class measures the total (integrated) radiation emitted from a surface calorimetrically. The second class (optical type) compares by observation with the eye the monochromatic radiation intensity of the object in the visible-wavelength range with a known monochromatic radiation intensity. Each pyrometer must be calibrated by viewing with it objects with known emitted radiation intensity.

In the case of a "free" gray body, a body which is only emitting and not reflecting or transmitting power, either the emissivity of the surface has to be known or it has to be increased artificially to the value 1 when the true temperature is to be determined from a pyrometer reading. Otherwise, an apparent temperature is read.

A number of apparent temperatures are used in pyrometry. The optical pyrometry definitions for "free" bodies are discussed first for reference to our case of imposed reflective and transmissive terms.

The apparent monochromatic temperature, T_λ , is the temperature of a black body which, at a defined wavelength in the visible range (usually but not necessarily at $\lambda_r = 0.665\mu$), has the same radiation intensity as the surface under consideration. The basis of the measurement is Planck's law.

$$i_{\lambda bn} = \frac{2C_1}{\lambda^5 (e^{C_2/\lambda T} - 1)} \quad (1)$$

According to this definition and Equation (1):

$$\frac{1}{e^{C_2/\lambda T_\lambda} - 1} = \epsilon_\lambda \frac{1}{e^{C_2/\lambda T} - 1} \quad (2)$$

At temperatures occurring in engineering applications, the first term in the denominator of the above equation is large compared with 1, and the 1 can be neglected without causing an error which would conflict with the obtainable accuracy. This equation then can be transformed to the following relation:

$$\frac{1}{T} = \frac{1}{T_\lambda} + \frac{\lambda}{C_2} \ln \epsilon_\lambda \quad (3)$$

ϵ_λ denotes the monochromatic emissivity of the surface. This equation again is for a free body which is not reflecting or transmitting any additional power.

A calorimetric pyrometer makes use of the total radiation temperature T_t . This is the temperature of a black body when it emits the same total radiation intensity as the surface toward which the pyrometer is directed. From this definition and the Stefan-Boltzmann equation:

$$e_b = \sigma T^4 \quad (4)$$

it follows that the relation between T_t and the true surface temperature T is

$$\sigma T_t^4 = \epsilon \sigma T^4 \quad (5)$$

or

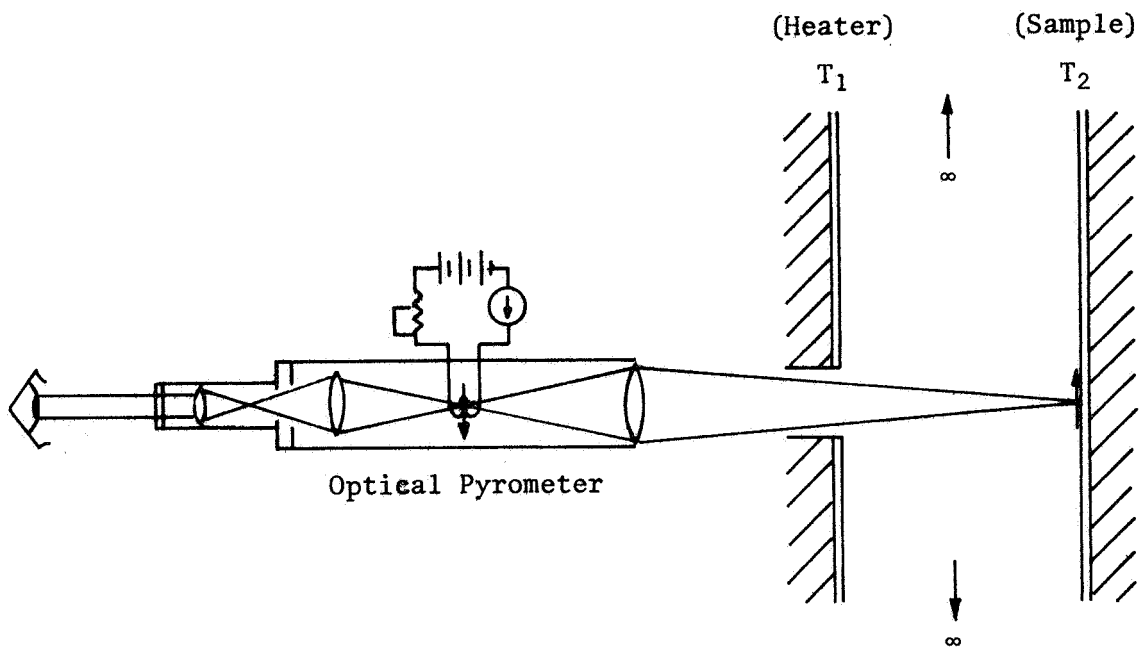
$$T = T_t / \sqrt[4]{\epsilon} \quad (6)$$

For the experimental program, an optical pyrometer was used. The analysis of our problem of included reflection and transmission will be presented for this type of pyrometer, which is the more difficult of the two types to analyze. The analytical development for the calorimetric type follows simply, and is not presented here. Numerical results are presented, however, for both types.

ILLUSTRATIVE EXAMPLE OF THE REFLECTION PROBLEM

Figure A2(a) shows a one-dimensional version of the tube sample-temperature measurement problem. The heater temperature T_1 is greater than that of the sample T_2 . The optical pyrometer is viewed through an inconspicuously small hole in the heater to focus on T_2 . The problem has two radiating surfaces.

Figure A2(b) describes the monochromatic radiative power transfer between two gray parallel surfaces whose distance apart is small compared with their size, so that practically all radiation emitted initially by one surface, say 1, falls upon the second, 2. That not absorbed initially by 2 on the first pass is reflected. This radiation travels in this way back and forth in diminishing quantity between the surfaces



a. Geometry

Figure A2. - Basis for the illustrative example of the reflection problem.

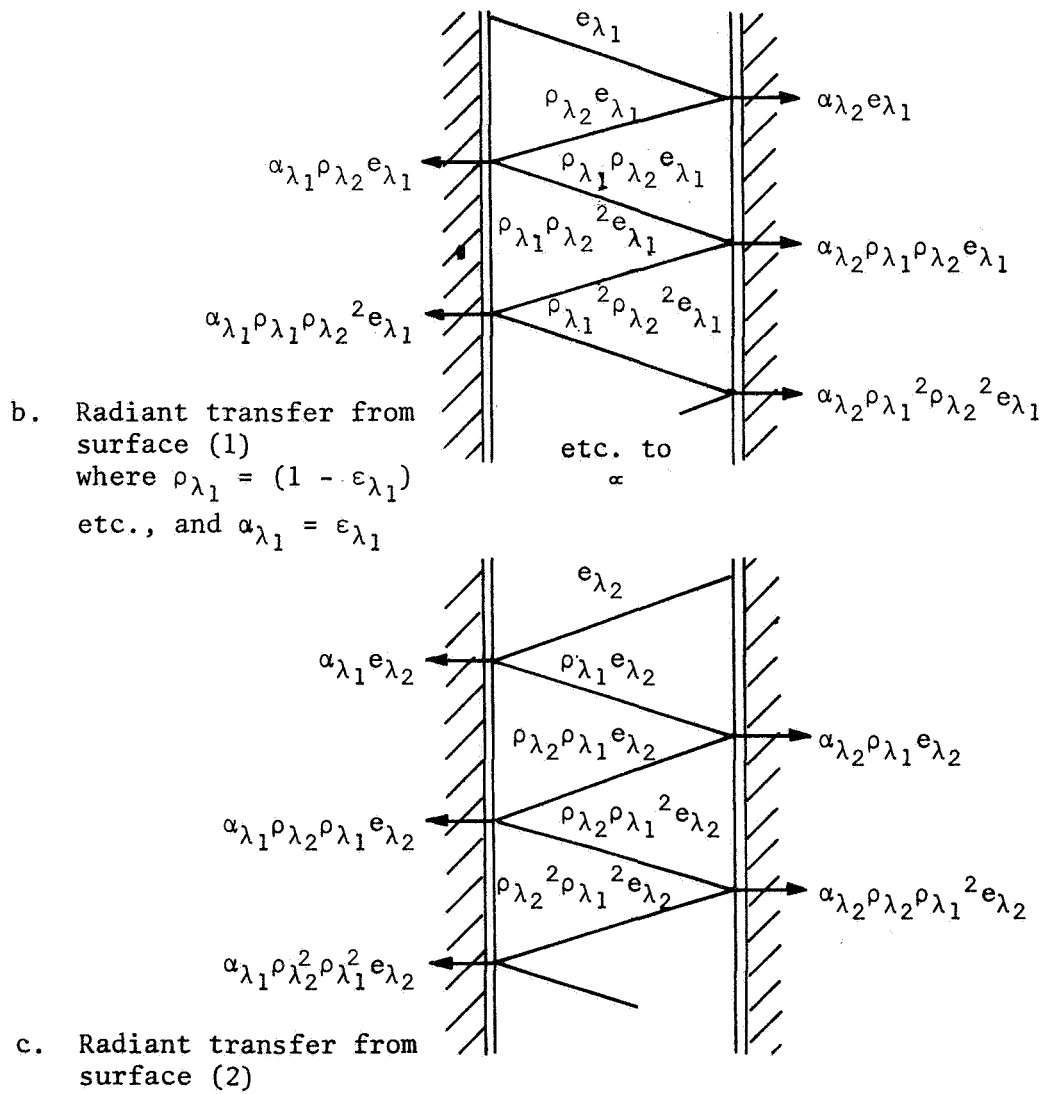


Figure A2. - Concluded.

until it is finally absorbed. Likewise, that emitted by 2 is treated in the same way, Figure A2(c). The net heat transfer is the summation of these two processes.

The power appearing to the optical pyrometer to emanate from T_2 is a composite of the total of two terms:

(1) That radiatively emitted from the surface at T_2 , e_{λ_2} , and all its subsequent reflections off to surface 2, namely:

$$= e_{\lambda_2} \sum_{n=0}^{n=\infty} [1 + (1 - \epsilon_2)(1 - \epsilon_1) + (1 - \epsilon_2)^2(1 - \epsilon_1)^2 + \dots + (1 - \epsilon_2)^n] \quad (7)$$

when $(1 - \epsilon_2)(1 - \epsilon_1) < 1$

$$= e_{\lambda_2} \left[\frac{1}{1 - (1 - \epsilon_2)(1 - \epsilon_1)} \right] \quad (8)$$

and

(2) that multiple reflection off of surface 2 that was first emitted from surface 1 as e_{λ_1} , namely:

$$= e_{\lambda_1} \sum_{n=1}^{n=\infty} [(1 - \epsilon_2) + (1 - \epsilon_1)(1 - \epsilon_2)^2 + (1 - \epsilon_1)^2(1 - \epsilon_2)^3 + \dots + (1 - \epsilon_1)^{n-1}(1 - \epsilon_2)^n] \quad (9)$$

which when $(1 - \epsilon_2)(1 - \epsilon_1) < 1$

$$= e_{\lambda_1}(1 - \epsilon_2) \left[\frac{1}{1 - (1 - \epsilon_2)(1 - \epsilon_1)} \right] \quad (10)$$

The total emissive power appearing to emanate from T_2 then is the sum of equations (8) and (10), or

$$= [e_{\lambda_2} + e_{\lambda_1}(1 - \epsilon_{\lambda_2})] \left[\frac{1}{1 - (1 - \epsilon_{\lambda_2})(1 - \epsilon_{\lambda_1})} \right] \quad (11)$$

noting:

$$e_{\lambda} = \epsilon_{\lambda} \pi i_{\lambda bn} \quad (12)$$

that is, monochromatic emissive power, e_{λ} , is proportional to the normal monochromatic radiation intensity $i_{\lambda bn}$ and emissivity ϵ_{λ} . Planck's law, equation (1) becomes

$$e_{\lambda b} = \frac{2\pi C_1}{\lambda^5 (e^{C_2/\lambda T_{\lambda}} - 1)} \quad (13)$$

Defining the apparent monochromatic temperature, T_{λ} , as before

$$\frac{1}{(e^{C_2/\lambda T_{\lambda}} - 1)} = \left[\frac{1}{(e^{C_2/\lambda T_2} - 1)} + \frac{(1 - \epsilon_{\lambda_2})}{(e^{C_2/\lambda T_1} - 1)} \right] \left[\frac{1}{1 - (1 - \epsilon_{\lambda_2})(1 - \epsilon_{\lambda_1})} \right] \quad (14)$$

Again, as before, the minus 1 term may be ignored, but the equation can not be neatly and explicitly solved for T_2 analogously for the free gray body, as was done in equation (3). The solution is shown in Figure A3 numerically computed for the case of heater temperature, T_1 , of 1941°K for a range of sample temperatures, T_2 , from 1940 to 1500°K. In effect, the greater the difference between sample and heater, the more insensitive the indicated pyrometer measurement is to true sample temperature. In fact, after a difference of approximately 200°K the pyrometer appears to mirror the "heater" temperature more than anything else.

It is important to note in Figure A3 that if $T_1 = T_2$, the heater and sample are at the same temperature, 1940°K here, and we have the important case (for the geometry of Figure A2) of the "hohlraum", or black body cavity. Regardless of the emissivities the observed equals true or black body temperature. (Recall that the pyrometer temperature scale is calibrated in terms of black body radiation.) It is this well-known concept that is used here in a special experiment to measure true tube sample temperature. The inside of the tube via a small drilled hole is the hohlraum.

This simple analysis prompted the author to make a more careful, sophisticated analysis presented subsequently and to study the transmission problem.

	<u>TEMPERATURE</u>	<u>EMISSIVITY ϵ</u>	<u>MATERIAL</u>
HEATER	1941°K	0.80	GRAPHITE
SAMPLE	VARIABLE	0.50	ZIRCONIA

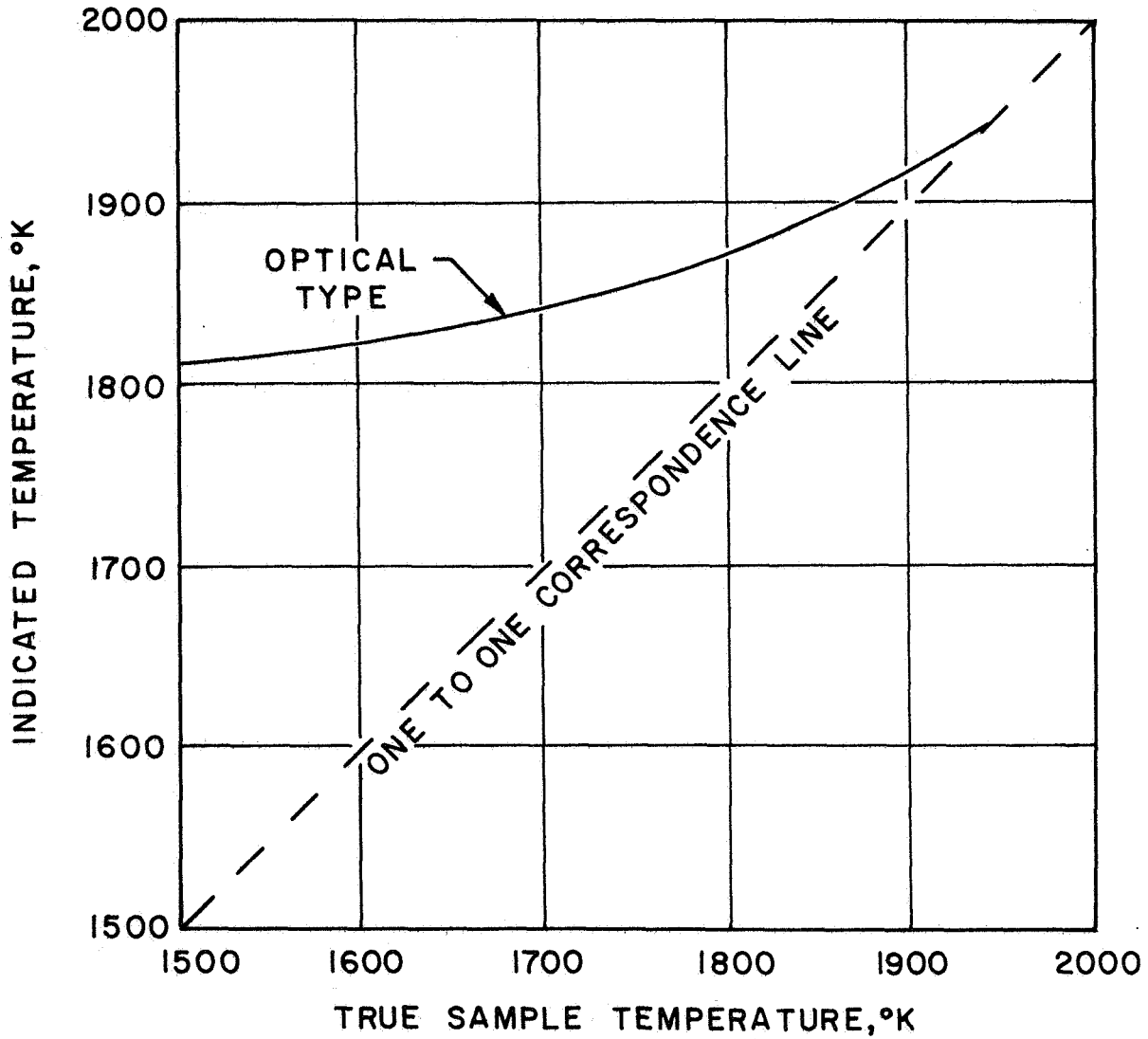


Figure A3. - Pyrometer indicated temperature as a function of true (one-dimensional model) tube sample temperature.

ILLUSTRATIVE EXAMPLE OF THE TRANSMISSION PROBLEM

Zirconia and thoria have both been found to transmit radiant power in the thicknesses involved here (see Table AI). Reference A2 notes that the spectral normal transmittance, τ_λ , measured behind a heated specimen of ZrO_2 , 1 mm and 2 mm thickness, were 0.04 and 0.03, respectively. This corresponds to passage through one or two walls of the sample, respectively

An illustrative example shows that the influence of this energy term upon the pyrometer measurements problem is seen to be rather inconsequential. The effect may be lumped into the reflective correction problem.

Figure A3 shows the one-dimensional version of the problem of a "tube" being heated by a surrounding heater. The first interaction only (reflection and transmission) is shown for simplicity.

From the law of conservation of energy,

$$\rho_\lambda + \alpha_\lambda + \tau_\lambda = 1 \quad (15)$$

Assuming the reflected spectral energy remains surface-oriented and independent of depth of specimen, then the sum of absorptivity, α , and transmissivity, τ , remains a constant. In the case of a thick specimen, 6 mm or more (reference A2),

$$\alpha'_\lambda = \epsilon_\lambda \quad (16)$$

from Kirchhoff's law, and where α'_λ is the "thick" absorptivity. Therefore,

$$\alpha'_\lambda = \alpha_\lambda + \tau_\lambda \quad (17)$$

From symmetry, the energy term from surface (2) as viewed by the pyrometer is seen to be, from Figure A4,

$$\begin{aligned} & e_{\lambda_1} (\rho_{\lambda_2} + \rho_{\lambda_2} \tau_{\lambda_2}^2 + \tau_{\lambda_2}^2) \\ & = e_{\lambda_1} \left[(1 - \epsilon_{\lambda_2}) + (1 - \epsilon_{\lambda_2}) \tau_{\lambda_2}^2 + \tau_{\lambda_2}^2 \right] \end{aligned} \quad (18)$$

wherever there was a $(1 - \epsilon_{\lambda_2})$ term in equation (14). The $(1 - \epsilon_{\lambda_1})$ terms stand. The resultant apparent monochromatic temperature, T_{λ_1} , for both reflectivity and transmissivity may be calculated from

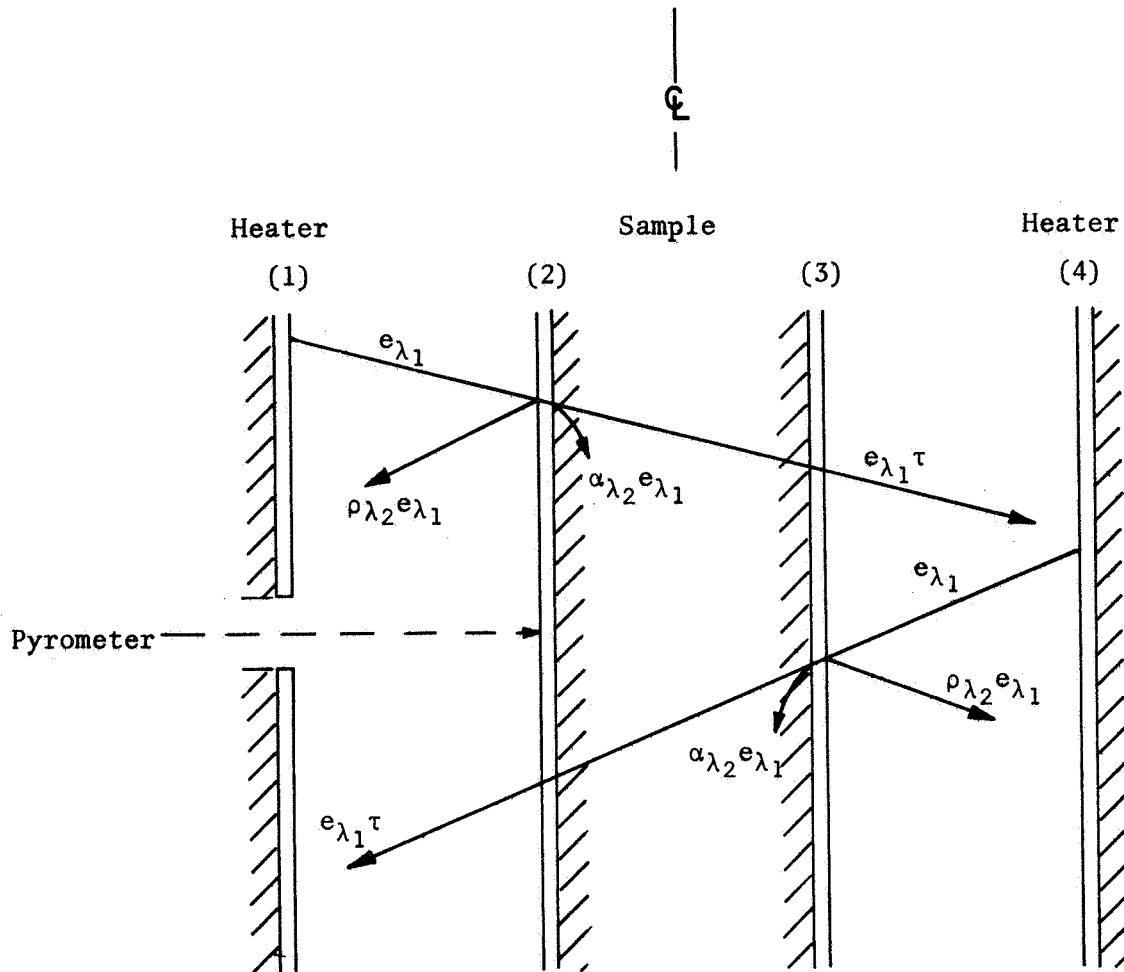


Figure A4. - Basis for illustrative example of the transmitted power increment influence on pyrometer measurement.

$$\frac{1}{(e^{C_2/\lambda T_{\lambda_1}} - 1)} \approx \left[\frac{1}{(e^{C_2/\lambda T_1} - 1)} + \frac{(1 - \epsilon_{\lambda_2}) + (1 - \epsilon_{\lambda_2})\tau_{\lambda_2}^2 + \tau_{\lambda_2}^2}{(e^{C_2/\lambda T_1} - 1)} \right] \times \left[\frac{1}{1 - [(1 - \epsilon_{\lambda_2}) + (1 - \epsilon_{\lambda_2})\tau_{\lambda_2}^2 + \tau_{\lambda_2}^2](1 - \epsilon_{\lambda_1})} \right] \quad (19)$$

The net effect of transmittance is that of increasing the effective reflectivity in this example from 0.5 to 0.54, which is rather inconsequential.

For the following analysis a net reflectivity of 0.5 was used.

ANALYSIS OF THE ACTUAL SAMPLE HEATER PROBLEM

The problem represented by the geometry of Figure A1 requires that the following additional factors be included over those of the illustrative examples:

- (1) Two-dimensionality instead of one
- (2) Three members instead of two
- (3) The non-simple shape of the heater requiring shape factor evaluation instead of the assumption of $F = 1$

Method

A new method is developed which accounts for the above factors. This is referred to here as the "accounting method". Here the emission temperature character of the radiation is preserved in the analysis. This spectral identification of power is essential for each energy term for optical pyrometry interpretation. The power radiating from each surface is in turn evaluated in terms of the surfaces of the system where they are ultimately absorbed. The emission energy (transaction 1) is first distributed to all possible surfaces (accounts) for each emitting surface. The amount initially absorbed is accounted for and that available to be reflected or transmitted noted. The first reflection from each surface (according to the shape factors of the receiving surfaces) is then distributed to all possible surfaces according to the reflecting surfaces' shape factors, completing transaction 2. The simplification of the method then comes in balancing the accounts and treating only one (the sum) emission energy term from each surface. These transactions are repeated until all surfaces are reflecting trivial terms. Two matrices are thus formed: the absorption and the reflection.

The absorption matrix may be treated as the heat transfer matrix in the Stefan-Boltzmann equation, Equation (4). It also may be used with Planck's law to help determine, along with the reflection matrix, the apparent monochromatic temperature for optical pyrometry purposes.

Shape Factors, F

Unlike the illustrated problem, the different surfaces of Figure A1 have been shape factors relative to each other differing from unity. These have been evaluated from basic definitions to the use of conservation and reciprocity relations. Descriptive geometry techniques were employed to evaluate the key heater shape factors. The results of analysis have been summarized in Table AII which lists the shape factors F identified by their subscripts H, S and W for heater, tube sample and tungsten shield, respectively.

TABLE AII. - SHAPE FACTORS MATRIX

From/To	H_i	H_o	H_e	S	W
Heater _{inside} , H_i	0.098 ⁴	0	0.149 ²	0.748 ²	0.005 ²
Heater _{outside} , H_o	0	0	0	0	1.00 ⁴
Heater _{ends} , H_e	0.198 ¹	0	0.230 ¹	0.187 ³	0.385 ³
Sample, S	0.664 ³	0	0.100 ¹	0	0.236 ⁴
Shield, W	0.001 ¹	0.304 ²	0.051 ²	0.058 ²	0.586 ⁴

Notes: ¹Fundamental definition, Reference A1, p. 395.

²Reciprocity.

³Symmetry.

⁴Conservation.

The areas of the surfaces are given in Table AIII. Consolidating the heater to one surface is based upon Figure A1 and Table AIII.

TABLE AIII. RADIATING SURFACE AREA

Element	Area cm ²
Heater _{inside} , H _i	4.452
Heater _{outside} , H _o	6.161
Heater _{ends} , H _e	2.677
Heater _{total} , H _t	13.290
Sample, S	5.026
Shield, W	20.271

The shape factors are shown in Table AIV.

TABLE AIV. - CONSOLIDATED SHAPE FACTOR MATRIX

	Area cm ²	H _t	S	W
H _t	13.290	0.169	0.287	0.542
S	5.026	0.764	0	0.236
W	20.271	0.356	0.058	0.586

Here the heater is treated as one surface and the shape factor is denoted by subscript H_t.

As a result of the "accounting" method, the Table AV matrix is shown which represents the energy absorbed by each surface which is in turn radiated to every other surface.

TABLE AV. - ABSORPTION MATRIX. RADIANT HEAT TRANSFER BETWEEN SURFACES

	Total Emitted	K Absorbing Surface(Cm ²)			
		H	S	W	
Emitting Surface	H	11.164	4.699	1.914	4.488
	S	2.513	1.909	0.072	0.6284
	W	8.717	4.514	0.521	3.671
Total Absorbed		<u>11.122</u>	<u>2.507</u>	<u>8.7874</u>	
Percentage Error*		0.4	0.7	0.8	

$$\frac{\text{*Emitting-Absorbed}}{\text{Emitted}} \times 100$$

The coefficients, K, carrying the dimensions of square centimeters given in the absorption and reflection matrix are defined according to

$$K = \epsilon_{\lambda} A F \phi \quad (20)$$

where ϕ represents the fraction of original emission H, S or W involved. The matrices are independent of temperature, except perhaps for how emissivity may vary with temperature. The monochromatic power absorbed or reflected is defined by

$$Q_{\lambda} = \epsilon_{\lambda} A F \phi e_{\lambda b} = K e_{\lambda b} \quad (21)$$

where $e_{\lambda b}$ is defined by equation (13) giving

$$Q_{\lambda} = \frac{K 2\pi C_1}{\lambda^5 (e^{C_2/\lambda T_{\lambda}} - 1)} \quad (22)$$

If total heat transfer is involved, then the K factor from the absorption matrix may be used with the Stefan-Boltzmann law as shown in

$$Q = K\sigma T^4 \quad (23)$$

The latter is used for the calorimetric pyrometer calculations.

The above matrices are used to calculate the monochromatic apparent temperature for the problem described by Figure A1 as follows. The original power emitted by S is

$$Q_{\lambda E} = K_{ES} e_{\lambda b_S} = 2.513 e_{\lambda b_S} \quad (24)$$

The power reflected by S from H, S and W summed is:

$$Q_{\lambda R} = K_{RH} e_{\lambda b_H} + K_{RS} e_{\lambda b_S} + K_{RW} e_{\lambda b_W} \quad (25)$$

The power seen by the optical pyrometer is the summation of the power emitted or reflected by S as defined by the sum of equations (24) and (25). This is equated to equation (22) to solve for T_{λ} , the apparent monochromatic temperature. K in this case is considered to have an $\epsilon_{\lambda} = 1$, a shape factor of 1, and the area used is taken from Table AIII for the sample, 5.026 cm². The optical and calorimetric pyrometers respond to the true sample temperature of the geometry and properties of Figure A1 given in a manner described in Figure

TABLE AVI. - REFLECTION MATRIX

		Reflected Energy		
		H	S	W
Original	H	0.896	1.914	5.952
Source of	S	0.363	0.072	0.681
Power	W	<u>0.860</u>	<u>0.521</u>	<u>4.868</u>
Total Reflected		<u>2.119</u>	<u>2.507</u>	<u>11.501</u>

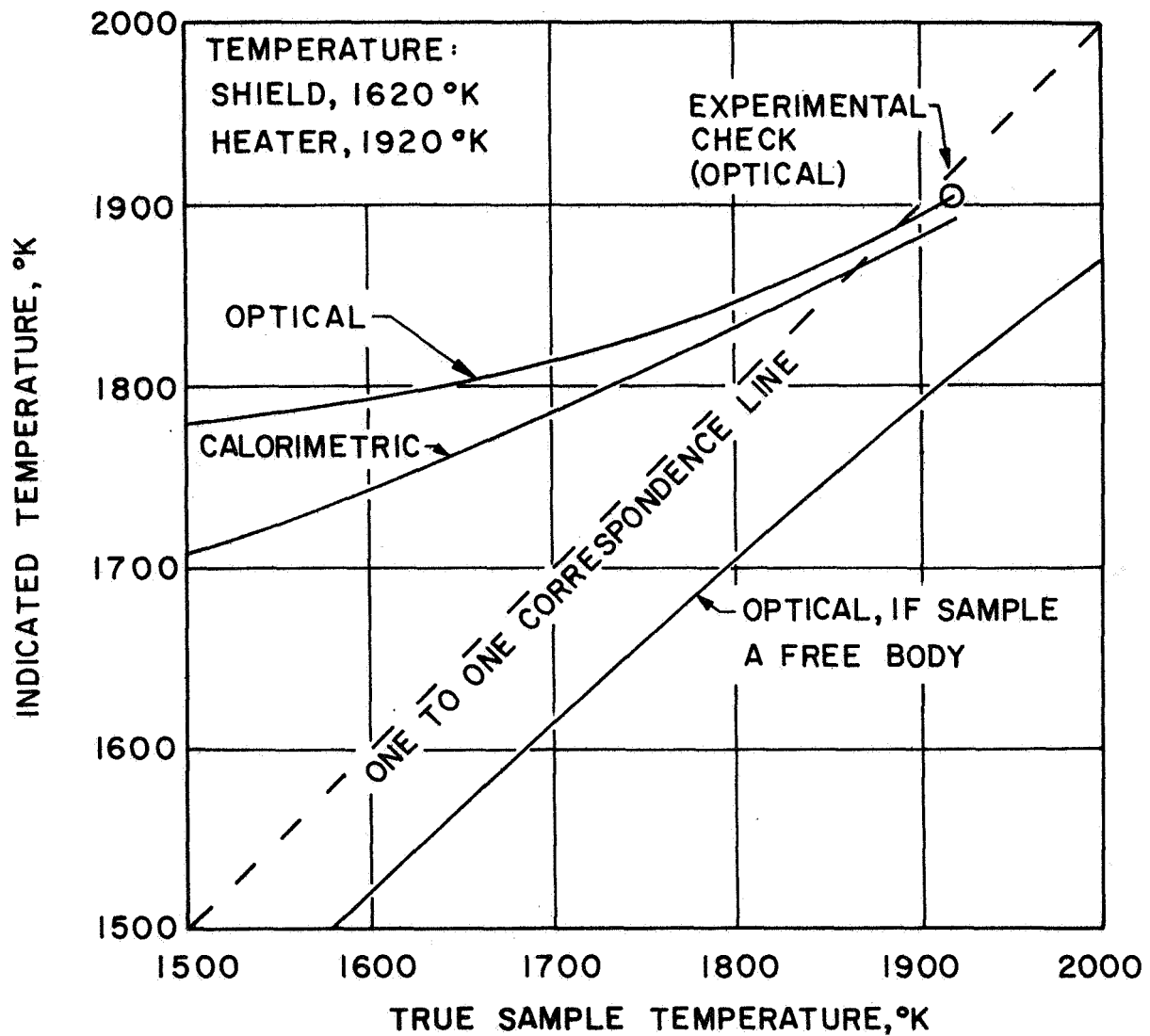


Figure A5. - Calculated pyrometer indicated temperature as a function of true sample temperature for geometry of Figure A1.

EXPERIMENTAL VERIFICATION

The following experiment was performed in order to verify the preceding analysis. Referring to Figure A1, an identical zirconia tube sample was used in which a 0.76 mm hole was drilled through the sample wall next to the normal pyrometer viewing site. As was analytically illustrated in the example, and is also a well-known fact, a black body ($\epsilon = 1$) was realized in the small opening, or hohlraum. End effects, within the tube and which are small, were made insignificant by closing the tube in the heated zone with zirconia wool insulation. The pyrometer measurement in the hohlraum is the true sample temperature. The temperature of the graphite heater needs only a small correction due to the radiation reflection term from the tungsten shield and the emissivity of the graphite; hence, the essentially true temperature of the graphite heater can be determined via equation (14). Comparative measurements were made over a range of temperatures of the tube sample outer wall and hohlraum, graphite heater, and tungsten shield. From Figure A5 it can be seen that the apparent temperature is very close to the true. When the corresponding data point is plotted on Figure A6, it is seen to agree reasonably well with the predicted optical pyrometer indicated temperature.

The best approach for precise measurements in the materials testing of ceramics in the configuration of Figure A1 is to keep the propellant flow to a low enough level so as not to exceed a 60°K indicated temperature difference between the heater and the sample.

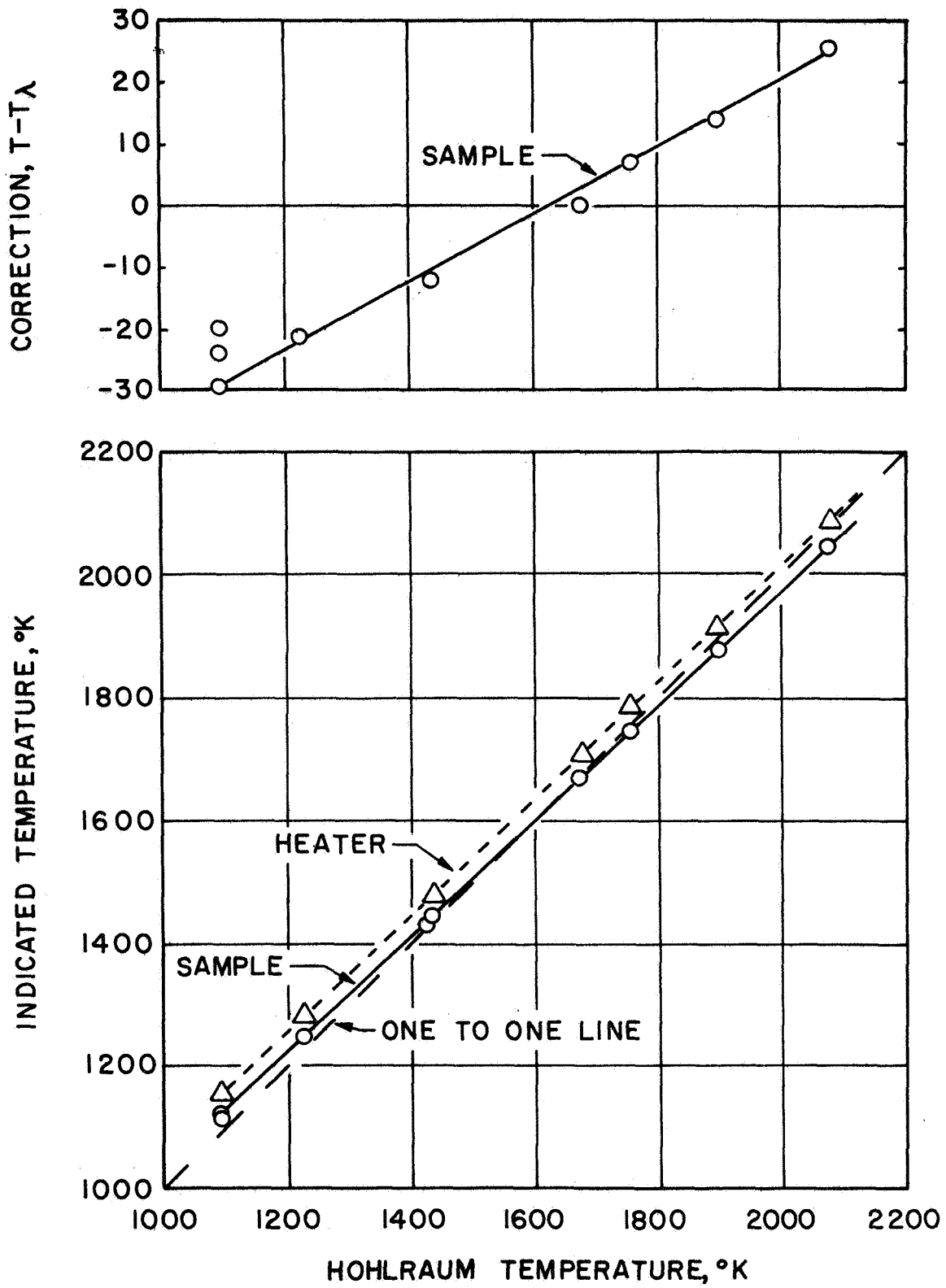


Figure A6. - Indicated monochromatic temperature ($\lambda = 0.65\mu$) of sample and heater as a function of sample hohlraum temperature.

SYMBOLS

A	area, cm
C_1	radiation constant, Planck's law, 0.59525×10^{-12} watt cm ²
C_2	radiation constant, Planck's law, 1.4387 cm K
e	emissive power, watts cm ⁻²
F	radiation shape factor
i_λ	monochromatic radiation intensity, watts cm ⁻³
K	coefficient defined by equation (20)
Q	heat flow, watts
T	temperature, °K
α	absorptivity
ϵ	emissivity
λ	wavelength, cm
μ	micron, cm ⁻⁴
ρ	reflectivity
σ	Stefan=Boltzmann constant, 5.67×10^{-12} watts/cm ² K ⁴
τ	transmissivity
ϕ	fraction of initial emitted power involved in transaction

Subscripts:

b	black body
e	end surface of heater leg
E	emitted
H	heater
i	inside circumferential surface of heater
n	normal
o	outside circumferential surface of heater
R	reflected
S	tube sample
t	total radiation over all wavelengths
T	total surface of heater
W	shield
λ	monochromatic
1	surface 1
2	surface 2

HOHLRAUM EXPERIMENT DATA (°C)

<u>Data Point</u>	<u>Hohlraum Temperature</u>	<u>Apparent Sample Tube Wall Temperature</u>	<u>Apparent Graphite Heater Temperature</u>	<u>Apparent Tungsten Shield Temperature</u>	<u>Apparent Insulation Temperature</u>
02	820	840	878	--	--
03	822	846	880	--	--
04	821	850	878	--	--
05	954	975	1005	--	--
06	1160	1172	1206	866	--
07	1398	1398	1431	--	--
08	1481	1474	1514	1170	865
09	1620	1606	1642	1314	920
10	1802	1776	1813	1490	979
11	1394	1394	1426	1077	840
12	1155	1165	1202	865	--

All measurements were made with a Micro Optical Pyrometer manufactured by the Pyrometer Instrument Co., Inc., Bergenfield, N. J., Model #95, Serial No. M6305.

REFERENCES

- A1. Eckert, E.R.G.; and Drake, Robert M., Jr.: Heat and Mass Transfer. 2nd ed., McGraw-Hill Book Company, Inc., 1959, pp. 353-438.
- A2. Noguchi, Tetsuo; and Kozuka, Takeshi: Temperature and Emissivity Measurement at 0.65μ with a Solar Furnace. Solar Energy, vol. 10, no. 3, 1966, pp. 125-131.
- A3. McMahon, W. R.; and Wilder, D. R.: Hemispherical Spectral Emittance of Selected Rare Earth Oxides. J. Am. Ceram. Soc., vol. 51, no. 4, April 1968, pp. 187-192.
- A4. Richmond, Joseph C.: Effect of Surface Roughness on Emittance of Nonmetals. J. Opt. Soc. Am., vol. 56, no. 2, Feb. 1966, pp. 253-254.
- A5. Comstock, D. F., Jr.: Measurement of Thermal Radiation Properties of Solids. NASA TR SP-31, 1963.

APPENDIX B

DEFINITIONS OF PERFORMANCE PARAMETERS

Specific impulse, I_{sp} , sec.

$$I_{sp} = \frac{\Delta F}{\dot{m}g}$$

where

F = thrust to be measured by dynamometer, N

\dot{m} = propellant mass flow, Kg - sec⁻¹

Efficiency - electric power overall, η_o^*

$$\eta_o^* = \frac{\Delta \dot{m} I_{sp}^2 g^2}{2P_e} = \frac{F I_{sp} g}{P_e}$$

where

P_e = electrical power input, watts

Efficiency - total power overall, η_o

$$\eta_o = \frac{\Delta \dot{m} I_{sp}^2 g^2}{2(P_e + P_i)} = \frac{F I_{sp} g}{2(P_e + P_i)}$$

Initial power in gas, P_i , watts

$$P_i = \dot{m} h_i 4184$$

h = enthalpy of an ideal gas above zero, kcal/kg (ref. B1)

Power in the jet, P_j , watts

$$P_j = P_e + P_i - P_l$$

P_l = heat lost from the thruster prior to exhaust jet, watts

Heater efficiency, η_H

$$\eta_H = \frac{\Delta P_j}{P_e + P_i}$$

Nozzle efficiency, η_N

$$\eta_N = \frac{\Delta}{2P_j} \frac{F I_{sp} g}{g}$$

or

$$\eta_N = \frac{\Delta}{\eta_H} \frac{\eta_o}{g}$$

REFERENCES

- B1. JANAF Thermochemical Tables, Second Edition, National Bureau of Standards, NBS 37, June 1971.